University of Strathclyde

Strathclyde Institute of Pharmaceutical and Biomedical

Sciences

Model-Based Design of Scalable Continuous Mixed-mode Crystallisation

Jenna Johnston

Thesis submitted for the degree of Doctor of Philosophy

Supervisors: Prof Alastair Florence and Dr Cameron Brown

November 2023

Declarations

This thesis is the result of the author's original research. It has been composed by the author and has not been previously submitted for examination which has led to the award of a degree.

Signed: Date:

Abstract

Crystallisation is a complex process that consists of multiple mechanisms that can compete for solute particles in solution. Subsequently, modelling the crystallisation process accurately is challenging. Within this work, two different types of crystallisation, two different solute systems and two methods of parameter estimation have been modelled using population balance modelling software. The ability to model a system of interest allows the model to then be considered as a digital representative of the process. The mechanistic model can then be used to test the process under new conditions and ultimately allow for optimisation of the process for given process outputs.

The main component system of interest for this work has been lactose and water. A mechanistic model of a seeded cooling lactose crystallisation has been achieved within this work. The characteristic slow growth and nucleation kinetics of lactose were seen experimentally and as such evaporative crystallisation was then focused upon. The development of a vacuum-induced evaporative crystalliser was attempted to circumvent the slow kinetics seen from the cooling lactose crystallisation work. The kinetics of this system were far faster and a representative model was built for this process. Despite a noisy and difficult process platform a sufficient model was built describing the primary nucleation, growth and agglomeration kinetics of the system. An innovative approach to process design was endeavoured to combine the two models and develop a multi-mode platform for the recovery of lactose from water. This allowed for the fast nucleation rate of an evaporative crystalliser to be utilised while combining with a multi-stage cooling crystallisation to improve yield recovery.

The ultimate goal of this work is to show the usefulness of developing mechanistic models. The models developed within this work allowed for the optimisation of given crystallisation processes for focused optimisation objectives. Optimisation of crystallisation without further experimentation allows for well-defined and designed processes to be built while performing minimal experiments and producing less waste. Finally, within this work, the combination of mechanistic models has been attempted to develop a multi-mode crystallisation platform. This approach allowed for an entirely simulation-based design of a continuous platform made up of both evaporative and cooling crystallisation stages. From this work, the ability to model effectively and utilise mechanistic models to reduce experimentation and waste has been clearly demonstrated.

Acknowledgements

I would like to thank my supervisors, Prof. Alastair Florence, and Dr Cameron Brown, for their guidance and support throughout my PhD journey. In particular, Dr Cameron Brown for being a sounding board for problems and ideas which was invaluable in the completing of this thesis. Additionally, this project would not have been possible without the ESPRC CMAC Future Manufacturing Research Hub for both the brilliant facilities and the extremely helpful and talented individuals I was lucky to work with. I am also incredibly grateful to Dr Humera Siddique for her guidance and encouragement over the years. I would also like to mention the brilliant support and expertise I received from my industry supervisor, Dr Anna Jawor-Baczynska both during and after my placement.

A specific thank you must be reserved for my family who have encouraged me in everything in my life. In particular, my parents instilled in me from a young age the importance of pushing myself and working hard while always reminding me that family is truly what it's all about. I deeply appreciate all the joy and laughter my family have brought me throughout my PhD and my life.

Finally, a special thank you to my partner, Cameron Black. Without whom I know I would not be where I am today. His constant love and support have been a source of strength throughout the highs and lows of my PhD. I owe my sanity to him and the sound of his laugh.

Contents

1 Introduction

1.1 Crystallisation Background

Crystallisation is a key unit operation within many industrial processes as it is a widely used method of purification and isolation[1]. The purification and isolation of compounds via crystallisation have a clear purpose for manufacturing, particularly when considering the pharmaceutical industry's need for high-purity drug substances and avoidance of contamination in products to assure patient safety. Crystallisation is the process of producing solid particles in the form of crystals of solute from a solution. This process can produce highly pure crystals due to the highly ordered structure and precise molecular level recognition required for incorporation into a crystal structure during nucleation and growth from solution. This limits the introduction of foreign molecules within the structure and as such improves the purity of the recovered solid particles from crystallisation [1].

The inducement of crystallisation is commonly driven by controlling the supersaturation levels within the solution [2]. Supersaturation can be achieved by several methods and as such a variety of different modes of crystallisation processing can be used in different products and industries. Specifically: evaporative, cooling, reactive, and antisolvent [1]. The focus of this research is primarily cooling crystallisation but with some additional consideration of evaporative crystallisation under vacuum conditions to investigate the ability to apply digital design approaches to pharmaceutical crystallisations.

Cooling crystallisation is a commonly used method of purification within both the pharmaceutical industry and the fine chemical industry. In this case, supersaturation is introduced by the reduction of solubility of solute by reducing the temperature of the solution [3].

When discussing the design, operation or control of cooling crystallisation or any type of crystallisation, it is important to consider how the process conditions affect the different crystallisation mechanisms. The crystallisation process can be tentatively split into nucleation and growth mechanisms. The nucleation stage of crystallisation is the initial formation of the smallest stable solute nuclei upon which subsequent growth can begin with the attachment and integration of more solute molecules into the crystal structure. This is a highly simplified description of crystallisation without any inclusion of additional processes such as breakage or agglomeration within the system that can affect the outcome of the overall process. Nucleation is a complex process that is stochastic in nature. Although the nucleation events themselves are not directly predictable, repeated experimentation under identical conditions results in a probability distribution [4]. Additionally, the different mechanisms within crystallisation are not restricted to occurring consecutively instead the different aspects can occur in parallel to each other such that nucleation events occur alongside growth, breakage or agglomeration [5]. The solution conditions also change during nucleation as supersaturation is depleted and new secondary nucleation sites are created. Taken in combination, these factors make modelling crystallisation processes challenging. The presence of multiple mechanisms operating competitively throughout process operation can lead to the production of material with variable attributes. This is particularly true with respect to crystal size distribution (CSD) as there will be the production of nuclei and growth in parallel allowing different extents of growth to occur for different nuclei and seeds typically resulting in a broad CSD comprising fines and larger particles. To achieve greater control over the process it is highly desirable to understand the relationship between process parameters and the crystallisation rate process outcomes in order to design and operate crystallisations capable of reproducibility and delivering consistent product quality.

1.1.1 Continuous Crystallisation Processes

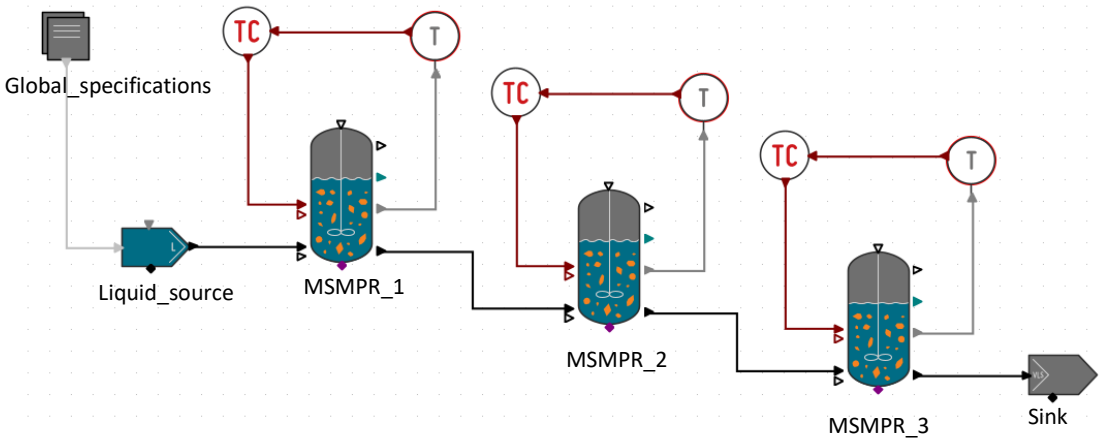

Figure 1-1 - A schematic representation of a mixed suspension, mixed product removal (MSMPR) 3-stage cascade from gPROMS FormulatedProducts version 2022.1.0 (gFP) [8]*. Flowsheet components are defined as follows; "Global_specifications" links to model background data such as solubility, "Liquid_source" supplies feed stream properties and flow to cascade, "Sink" receives and monitors product flow, "T" and "TC" define temperature sensor and temperature controller respectively.*

Despite crystallisation being one of the earliest process unit operations in history, the process itself remains relatively poorly understood [6]. There have been great research advances in the last few decades and this growth in knowledge has allowed vast strides in the design and control of the crystallisation process[7]. Whilst pharmaceutical manufacturing largely relies on batch processing, the increased understanding of crystallisation processes has also allowed the development of continuous platforms such as depicted in Figure 1-1 [8][9]. Currently, the pharmaceutical industry heavily favours batch processes, specifically, with respect to crystallisation for simplicity and robustness [10]. The use of batch compared to continuous processes is less demanding on process understanding of the crystallisation mechanisms involved to achieve acceptable results [9]. However, with there being great strides in the flow chemistry and continuous synthesis of active pharmaceutical ingredients (API) there is considerable interest in continuous crystallisation processes to allow more integrated continuous processing [10].

Continuous processing has a number of advantages when compared with batch processing. The use of continuous crystallisers can lead to reduced batch-to-batch variability of product characteristics that can be seen when comparing different batches of the same product [8][9]. More consistent primary particle or crystal attributes are also an advantage in terms of slurry and powder properties as there will be less variance, and the processing downstream can be more easily controlled [9]. There is also an improved ability to exert control over continuous processes as any necessary changes to process conditions can be implemented quickly and on a smaller volume of process solution. As such, the consequences of disturbances can be limited more effectively [10]. However, the level of control required for an effective continuous process is higher and subsequently more enhanced process design is needed as well as a greater understanding of the process [11]. The details of designing controllers for various continuous pharmaceutical manufacturing platforms have been well described by Benyahia et al [12]. More enhanced control measures means that control systems can be implemented in such a way as to obtain direct control over ideal particle attributes including size and morphology throughout the process and subsequently produce less waste in the form of off-spec products [13][14][11]. This concept has been shown through the development of a continuous sonocrystallisation platform for the crystallisation of lactose with particle size control through the D50 by Siddique et al [15]. Continuous processes are also easier in terms of scale-up when compared to batch systems which can allow the system to vary production rate relative to requirements [9]. Overall, the potential for continuous manufacturing of pharmaceuticals is of growing interest due to the reduced capital due to smaller sized vessels, flexibility of production scale and more robust processes through enhanced control [11][16][17].

1.1.2 Crystallisation Mechanisms

As previously discussed, the crystallisation process is complex and made up of numerous mechanisms. These different mechanisms have numerous mathematical models that can be used to describe them. The coupling of these individual mechanisms allows the full crystallisation process to be described for a given system. As such, the defining of the individual mechanisms and the model equations used to define them is fundamental in the ability to model their behaviour.

1.1.2.1 Nucleation

Nucleation is the process by which new solid particles are created from supersaturated solutions. The formation of nuclei and the rate of nucleation is key to all unseeded crystallisation processes. Nucleation can be further split into primary and secondary nucleation mechanisms. Primary nucleation is nucleation that takes place in the absence of any solute particles. Primary nucleation is either regarded as homogenous in which the nuclei form in a system with no foreign bodies or heterogeneous where the presence of non-solute particulates aids the nucleation process. This latter scenario is largely thought to describe most practical crystallization applications.

There are a number of different expressions that can be used to describe nucleation rate[18][19][20]. The simplest form is the empirical expression that follows the power-law model[20]. B represents the primary nucleation rate, which has been described in Equation 1 in terms of; the nucleation rate constant, the gas constant, temperature, supersaturation and supersaturation order denoted by k_b, R, T, S and b, respectively. The activation energy term, $E_{a,b}$, has also been included in this model to allow for additional variables for the fitting of the expression to measured data.

Equation 1

$$B = k_b e^{\frac{-E_{A,b}}{RT}} S^b$$

Secondary nucleation is defined as the formation of small nuclei in the presence of seed crystals of the same system. This type of nucleation is further divided by the two mechanisms which produce the stable nuclei: the attrition of seed particles; and the removal of clusters at the seed surface. The defining difference between these two mechanisms is that one is the physical removal of small particles from the seed particle and the other is a phase shift from liquid to solid to form nuclei without altering the initial seed particle. There is much discussion around the definitions of these two mechanisms and whether attrition should be described as nucleation given that there is no phase change present[21].

Secondary nucleation has been found to be the more dominant nucleation mechanism in industrial crystallisers and as such there has been significant research into this area. In particular, the effects of attrition-based secondary nucleation have been intensively studied in literature[23]–[28]. Equation 2 describes the attrition of particles due to collisions between the particle and the impeller. This equation can be split into three sections: kinetics, stirrer effects and seed effects. The kinetics of the system are represented by the rate constant, $k_{n,c-i}$, relative supersaturation, S_{rel}, and supersaturation order, n_{c-i}. The stirring effects are described by the energy dissipation rate, the impeller pumping number and power number denoted by ε, N_Q and N_p, respectively. Finally, seed effects on nucleation rate are captured by shape factor k_v, particle density, ρ_p and the volume of particles captured by the third moment limited by the minimum size expected to be prone to attrition, $L_{min, c-i}$.

Equation 2

$$J_{att} = \exp\left(\ln(k_{n.c-i})\right) {S_{rel}}^{n_{c-i}} \left(\frac{N_Q}{N_P}\right) \varepsilon k_v \rho_p \int_{L_{min.c-i}}^{\infty} L^3 n(L) dL$$

1.1.2.2 Growth

The growth of crystals in a saturated system is the increase in initial particulate size by the uptake of solute molecules from the solution. The increase in particle size through time during the crystallisation process is defined by the growth rate and there are different models that can be used to define growth rate. The most commonly used model to define growth rate is a power law type formula as shown in Equation 3[25]. These different models differ by varying the definition of the supersaturation driving force for growth in absolute or relative terms as displayed in Equation 6 and the inclusion of a diffusion step.

Two basic growth models are to be investigated for fitting the growth rates of the systems studied within this work: the two-step kinetic model and the power law. The two-step model considers growth across two stages: the diffusion of solute molecules from the bulk to the crystal surface; and the integration of solute molecules into the crystal structure's surface[25], [26]. The growth rate of the diffusion step is shown in Equation 4 and is defined in terms of the solute concentration, C, solute concentration at the crystal surface, C_i, the crystal density, ρ, and finally the volume diffusion constant, k_d. The subsequent growth rate of the surface integration step is described in the form of the power law expression shown in Equation 3. This equation has incorporated the temperature effects through the inclusion of activation energy, $E_{A,g}$. Ultimately, the growth rate is determined by the rate constant, k_g, supersaturation, S, and supersaturation order, g.

Equation 3

$$G_{Surf}(L) = k_g e^{\frac{-E_{A,g}}{RT}} S^g$$

Equation 4

$$G_{diff}(L) = k_d(L) \frac{C - C_l(L)}{\rho_c}$$

The diffusion step is made system-specific with the use of the effective diffusivity correction factor, α, through the relationship with the diffusion coefficient, D_{AB} in Equation 5. The diffusion coefficient constant is additionally described by the Boltzmann constant, k, temperature, T, dynamic viscosity, μ, and the molecular diameter of the solute, d_m. If the system in question is known or found to be surface integration limited, then the need for modelling of the diffusion step is negated and the power law will be sufficient. The cooling crystallisation of paracetamol form I from ethanol was found to be an example of a surface integration limited system by Mitchell et al[27]. The driving force defined within the surface integration step can be defined as absolute or relative as shown in Equation 6 depending on the system[8].

Equation 5

$$k_d(L) \propto D_{AB} = \alpha \frac{kT}{6\pi\mu \frac{d_m}{2}}$$

Equation 6

$$S = \frac{C_l - C^*}{\rho_c} = \frac{C_l - C^*}{C^*}$$

1.1.2.3 Agglomeration

Agglomeration is the process in which individual particles adhere together to form large, clustered particles referred to as agglomerates [28]. The presence of agglomeration within a process can be considered in both a positive and negative view depending on desired process outputs and the ability to control the agglomeration rate. The use of spherical agglomeration to control particulate size has been a recent development in the crystallisation industry[29]. Additionally, there are research areas focused on the limiting of agglomeration within a process to ensure primary particles are produced such as the work of Terdenge et al that utilised gassing to reduce the agglomeration rate[28].

When investigating agglomeration with a view to determining and modelling any rate processes taking place, there are two factors to consider: collision rate and agglomeration efficiency. Within gPROMS FormulatedProducts version 2022.1.0 (gFP), the rate of collision of particles is simulated by the agglomeration kernel and is not part of the investigation when fitting size data. Alternatively, the overall agglomeration rate is made system-specific through the agglomeration efficiency which describes the effectiveness of colliding particles to produce stable agglomerates.

A key point of interest for parameter estimation for developing a model that accurately describes the impact of agglomeration on product PSD is to identify reliable estimates for the parameters in Equation 7 [30]. This equation shows the semi-empirical model that links Mumtaz number, A_{50}, to agglomeration efficiency, Ψ. A_{50} is a dimensionless number

describing the strength of the crystalline bridge between the two individual particles joining to form the agglomerate and is the unknown term to be estimated when fitting the agglomeration term within the model. The remaining terms of Equation 7 are defined as growth rate, G, dynamic viscosity, μ, characteristic mean length of new agglomerate, $d_{3.0}$, and mean shear rate, ɣ.

Equation 7

$$\psi = \frac{\frac{\boldsymbol{A_{50}} G}{\mu {d_{3.0}}^2 \gamma^2}}{1 + \frac{\boldsymbol{A_{50}} G}{\mu {d_{3.0}}^2 \gamma^2}}$$

1.1 Population Balance Modelling

Population balances have been used in many different industries as a way of describing the progression of particulate systems over time and have been applied to model varied systems from biological populations to aerosols[31]. Randolph and Larson were the driving force in using population balances with respect to crystallisation processes [32]. The basic premise of population balance modelling is rather simple, utilising the well-established methods in chemical engineering of using mass and/or energy balances to describe and monitor changes during processes[33]. However, in the case of population balance modelling, this allows further discrimination of the changes taking place during the process and describes the distribution of mass across the population of particles as governed by the different rate processes that describe the birth, growth and death of crystals. The birth of crystals needs to be considered from three mechanisms: nucleation, agglomeration, and breakage. Subsequently, the death of crystals also needs to be considered across three mechanisms: dissolution, agglomeration, and breakage. Population balances allow the progression of the

crystals through the crystallisation process being studied to be accounted for on a probability basis.

The basis of the population balance described by Randolph and Larson is the continuum mechanics framework that relies on the principles of conservation of mass, energy and momentum and assumes the system can be modelled as a continuous medium [32]. In this framework, the evolution of particulate properties in a system is described in two separate spaces. The first is the physical space, this depicts the physical location within the design space and is described by the external coordinates. The second space depicts the abstract property space, which depicts a defining property of the particles, such as length[33]. The abstract space is described by internal coordinates which can be defined in continuous or discrete terms[34]. By assessing both design spaces the system can be fully described and can act as the basis of the model [32]. A well-mixed process can be described by the characteristic length of particles through time using the 1D PBE described by Majumder et al., in 2011 as shown in Equation 8[35]. The PSD within the system is defined by n(L,t), the growth rate by G, Q defines the rate of the nucleation, agglomeration and breakage as denoted within Equation 8.

Equation 8

$$\frac{\partial}{\partial t}n(L,t) + \frac{\partial}{\partial L}\big(G(L,t)n(L,t)\big) = Q_{nuc} + Q_{agg} + Q_{break}$$

1.1.1 Solving Population Balance Equations

Population balance equations allow a particulate process to be simulated based on the probability of events and therefore take into account uncertainties and stochastic effects in

the birth, growth and death of particles depending on the process conditions that will influence how the particle distribution evolves over time [32]. The equations being utilised are in an integro-differential form when including agglomeration and breakage terms and are usually solved by numerical methods as they are too convoluted for analytical solutions to be practicable [36]. As such, a great deal of research has been put into developing adequate numerical solution methods, such as finite element. These numerical solution methods, attempt to better describe processes in relation to computational time and enable the most appropriate approach to be implemented for any application.

1.1.1.1 Analytical Solution

As highlighted earlier, population balance equations are often too complex for analytical solutions to be attempted. However, in simpler cases, these equations can be solved analytically by applying some simplifying assumptions [36]. In the case of MSMPR, which this research is focused on, a solution can be found by assuming: steady state operation, uniform mixing, no hold-ups or losses from the system, that growth is uniform and independent of size and agglomeration and attrition are negligible. The MSMPR is therefore assumed to have no crystals within the inflow, the product and the contents of the crystalliser at any one time are identical and the system is well-mixed. This form of analytical solution was described by Randolph et al for a multi-stage cascade with nucleation in each vessel. However, it was stipulated it could be used for single vessel systems for any specified component system so long as the assumptions stated hold true[37].

1.1.1.2 Method of Moment

Equation 9

$$\mu_i = \int_0^\infty n(L,t)L^i(t)dL$$

The Method of Moments is a commonly used method of solving population balance equations and was pioneered by Randolph and Larson and Hulburt and Katz [36]. This method takes the population balance equations and converts them into moments. The moment equation can then be used to identify the global properties of the system. The transformation of the population balance equations into the form of moments reduces the number of calculations required and therefore reduces the computational power needed for the solution compared to other methods. The transformation of population balance equations to moments can be completed using Equation 9 [38]. This equation calculates the i^{th} moment, μ_i, from the number density function, n, and the characteristic size of crystals, L. The use of the method of moments is so important to solving the population balance equations (PBE) as it reduces the partial differential equation to a simpler set of ordinary differential equations assuming no agglomeration, breakage or size-dependent growth is present [38]. This simplification allows the solving of these equations to be far simpler than that of analytical methods.

The crystallisation process can most often be described by using the first four moments. The different moments all depict different properties of the system's distribution per unit volume: 0^{th} moment corresponds to the total number of particles, 1^{st} moment gives the total length of particles, 2^{nd} moment gives the total surface area of the crystals and finally, 3^{rd} moment gives the total volume [38].

There are a number of different methods of moments used in describing crystallisation. These different methods vary in their ability to describe different mechanisms. For instance, the Standard Method of Moments (SMOM) cannot account for agglomeration or breakage within the system. Therefore, methods such as the Quadrature Method of Moments (QMOM) and other manipulations of SMOM have been developed to depict the complicated mechanisms of crystallisation more accurately [36]. These different methods often give rise to greater computational requirements. Therefore, there needs to be a trade-off depending on the prevalence of the different crystallisation mechanisms within the process being assessed.

A disadvantage of using the method of moments for solving population balances is that the raw information of the distribution is lost during the transfer. Therefore, this means the distribution is not reproducible and instead needs to be inferred based on deconvolution methods and a priori knowledge [36][39]. There have been some very promising progressions of the SMOM to incorporate the more challenging mechanisms such as agglomeration. The work of Attarakih et al has allowed for a general method that can be manipulated to revert to QMOM and other sectional methods. This method defines the system by separating between primary particles used for reconstructing the distribution and secondary particles that contain information for particle interactions. This distinction allows for accurate solving of the population balance equations without losing the shape of the distribution[39].

1.1.1.3 Discretization method

Discretization methods are based on the sectioning of the internal coordinates into designated bins to transform the PBEs into a set of differential equations that can then be solved directly[40]. A clear advantage of the discretization methods for solving population

balances is that the original distribution is preserved, and no prior knowledge of the system's behaviour is required. However, this leads to an increase in computational power requirements [36]. The computational power is directly related to the chosen bin size and therefore depends heavily on the broadness of the distribution of the system. With advances in the wide accessibility of powerful computational resources, the use of discretization methods is becoming more common [36].

1.1.1.3.1 Method of Characteristics

In this method, the original partial differential equation is transformed into ordinary differential equations by discovering curves along the L-t plane. The solution of these ordinary differential equations is based upon a characteristic such as length can then be utilised to solve the original partial differential equation. A disadvantage to this method is the high computational time required to solve such a large number of equations. This method of solving population balance equations is often coupled with other methods to improve the efficiency of solving the equations.

1.1.1.3.2 Finite Difference Method (FDM)

This method utilises difference equations in order to approximate the differential equations of the PBEs. The use of this method is particularly suited for building population balance models while incorporating computation fluid dynamics (CFD) which is often based upon using finite element or finite volume methods [36]. The inclusion of PBE can be achieved by direct input of PBE to CFD code[36]. The combining of CFD with PBE has been utilised by John et al., to study the effect of the location of inlets on the flow field within a cavity and ultimately how this impacts the growth rate and primary nucleation rate of calcium carbonate[41].

1.1.1.3.3 Finite Element Method (FEM)

In this method, the partial differential within the PBEs is converted into integral forms [36]. The numerical solution of which requires the system to be discretized. Once the continuum is discretised, solutions for the differential equations across the individual sections can be found using iterative solver methods [36][42]. From summing up these solutions, global solutions of the system can be found [43]. The advantage of FEM over FDM is that the discretization of the domain does not need to be uniform and therefore the higher resolution can be applied where needed and not across the whole domain which greatly reduces computational load [36].

1.1.1.3.4 Finite Volume Method (FVM)

Finite volume is similar to finite element in that the function being fit is discretized and values are calculated in line with this. However, finite element defines functions to represent the individual discretised points whereas finite volume utilises integrals to give average values at the individual points. The use of FVM has been utilised in other research areas such as aerodynamics and its efficacy for population balance modelling has been discussed when considering high-resolution methods[44].

1.1.1.4 Monte Carlo Method

The basic premise for Monte Carlo solving methods is the input of randomly generated numbers from a specified distribution into the equations of interest and the most frequent solutions will correspond to the true solution. There are a number of advantages to this method of solving population balance equations. The random input produces a dependable set of results that closely depict the crystallisation process being studied. However, to

thoroughly and accurately use this method a large number of particles need to be tracked [45]. As such, there is a correspondingly high computational time for this method [36].

1.1.2 Parameter Estimation

The research described by Pérez-Calvo, Kadam and Kramer [30] and Bari and Pandit [46] discuss the use of gFP as a method of defining the individual parameters of crystallisation. The gFP software has in-built rigorous parameter estimation abilities based upon maximum likelihood optimisation solvers [46]. The basis for solving and defining the parameter estimates from experimental results within gFP is simply done by minimizing the objective function, Φ, in Equation 10[30]. This equation is defined by the number of measurements, NT, the parameters being estimated, θ, the number of experiments being used, NE, the number of measured variables in the i^{th} experiment, NV_I, the number of measurements of variable j for experiment I, NM_{ij}, the variance of the k^{th} measurement of variable j in experiment I, σ_{ijk}^2, the measured value of the k^{th} measurement of the j^{th} variable in experiment I, $\tilde{Z}_{ijk}$, and finally the predicted counterpart of $\tilde{Z}_{ijk}$, Z_{ijk}. In the case of gFP, the population balance is solved and modelled by the high-resolution fidelity finite volume scheme with flux limiting function (HRFVS-FL) which has been widely described in the literature and adopted in a number of industrial applications [47][48][49].

Equation 10

$$\Phi = \frac{NT}{2}\ln(2\pi) + \frac{1}{2}\min_{\theta}\left\{\sum_{i=1}^{NE}\sum_{j=1}^{NV_i}\sum_{k=1}^{NM_{ij}}\left[\ln\left({\sigma_{ijk}}^2\right) + \frac{\left(\tilde{z}_{ijk} - z_{ijk}\right)^2}{{\sigma_{ijk}}^2}\right]\right\}$$

1.1.2.1 Model Design Methods

Parameter estimation is a key step in the development of a mechanistic model of crystallisation. The ability to define the parameters of crystallisation allows a true

representation of the particular crystallisation system to be described. As the resulting model is to be the basis for optimisation and to inform greater process understanding, the accuracy of the parameters and subsequent model is paramount. The method of retrieving sufficient parameters to adequately describe the crystallisation process will have a large effect on the accuracy of the mechanistic model produced.

The modelling of crystallisation is such a complex problem due to there being a number of different mechanisms taking place and potentially interacting within a system simultaneously. These numerous mechanisms of crystallisation are competing for solute molecules in solution and all have different effects on the crystal size distribution (CSD) of the product. It is therefore important to accurately depict the different mechanisms in order to get a true representation of the overall system. In the next section, the different methods of uncoupling these parameters are discussed in detail.

1.1.2.2 Simultaneous Parameter Estimation

A method of determining growth and primary nucleation kinetics has been discussed by Nagy et al based upon the metastable zone width of the system [50]. The advantage of this method is the simplicity of the experiments required. The defining of the metastable zone width is usually a prerequisite to performing a controlled crystallisation and as such is often studied regardless of the need to build a mechanistic model. The knowledge gained from defining the metastable zone width (MSZW) allows for effective experimental design in terms of seeding and the cooling profile with maximum tolerable supersaturation levels before primary nucleation occurs. The expansion of knowledge gained from MSZW experiments is an efficient method of investigating the kinetics of the system without the need for numerous experiments. The system investigated in the work of Nagy et al utilises in-situ analysis

methods to assess the kinetics of a paracetamol-water system. The concentration within the system was continuously monitored using a Fourier-transform infrared spectroscopy (FTIR) probe. This allowed the concentration changes and depletion of supersaturation induced by the presence of nucleation or growth to be monitored and assessed. Additionally, the use of a focused beam reflectance measurement (FBRM) probe allows crystal size distribution (CSD) to be assessed. The recorded chord length distribution (CLD) can be used to estimate the CSD by utilising a shape factor. This estimation of the CSD allows for growth to be assessed with direct respect to the crystals grown within the system as opposed to merely inferred from concentration changes.

The experiments designed for this method of kinetic data collection are centred around unseeded desupersaturation experiments. The induction times of the system can be assessed in this manner and will allow for systems where primary nucleation is the only form of nucleation taking place. This can be assumed as the nuclei present are too small to allow for secondary nucleation to take place. The growth of particles formed can be monitored via FBRM and the resulting CSD data. The parameters of crystallisation can be assessed from these experiments while including their dependence on supersaturation levels and the cooling rates applied to the system. The primary nucleation and growth parameters can then be assessed simultaneously with the use of a generic dynamic model and the incorporation of the MOM.

This method however has a number of disadvantages in providing reliable estimates of the parameters describing the process. For instance, the use of CLD to determine CSD increases errors within the system as CLD is known to inaccurately describe particle size due to the inherent method of measuring CLD not representing the true sizes but simply the cut of the particle that the FBRM laser detects[51]. This often leads to undersized predictions,

particularly when considering needle-like crystals. The parameters assessed within the work of Nagy et al., were limited to growth and primary nucleation[50]. This is also a clear disadvantage of this method as the effects of breakage and agglomeration can have great effects on the final outputs of a system. For instance, agglomeration and breakage have great effects on the final CSD which will ultimately affect downstream processing[52]. Secondly, the presence of breakage and attrition are key players when assessing secondary nucleation, which is widely recognised as the dominant nucleation mechanism in MSMPRs and is not considered in this approach.

1.1.2.3 Sequential Parameter Estimation

The estimation of crystallisation parameters sequentially has shown promising results. The methodology, which has been described by Pérez-Calvo, Kadam and Kramer [30] and Bari and Pandit [46], looks to uncouple the different parameters of crystallisation for specific mechanisms by limiting the presence of different and potentially competing mechanisms by altering the process conditions to favour a specific mechanism. By limiting certain parameters, other parameters can dominate under specified conditions and therefore the kinetics of the mechanism and specific parameters enable that to be modelled relative to crystallisation. Once individual parameters are defined and understood, their effect on crystallisation can be accounted for. This allows a wider range of parameters beyond growth such as nucleation and agglomeration to be assessed. In the analysis of agglomeration for instance, if the growth parameter is well understood the particle size distribution (PSD) of seed size can be broadened to include for a large span of sizes. The larger span of seed sizes has been shown to improve agglomeration efficiency[30]. The conditions in which agglomeration thrives are typically also favourable towards growth. Therefore,

agglomeration can only be assessed with any confidence once the growth parameters have been accounted for when looking at the resulting CSD of the product retrieved.

The reliability of results obtained from the parameter estimation approach within gFP is heavily dependent on the discretisation of the grid for population balance solving. It is important in this case to limit the bounds of the grid to appropriate sizes of crystal, dependent on the system being defined. As for the case of nucleation and growth the grid range must cover a suitable range to design the system. For instance, in the case of Pérez-Calvo, Kadam and Kramer a minimum crystal length of 1µm and a maximum of 5000µm were chosen.

1.1.2.3.1 Three-Step Sequential Parameter Estimation

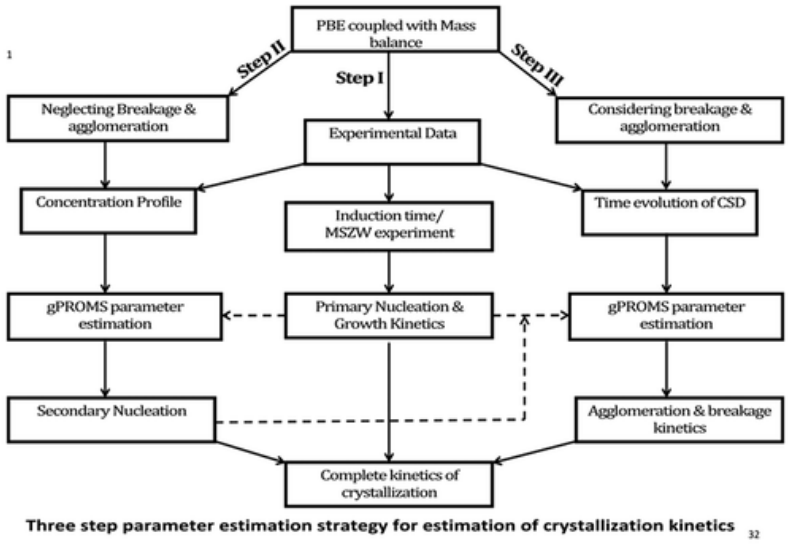

Figure 1-2 - Schematic depicting the ideology of the three-step method of parameter estimation [30]

The difference between the sequential method across these two papers is the method of decoupling the parameters experimentally. Perez-Calvo, Kadam and Kramer have separated growth into two terms (volume diffusion and surface integration) and agglomeration by

simply considering agglomeration to not affect the concentration of the solution [30]. This therefore allowed the surface integration mechanism of growth to be evaluated by seeded desupersaturation experiments where secondary nucleation was avoided by minimizing attrition. Any agglomeration terms could later be assessed by utilising the product CSD once growth could be accounted for with sizes in excess of achievable growth attributable to agglomeration. Similarly, secondary nucleation via attrition was accounted for by increasing collisions of the crystal with the stirrer by increasing the agitation rate. Finally, primary nucleation could be assessed when all other parameters were defined by minimising attrition and varying cooling rates in unseeded desupersaturation experiments.

This method of parameter estimation is similar to that described by Mitchell, Ó'Ciardhá and Frawley for determining the growth parameters of paracetamol from ethanol [27]. However, the solving of the population balances and the optimisation needed for estimating the chosen parameters were completed in MATLAB as opposed to gFP.

1.1.2.3.2 Five-step Sequential Parameter Estimation

The experimental method of the research completed by Bari and Pandit goes further in seeking to decouple different mechanisms. Growth and primary nucleation were assessed together by the use of induction time experiments. In this research, primary nucleation was thought to begin as soon as supersaturation was induced and the induction time represented the time taken for the nuclei produced via primary nucleation to grow to a measurable size [46]. From this viewpoint, the growth and primary nucleation terms were considered together. Induction time experiments also allow for secondary nucleation and agglomeration to be negated as the crystals will be too small in size to promote either mechanism at this initial stage. As primary nucleation can be defined purely on the number of crystals produced,

the changes in the concentration profile during induction time can be used to define the growth term of crystallisation[46]. Similar to the method described by Pérez-Calvo, Kadam and Kramer, agglomeration and breakage are assumed to have no effect on the concentration profile. With growth and primary nucleation defined in the previous set of experiments and agglomeration and attrition determined to not affect the concentration of the solution, any changes in concentration can be assumed to be caused by secondary nucleation. This was completed by constant cooling rate experiments. With nucleation and growth defined the product CSDs can finally be utilised alongside the optimisation systems within gFP to define agglomeration and breakage[46].

2 Aims and Objectives

Building on current best practices for modelling crystallisation processes, mechanistic models for different crystallisations were developed in this work. The development of crystallisation-mode-specific mechanistic models was achieved through the use of batch experiments. These small-scale batch experiments utilised process analytical technology (PAT) in the form of solute concentration and particle size monitoring through FTIR and FBRM probes. The modelling work for this thesis utilised the population balance modelling software from PSE, FormulatedProducts. This software also allowed for optimisation of the modelled process for different goals such as particle size, yield, and reduced batch time. Through the use of developed mechanistic models, the suitability and potential of different mixed-mode crystallisation platforms were tested without further experimentation and waste of material. The aims of this work are highlighted as follows:

- Develop mechanistic models of different crystallisation modes for the model system of lactose and water through a set of small, designed batch experiments.
- Develop a mechanistic model for the crystallisation of a late-stage development active pharmaceutical ingredient (API) compound from pre-existing data.
- Utilise the developed models for optimisation purposes for an array of optimisable objectives. In particular the optimisation of crystal mass recovery within particle size ranges of interest for the specified processes
- Utilise developed models of the lactose system to test the potential capabilities of different configurations for a continuous multimode crystallisation platform.

The overall goal of this work is to utilise the building of mechanistic models to gain a better understanding and optimisation of the crystallisation process for improved recovery and

tuneable particle size ranges. The use of models to aid in the development of processes allows fewer experiments to be performed and therefore reduces the waste in the development stages. This reduction in experiments focuses on the collection of efficient datasets that improve the sustainability of the work while still allowing for a better understanding of the system. Given the current push for better and more sustainable manufacturing practises, the use of mechanistic models to supplement the data needed for efficient manufacturing, through optimisation and simulation-based investigation of potential processes, has never been clearer.

2.1.1 Thesis Outline

Chapter 1 outlines crystallisation background theory, as well as methods of estimating crystallisation kinetic parameters. This chapter gives an overview of literature pertaining to developing mechanistic models of crystallisation processes. Chapter 3 details the methods used to build a mechanistic model of the cooling crystallisation process of lactose from water by means of sequential parameter estimation. The resulting model is then used as the basis for the optimisation of the system for an increase in yield while reducing batch time. Chapter 4 focuses on building a mechanistic model of a late-stage development compound from AstraZeneca by utilising pre-existing data from experiments with different aims. Chapter 5 outlines the designing of a semi-batch vacuum-induced evaporative crystalliser and the subsequent mechanistic modelling of the system. The model itself is then used for optimisation purposes for different process outcomes. Finally, Chapter 6 utilises the previously built cooling crystallisation model and the evaporative model as a way of investigating different configurations of a multi-mode platform. The capabilities and optimisation of these configurations are then discussed.

3 Mechanistic Model Development of Cooling Crystallisation

3.1 Introduction

This chapter is centred on the building of a mechanistic model of the cooling crystallisation of alpha-lactose monohydrate from water by means of sequential parameter estimation. The advantages and disadvantages of the different types of sequential parameter estimation were discussed in section 1.1.2.3 and within this chapter, the method outlined by Perez Calvo et al has been followed to develop a mechanistic model of the lactose cooling crystallisation process[30]. Lactose was chosen as the compound of interest for this work for a number of reasons, in particular its large-scale production and wide range of applications and the challenges caused by anomeric transformation, multiple solid forms and slow crystallisation kinetics of the system. The slow kinetics highlight the potential advantages of reducing the experimental work by means of simulated experiments. As such, the building of a mechanistic model relying on data from small-batch experiments will allow for the process to be represented digitally.

The additional complexity of modelling the system in terms of the mutarotation equilibrium and the formation of hydrate crystals was considered throughout the modelling process. The inclusion of these added complexities within the mechanistic model, will ensure that the model developed will be broadly applicable and robust in its ability to provide reliable predictions of the outcomes of the process. The end goal of this work is to utilise the model for optimisation purposes and to showcase the benefits of developing mechanistic models of crystallisation systems. The ability to optimise the process for different process output goals without the need for additional experimentation is a key advantage of building mechanistic models.

3.2 Lactose Crystallisation

3.2.1 Use in the Pharmaceutical Industry

Lactose is a naturally occurring disaccharide made up of galactose and glucose that is found within the whey of dairy products [53]. Whey is a by-product of dairy processing and is a serious consideration for waste processing. The lactose in whey is the largest source of biochemical oxygen demand (BOD) in the waste stream so it is important to remove the resulting lactose not only to reduce waste effects but as it is also a commodity in itself [54]. Lactose is widely used in not only the food industry but also as an excipient in the pharmaceutical industry where it is often added to the formulation of many tablets as a filler due to its relative affordability, availability and low toxicity [55].

3.2.2 Mutarotation

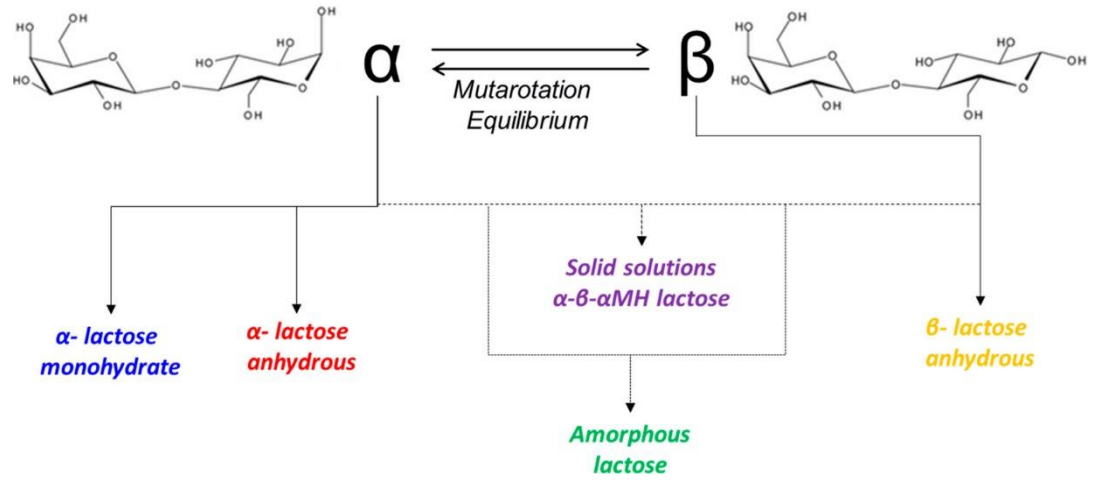

Figure 3-1 – Depiction of the mutarotation of lactose and the different possible crystal forms [53]

As shown in Figure 3-1 lactose exists as two isomers, α and β [53]. The transformation between these two isomers is undergone when in solution via mutarotation until equilibrium is reached. The method of crystallisation determines what form of lactose is produced with

the most commonly used form in the pharmaceutical industry being α-lactose monohydrate (ALM) [56]. Although this is not the most stable form, it is easily recovered as β-lactose has a higher solubility than that of its counterpart and as such crystallisers working under moderate temperatures will primarily produce ALM [53]. To crystallise the β form the crystallisation would have to operate at exceedingly high temperatures as crystallising below 93°C will favour α-lactose production [53][15]. As the α-lactose is crystallised the molecules in the solution undergo mutarotation and therefore more α-lactose is produced to account for the loss in solution [53]. This mutarotation consideration was found to have a limiting effect on the recovery as the equilibrium shift is temperature dependent and at lower temperatures, the equilibrium position reduces to an unfavourable yield recovery [57]. The focus of this work is centred on optimising the production of ALM crystals from water in terms of yield and particle size through the use of a mechanistic model.

3.2.3 Morphology

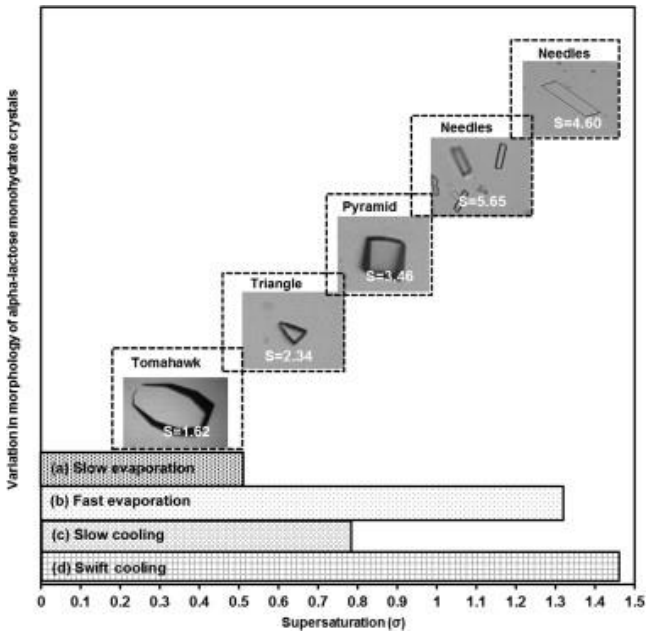

Figure 3-2 – Depiction of the different possible morphologies of lactose depending on the crystallisation process[58]

The characteristic shape of a slow-cooled α-lactose monohydrate is a 'tomahawk' shape which can be seen in Figure 3-2 [58]. The type of crystallisation, as well as the level of supersaturation at the beginning of crystallisation, has a great effect on the morphology of the produced crystals. It is important to control the morphology during the crystallisation process as this can lead to processing problems further down the line. For instance, needle-like crystals are notorious for their poor flow properties and as such have a high risk of blockages [59]. Such issues with downstream processes can incur high costs and therefore it is important to consider the morphology of crystals produced within a process to minimise such issues. The favoured tomahawk shape for ALM is typically achieved from cooling crystallisation at relatively low supersaturation [58].

3.2.4 Challenges in Industrial Crystallisation of Lactose

There are a number of issues with lactose crystallisation within an industrial context. For instance, the nucleation of lactose is very slow [54]. As such, it is common to use methods of inducing nucleation within the system such as sonication as discussed by Siddique et al for a continuous oscillating baffle crystalliser[15]. Alternatively, the slow nucleation kinetics are avoided through the use of seeding. Furthermore, the growth of lactose also has slow kinetics and is surface integrating limited as opposed to volume diffusion limited meaning that outside factors such as enhanced mixing cannot be used to aid the growth mechanism[60][56][57]. The rate of mutarotation was investigated as a possible limiting factor for the crystallisation of α-lactose but was found not to restrict the growth of crystals [57]. The slow growth and nucleation of lactose may be explained by the presence of impurities and ions when considering true lactose refining from whey [61]. However, in the case of this research, the lactose used is of pharmaceutical grade (≥99% total lactose basis) and therefore impurity levels should be sufficiently low to avoid interference with the

kinetics of crystallisation. The slow crystallisation kinetics, in this case, can be explained by the inhibiting effects that the presence of β-lactose can have when in solution [57]. This inhibiting effect of anomers is due to the likeness of the different anomers in solution blocking the inclusion of new solute particles into the crystal structure.

The slow nucleation kinetics is of clear concern when considering the lactose crystallisation process. As such, the use of ultrasound has been investigated for its ability to improve the rate of nucleation of lactose when in an aqueous solution [62]. The introduction of ultrasonic waves to the solution produces cavitation and the generation of gas bubbles. When these collapse, localised points of high temperatures and concentration are created[4]. The release of this energy within the system has been shown to induce nucleation. This can produce nuclei rapidly and also at lower supersaturation levels than is usually required [62][15]. Lactose crystallisation has been investigated within an array of different crystallisation platforms. The different crystallisers have been found to have significant effects on the crystallisation process, in terms of morphology, yield, and purity. The use of oscillatory baffle crystallisers has been investigated and it was shown that with the use of sonication, an appropriate continuous system can be implemented [15].

3.3 Model Basis

The parameter estimation experiments will allow kinetic data to be collected for the different mechanisms present in the investigated crystallisation process. Prior to parameter estimation of the crystallisation kinetics, the system itself was modelled to include physical properties as well as information specific to the crystallisation system. This prior modelling is important for physical properties that may vary throughout the experiment as well as particular impacts introduced by the solute when in solution. In the case of the lactose

system, there is increased complexity due to the mutarotation between alpha-lactose and beta-lactose when in an aqueous solution. This has a number of knock-on effects on other properties of the system. In the following sections, the basis of this will be explained in terms of; physical properties including viscosity and density, the solubility of ALM depending on beta-lactose concentration and temperature, and mutarotation kinetics.

3.3.1 Physical Properties Model

The physical properties of the model need to be adequately described to ensure the model depicts the true system in real-time. As such, the density and viscosity have been individually modelled as these properties are known to depend on both concentration and temperature. As such, the modelling of a cooling crystallisation is particularly susceptible to changes in viscosity and density which directly affect the very kinetics being studied.

The density and viscosity of lactose solutions have been researched in the literature with some success. The basis of this model is a set of expressions developed by Morison and Mackay [63]. The work performed by Morison and Mackay is restricted to the experimental range of 5-25 wt% and 10-50 °C. This range is lower than the working range of the work undergone within this research of around 15-65 °C and 20.19-36.98 wt%. As such, the extrapolation of these expressions may have some degree of error at higher concentrations and temperatures.

Equation 11

$$s.g. = \frac{\rho_s}{\rho_{water}(T)} = 1.000 + 0.3886w + 0.1158w^2$$

Equation 12

$$\frac{\eta}{\eta_o} = \frac{(1 + 0.5\varphi)}{(1 - \varphi)^2}$$

The density of the lactose solution can be found via Equation 11 which relates the ratio of solution density, ρ_s, and the density of water at a given temperature, $\rho_{water}(T)$ to the effect of changes in the concentration of lactose in wt%, w. The viscosity of the lactose solution, η, at the specified temperature and concentration can be calculated from Equation 12 through the effective volume fraction, ϕ, and the density of solvent, η_0. The set of expressions developed by Morison and Mackay [63] have all been combined and input within gFP to calculate the density and viscosity of the solution at any given time to define the physical properties of the system.

3.3.2 Mutarotation Kinetics Modelling

The relationship between α-lactose and β-lactose when in solution is an important factor in many of the mechanisms in the ALM crystallisation system and as such, it needs to be considered within the model.

The dissolution of lactose within water is followed by mutarotation of the molecule between the two anomers: alpha and beta. The mutarotation reaction has been studied and a governing equilibrium constant can be used to assess the concentration of the two anomers at any given time. The equilibrium constant can also aid in the assessment of the rate constants of the forward and backward reaction as can be seen in Equation 13. The equilibrium constant has been found in the literature to vary with temperature as shown in Equation 14 [64]. These relationships have been input to gFP to allow for accurate simulation of the mutarotation equilibrium within the solution with respect to time and temperature.

Equation 13

$$K_m = \frac{k_1}{k_2} = \frac{C_\alpha}{C_\beta}$$

Equation 14

$$K_m = 0.526 - 0.0003T + 2E^{-6}T^2$$

3.3.3 Custom Solubility Model

The solubility of lactose has an added complexity due to the subsequent mutarotation of the molecule when in an aqueous solution. The different anomers of lactose have different solubilities with beta's around ten times higher than that of alpha[65]. This difference in solubility is partly due to the mutarotation equilibrium lying in favour of the beta form with a ratio of 60:40 and as such the alpha dissolution will occur across two stages[66]. The first stage is the simple dissolution of ALM until the solution is saturated in relation to alpha-lactose. Following this, any excess alpha-lactose supplied will only dissolve once mutarotation of the previously dissolved solute lowers the concentration below saturation of beta and in turn, the system is shifted to an undersaturated state. The combined solubility of both anomers describes the total lactose solubility in water. The solubility of total lactose, $C_{l,s}$, has been studied in the literature extensively and the data acquired has been collated into a mathematical expression by McLeod in his 2007 thesis which can be seen in Equation 15[67].

Equation 15

$$C_{l,s} = 10.9109e^{0.02804T}$$

It is important that within this model the saturation and subsequent driving force for crystallisation are defined in terms of α-lactose as opposed to total lactose concentration. This will give an accurate representation of the driving process for the different crystallisation mechanisms under investigation. The definition of supersaturation of the system in terms of alpha-lactose can be seen in Equation 16[67].

Equation 16

$$S = \frac{C_{\alpha}(T)}{C_{\alpha,s}(T)}$$

An important consideration is the effect that the presence of the β-anomer in solution has on the concentration and solubility of ALM. The effect of the presence of different anomers on their solubility is an interesting phenomenon that is consistently seen in mixed carbohydrate systems[61]. The presence of additional carbohydrates has been found to lower the solubility of the original species. This lowering of solubility of ALM due to the presence of β-anomer has been described by Visser et al [68]. From this work, a correction factor has been suggested. A mathematical expression calculated from Visser's work describing the correction factor's dependence on temperature has been defined by McLeod and can be seen in Equation 17.

Equation 17

$$F = 0.0187e^{0.0236T}$$

The correction factor simply describes the dependence of the concentration of ALM in a saturated solution on the concentration of β-lactose. This dependence requires the definition of saturation described in Equation 16 to be updated as can be seen in Equation 18.

Equation 18

$$S = \frac{C_\alpha(C_\beta T)}{C_{\alpha,s}(C_\beta T)}$$

The calculation of these terms requires the relationships describing mutarotation and the solubility suppression to be utilised. The incorporation of mutarotation kinetics can be done by including the equilibrium constant K_m.

The correction factor, F, can be described as the gradient of the line depicting the relationship of ALM in a saturated solution with respect to β-lactose concentration. The equation for the gradient can be used to define the concentration of alpha-lactose, at saturation, corresponding to the concentration of β-lactose in equilibrium at the required temperature. With this definition and the use of the mutarotation equilibrium constant the required supersaturation ratio can be defined for a given lactose concentration, C_l, as shown in Equation 19[67]. This was input into gFP as a custom solubility equation.

Equation 19

$$S = \frac{C_l}{(C_{l,s} - F * K_m * (C_l - C_{l,s})}$$

3.4 Methods

3.4.1 Concentration Calibration Modelling

The ability to accurately monitor concentration during the crystallisation process is fundamental to the ability to assess the kinetics of the process. As such, building an accurate calibration model for the chosen spectra is a necessary prerequisite to ensure reliable data for modelling. The most suitable spectrometer was chosen based on the component system being monitored and the disparity between the spectra of the solute and solvent. Recording

concentration through the crystallisation process requires the incorporation of temperature effects. Therefore, a range of temperatures and concentrations that cover the working range of the crystallisation process being assessed are covered in the building of the spectral calibration model. A number of experiments were performed to record the required spectra of the specified system under an array of temperatures and mass compositions.

The use of projection-based regression methods such as PLS and PCR is the standard method for building calibration modes for spectral data such as FTIR [69], [70]. Univariate models are capable of describing the concentration of a system, however, are often not found capable of achieving suitable accuracy or robustness. The use of univariate methods also requires the selection of characteristic signals within the spectra that best describe the system, and this can be complex and slow depending on the system being studied. Alternatively, multivariate regression methods negate the need for manual selection of signals and are found to have a high degree of accuracy and can produce more robust models for systems with temperature-sensitive spectra[71].

The use of multivariate regression in the form of PLS and PCR for ATR-FTIR spectra is described in detail by Cornell et al 2008 [70]. An experimental plan is executed within this work to collate numerous spectra at different concentrations and temperatures to cover a wide range that may be seen during crystallisation processes. Within this work, the use of univariate and multivariate methods of building calibration models for concentration monitoring is compared. The use of multivariate regression was found to be superior to the univariate calibration model in terms of accuracy. More specifically, the use of PLS regression was better when using the same number of latent variables. Additionally, the inclusion of temperature as an input variable was found to have no resulting effect on the model's accuracy and therefore was not carried forward.

The concentration monitoring for total lactose concentration has an added level of complexity due to the presence of the mutarotation reaction when lactose is in water. Due to the mutarotation reaction, the lactose solution is actually made up of three components: water, alpha-lactose and beta-lactose. Therefore, the monitoring of the lactose concentration needs to incorporate the combination of beta and alpha-lactose. The ability to measure the concentration of the individual components via the monitoring of the IR spectra is not simple due to the inability to separate the peaks of the separate lactose anomers. Additionally, due to the relationship between mutarotation equilibrium and temperature, the onset of a temperature change corresponds to a shift in alpha and beta-lactose concentrations corresponding to the shift in equilibrium.

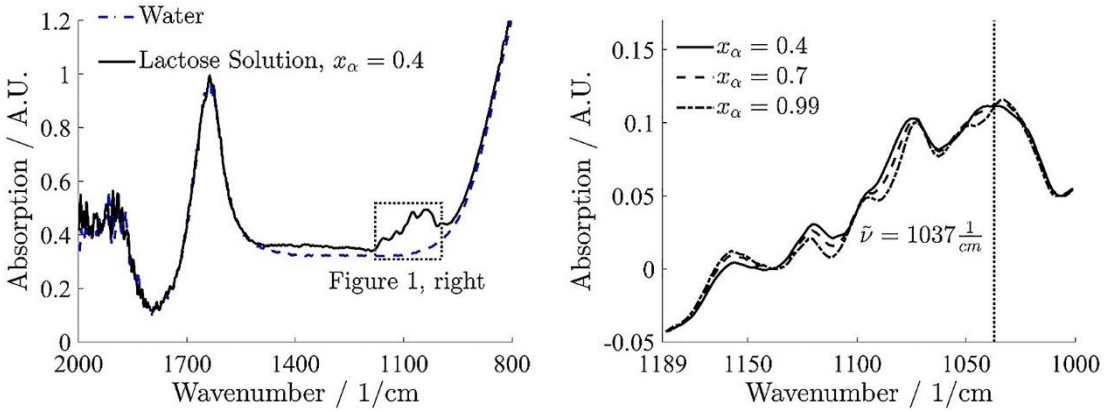

Figure 3-3 - FTIR spectra collected of a near mutarotation equilibrium solution of lactose: water solution with a concentration of 6.16g/100g lactose solution. x_α alpha mass fraction of total lactose [72].

The ability to accurately monitor lactose concentration via FTIR spectra has been investigated and described well by Schiele et al [72]. Within this work, the problem of monitoring anomer concentration has been investigated. The experiments performed within this paper found the unsuitability of standard calibration techniques such as PLS and PCR for the monitoring of total lactose concentration. Figure 3-3 shows spectra from Schiele's work that were collected over several hours that show the variation of spectra due to the concentration shift between alpha and beta-lactose due to mutarotation. The standard methods of developing

calibration models from spectra, such as PLS and PCR methods, are based on the area under the peaks of interest. The changing nature of the peaks regardless of constant total lactose concentration negates the use of PLS and PCR as suitable methods of building calibration models. This paper also highlighted the use of peaks which intersect for varying stages of mutarotation as suitable peaks to monitor total lactose concentration via polynomial fits and the incorporation of temperature.

3.4.1.1 Experimental Method

The working concentration and temperature range of interest for the system are highlighted in Table 1. The experiments were subsequently designed to encapsulate the workspace of interest while building the calibration model. A total of five different concentration experiments were proposed with additional experiments added where deemed necessary to build a more accurate calibration model. The temperature of each experiment was varied from at least 5°C above saturated temperature and cooled to the lowest temperature of interest or until nucleation was detected. The presence of nucleation defines the point at which the concentration of the solution is no longer known.

Component/Mode	Concentration (kg/kg)	Temperature(°C)
Lactose/Cooling	20-40	10-65

Table 1 - Working range of specified experimental work.

The following experiments were carried out in an EasyMax (Mettler Toledo) reactor system within a 100 ml vessel. Particle counts within the system were monitored continuously with the use of an FBRM probe. An FTIR ATR probe was also positioned within the system to collect spectra throughout the experiments to be used for the calibration modelling. A specified mass of solute was supplied to the empty vessel and subsequently topped up with pure

solvent to achieve the concentration of interest. The vessel was then heated within the EasyMax system to at least 5 °C above its corresponding saturation temperature and held for 20 min to allow for complete dissolution. Dissolution was confirmed by use of the FBRM probe before the system was then gradually step cooled in segments of 5 °C with a 10-minute hold. This was continued until nucleation was detected via the particle count or the lowest temperature of interest was reached. The detection of nucleation marks the loss of concentration data as the concentration from that point onwards no longer corresponds to the concentration following dissolution. This method was repeated across five concentrations covering the concentration and temperature range of interest.

3.4.2 Parameter Estimation Experiments

3.4.2.1 Experimental Theory

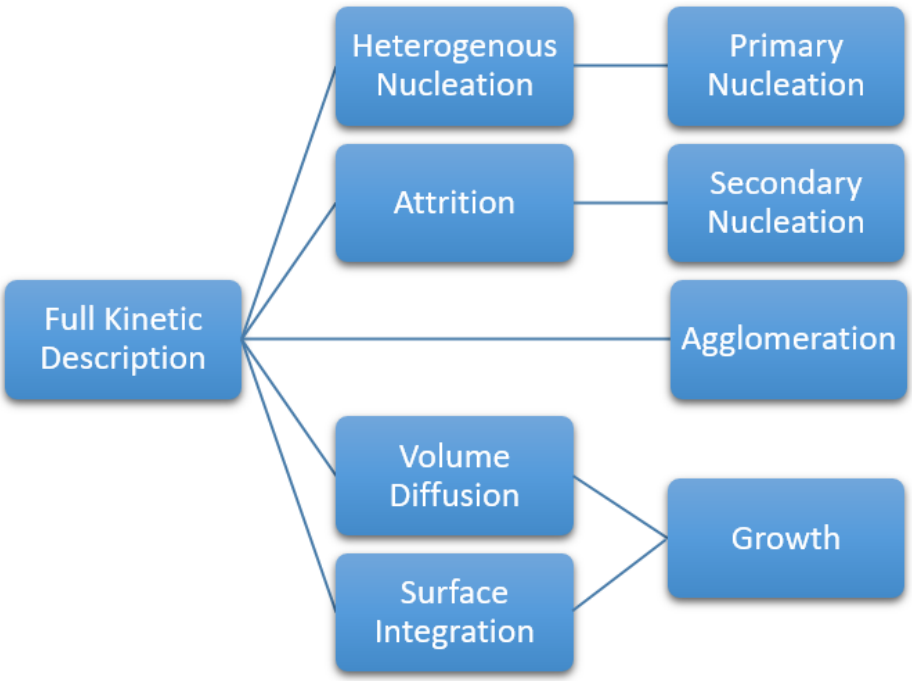

Figure 3-4 – Schematic depicting the building of a mechanistic model by individually assessing the different crystallisation mechanisms and collating them to build a full kinetic description of the process in question.

The crystallisation process can be split into individual mechanisms that when combined describe the overall process as can be seen in Figure 3-4. A mechanistic model of the process

gives a particular insight into how the different parameters interact relative to each other and with respect to process conditions. As the different parameters are often competing within the system it is important to try to only evaluate one parameter at a time by manipulating the process conditions. As different parameters are estimated and defined, their influence in later experiments can be accounted for to isolate the effects of the later studied parameters. Following the research described by Pérez-Calvo, Kadam and Kramer, five parameters of crystallisation are to be assessed within these experiments[30]. These parameters have been highlighted in Table 2.

Parameter	Experiment	Manipulation
Volume Diffusion	Isothermal dissolution	• Intermediate T
Surface Integration	Isothermal seeded desupersaturation	• Reduce seed size • Min RPM
Attrition	Isothermal seeded desupersaturation	• Increase seed size • Decrease seed mass • Max RPM
Agglomeration	Isothermal seeded desupersaturation	• Broaden seed PSD
Primary Nucleation	Induction time	• Min RPM

Table 2 - Summary of the individual crystallisation mechanism being investigated and the method of isolating the mechanisms for individual assessment.

Within this work, two-step growth kinetics are assumed, as such, volume diffusion and surface integration have been included in Table 2. The volume diffusion experiments have been carried out under isothermal dissolution conditions. This step is studied by assuming volume diffusion is the limiting factor affecting dissolution. From this assumption, volume diffusion is assessed experimentally by considering it as the inverse of growth, where surface integration is considered negligible.

Surface integration is the second step of growth and considers the uptake of solute molecules within the crystal structure itself following diffusion from the bulk fluid. The investigation of surface integration parameters is assessed by isothermal seeded desupersaturation experiments. To maximize growth kinetics within the system as well as minimise secondary nucleation due to attrition, the stirrer rate was kept low. The seed size was also reduced to reduce attrition with respect to collisions between the seeds and the impeller.

Following the characterisation of both growth terms, the attrition effects can be assessed, again via isothermal desupersaturation experiments. Secondary nucleation is assumed to only occur due to attrition from crystal-blade collisions. As such, attrition and therefore secondary nucleation is made dominant by increasing the stirring rate and seed size to increase collisions between the blade and the seed crystals. The increase of the stirring rate also reduces agglomeration efficiency and therefore reduces the presence of agglomeration. In order to limit the effects of growth on these experiments, the area for growth is decreased by not only increasing the size of the crystals but also reducing the amount of added seed.

The final set of isothermal desupersaturation experiments is used for assessing the effects of agglomeration on the crystallisation process. As growth and attrition have been fully characterized their effect on the final PSD can be predicted and as such the deviations from the predictions will allow the differences to be accounted for based on agglomeration. To improve the data obtained for assessing agglomeration within this system further experiments will be performed which use seeds with a broader CSD as agglomeration efficiency was found to improve with seed material made up of varied sizes.

Finally, primary nucleation is to be assessed by the use of induction time experiments across different supersaturation ratios. It is of course key to limit the presence of attrition and

therefore secondary nucleation effects. As such, the stirring rate was minimized. Concentration and temperature were varied to assess the full working range of this study.

3.4.2.2 Experimental Method

The ALM used for bulk material was purchased from Sigma-Aldrich, UK. The seeding material for these experiments was recrystallised from this material except for the 5 µm seeds (PSD shown in Figure 3-9) as these were purchased directly from DFE Pharma. Finally, all water used in these experiments was deionised and laboratory-grade.

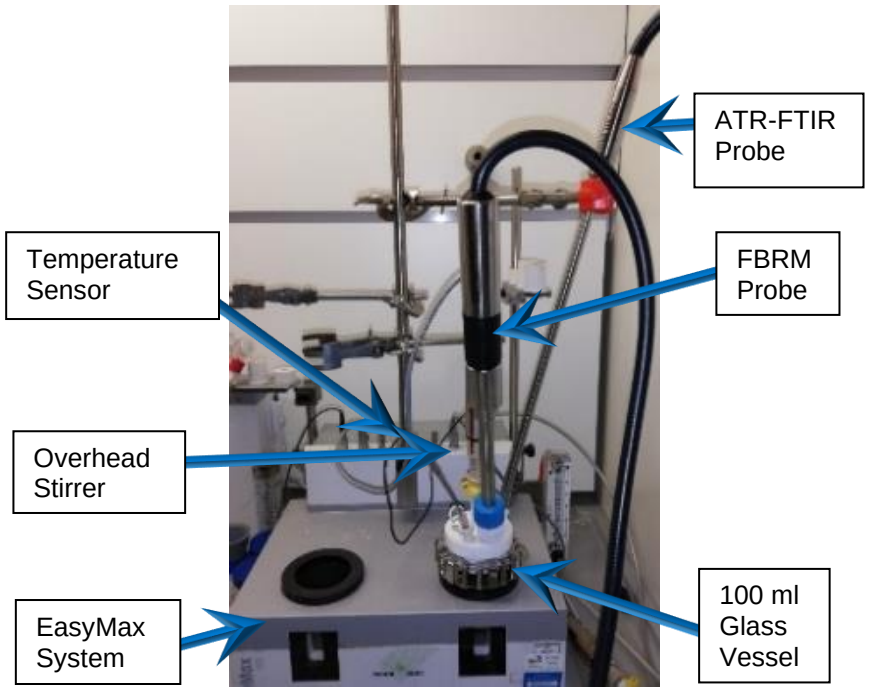

Figure 3-5 – Experimental set-up used for the determination of the crystallisation mechanisms.

The experimental set up used for parameter estimation experiments is shown in Figure 3-5. A chosen mass of ALM was weighed out and supplied to a corresponding mass of water within the 100 ml EasyMax vessel to achieve precise concentrations. The vessel and its contents were then heated to a temperature of at least 5°C above that of the saturation temperature for this concentration. The contents were then held at this temperature for an

hour to ensure complete dissolution. At this stage, the system was seeded in a manner specific to the mechanism of interest.

3.4.2.2.1 Seeding - Isothermal Dissolution Experiment

For the study of the kinetics of volume diffusion, the following seeding method was used. The vessel was cooled to a temperature that would induce a supersaturation ratio of 0.9. At this stage, 2.5g of seed was added that would just saturate the solution in the vessel.

3.4.2.2.2 Seeding - Isothermal Deseeded Supersaturation Experiments

For the experiments investigating surface integration, attrition and agglomeration, the following seeding method was used. The temperature of the solution was dropped in order to attain the chosen supersaturation ratio of interest as stated in Table 3. At this stage, the seed was added to the vessel via a syringe with the use of a room-temperature saturated solution of lactose and water as the carrier fluid. The system was then held at this temperature for a minimum of five hours to allow time for the mechanism being investigated to have a significant effect on the system and particle size.

3.4.2.2.3 Experimental Analysis

The experiments were monitored in situ with two process analytical tool (PAT) probes: FTIR (ReactIR, Mettler Toledo) and FBRM (G400, Mettler Toledo.) The FTIR probe allowed for continual concentration monitoring of lactose in solution while the FBRM probe was used as a way of monitoring the presence of particles throughout the process. The monitoring of particle count is important to ensure complete dissolution prior to seeding as well as to assess the presence of nucleation. The particles produced and recovered experimentally

were analysed using a laser diffractometer (Mastersizer 3000, Malvern Instruments) for size analysis as well as X-ray powder diffraction (XRPD) to assess form.

3.4.2.2.4 Process Conditions

Exp.	Concentration (mass %)	Saturated Temperature (°C)	Seeding Temperature (°C)	Seed Mass (g)	Supersaturation Ratio
(a)	35.13	60	50.17	0.89	1.2
(b)	35.13	60	42.48	1.44	1.4
(c)	29.18	50	40.95	0.69	1.2
(d)	29.18	50	33.75	1.12	1.4
(e)	23.84	40	24.76	0.87	1.4

Table 3 - Experimental plan used to assess growth rate. Mass % in this case is defined as the mass of lactose in solution as opposed to ALM. Across these experiments, the stirring rate was held constant at 400 RPM.

3.4.3 Modelling Experiments

3.4.3.1 Parameter Estimation

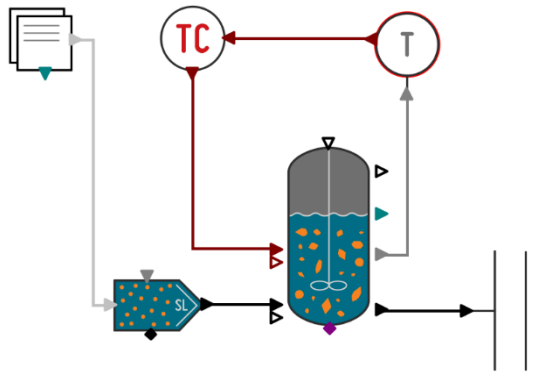

Figure 3-6 - Depiction of flowsheet within gFP used for the parameter estimation of the unknown variables concerning growth as well as the flowsheet used for simulation.

Within gFP, a number of flowsheets representing the performed experiments were created (Figure 3-6). These flowsheets are individually made to match the process conditions of each experiment. With the complete set of experiments represented within gFP and the

concentration profiles input, parameter estimation of the unknown growth constants can be assessed. As stated previously, the chosen growth model is a two-step kinetic Mersmann model and the constants being assessed are growth rate constant, supersaturation order and effective diffusivity. Additionally, the discretisation of the grid for this work is specified as 0.1µm to 1000µm using a logarithmic scale with 50 grid points.

3.4.3.1.1 Modelling Amendments

This model has the capability to predict the α and β-lactose equilibrium for changes in process conditions based on previously determined mutarotation kinetics [64]. This allowed the experimental conditions including timings to be input to achieve accurate predictions of the α and β equilibrium that would be representative of the true concentrations at specific times experimentally. Additionally, the size of the seed particles was specified by the laser diffraction bins obtained experimentally. The seed size was constant for all the surface integration experiments.

3.4.4 Goodness of Fit Test

The ability of the model to accurately predict the measured data is assessed via a goodness of fit test. Within this test, the predictions and the measured values are compared via the weighted residual and the expected weighted residual[73]. The expectation for a perfect model would be the difference between these two values to be zero and this describes the null hypothesis of this test. χ^2 and $\chi^2_{critical}$ are used to describe whether this null hypothesis has been met. If the χ^2 value is found to be less than the critical value it can be defined as statistically insignificant and therefore the goodness of fit test can be considered passed[73].

3.4.5 Global Systems Analysis

Global system analysis was used to investigate the process output's sensitivity to the variation of the input process conditions as well as the variance from the fitted kinetic parameters. The variance of the fitted kinetic parameters was investigated in relation to their effects on the crystal mass recovery and particle size. Pseudo-random sampling allows values for the fitted kinetic parameters within the given variance bounds to be simulated and the resulting process outputs values compared. This analysis allows the uncertainty of the model developed to be assessed in regard to the resulting variation in process endpoints.

Alternatively, this analysis allows the process conditions to be varied to allow for an awareness of the potential attainments capable of the tested system. This allows for insight into process conditions with the most significant influence on the process outputs. This insight can then be used to focus the optimisation of the process. The temperature and concentration of both anomers have been linked corresponding to the equilibrium at the given temperature.

3.4.6 Optimisation

The optimisation of the cooling crystallisation process within this work has been investigated for a number of chosen objective functions. An approach to optimising a variety of crystallisation platforms has been described in detail by Vetter et al[74]. This paper describes a method to utilise optimisation functions to discover and define attainable regions for given process outputs such as particle size via manipulation of process conditions within acceptable ranges. This form of optimisation is set up to allow for variation of specified process conditions within given ranges with the aim of optimising a chosen process output. The process conditions chosen for the purpose of optimisation are decided from the results of the global systems analysis of the variation of the process conditions. The optimisation of the process is also limited by specified constraints selected due to the physical and practical

considerations of running the proposed optimised pathway. This work has utilised inequality endpoint constraints to focus the optimisation within workable regions. For instance, selecting an endpoint constraint of a yield of greater than 70 % will guide the optimisation to not accept any found maxima below this constraint.

3.5 Results

3.5.1 Concentration Calibration Model

Preliminary attempts at building the calibration models for the lactose system were trialled with the use of PLS regression using both the MATLAB plsregress function (version R2020a) and the EigenVector PLS_Toolbox (version 8.9.1 [75]) capabilities. The initial findings from this work were that at moments where there were shifts in the mutarotation equilibrium, such as temperature changes, the calibration model would perform poorly. This is in agreement with the work by Schiele et al discussed previously[72]. As such, polynomial relationships were used to describe the system for subsequent analyses.

Due to the issues with temperature seen using the PLS and PCR calibration models for concentration prediction, the use of temperature as an input variable for the prediction of concentration was investigated. This links the temperature and peak height at any given time to the resulting concentration. The calibration data is used to assign the variables of the polynomial. Ultimately, a defined polynomial equation can then be used to predict concentration from temperature and peak height.

Prior to building the calibration model, an appropriate wavelength to assess concentration with minimal temperature effects must be assigned. Additionally, a corresponding wavelength is needed to be used for the baseline correction. The spectra from the calibration set were assessed to gauge wavelengths that show minimal variation with changing

temperatures. Pairs of these points were assessed to gauge the best baseline and peak combination to improve the prediction of concentration for the calibration models independently.

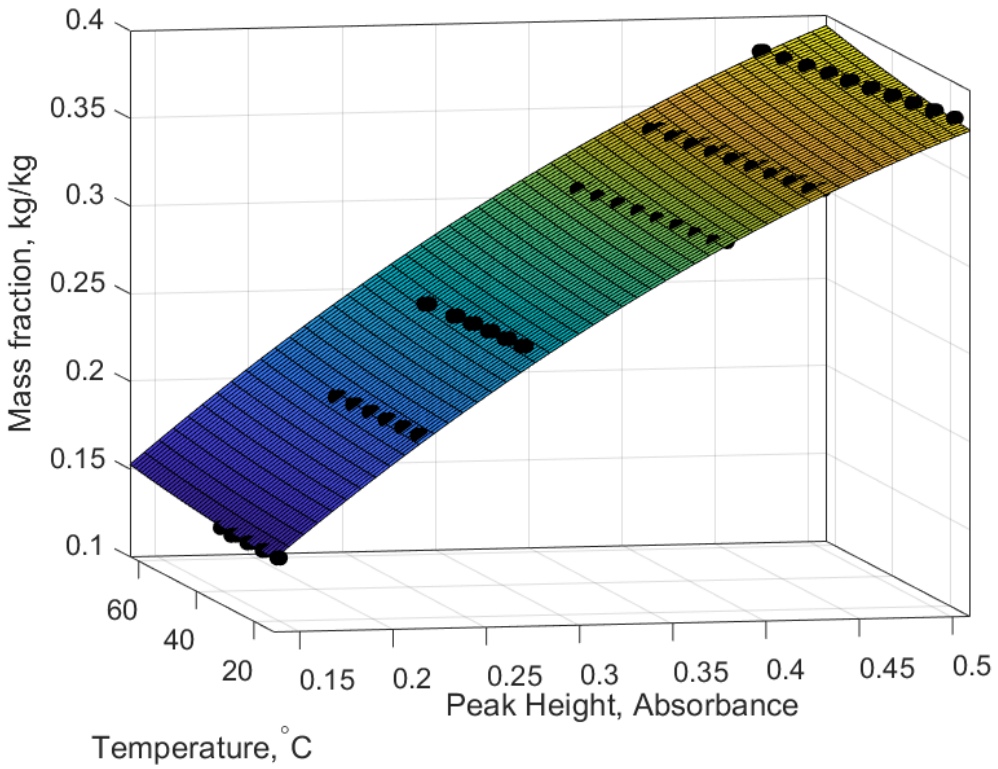

Figure 3-7 - Surface depicting the polynomial calibration relationship between peak height, temperature and concentration in $kg_{solute}/kg_{solution}$. The peak height at 1018.1cm^{-1} with respect to the baseline at 1141.1 cm^{-1} was used for the monitoring of the concentration. Black data points show the collected data from experimental calibration work.

The fitting of the polynomial equation describing the relationship between the peak height, H and temperature, T, for the cooling crystallisation work began by finding the optimal peak and baseline paring. Pairings between 950 and 1200 cm^{-1} were investigated, and the optimal pairing was found to be 1018.1 cm^{-1} and 1141.1 cm^{-1}. The surface polynomial was defined as shown in Equation 20. The fitted polynomial was then tested against two validation experiments that covered a range of two intermediate concentrations with varying

temperatures. It should be noted that the peak height has a much stronger relationship to concentration than that of temperature but from the work described by Schiele et al the incorporation of both variables is found to produce a robust calibration model[72].

Equation 20

$$C(H,T) = 0.303 + 0.0710H + 3.34 \times 10^{-3}T - 8.65 \times 10^{-3}H^2 + 4.94 \times 10^{-4}H + 3.89 \times 10T^2$$

The fitted polynomial's ability to describe the concentration from the measured variables is displayed in Table 4 in the form of a high R^2 value of 0.9983 and low RMSE values. The RMSE values for the calibration data and the validation data show the high accuracy that the developed calibration model is capable of. As such, the accuracy of the calibration model was deemed acceptable for use for concentration predictions for all future cooling lactose concentration crystallisation experiments.

Model	R^2	RMSE (kg/kg)	RMSE (val) (kg/kg)
Cooling/lactose	0.9983	0.0031	0.0036

Table 4 - Cooling lactose calibration model results.

3.5.2 Parameter Estimation Experiments

3.5.2.1 Nucleation Investigation

Induction time experiments were performed at the highest concentration of interest, 35.13 wt%, and the temperature was set to investigate the supersaturation ratios of 1.2 and 1.4. The induction time experiments were found for a supersaturation ratio of 1.2 to be greater than 100 hours. The exceedingly slow induction time was considered not industrially relevant especially when coupled with the fact that lactose is typically crystallised in seeded conditions[76]. As such, the need to model the primary nucleation of lactose within this cooling system was unnecessary.

Similarly, secondary nucleation was also investigated for this system using isothermal seeded desupersaturation experiments using a larger seed size with a D50 of 119 µm to increase the number of crystal-impeller collisions and aid attrition. This was tested at the highest concentration and supersaturation ratio investigated as part of the surface integration experiments as seen in Table 3. Under these conditions, with an increased stirring rate of 900 rpm, the recorded particle count was shown to hold steady and no signs of nucleation were observed. This was found to be in line with literature where a threshold of supersaturation ratio of 1.6 has been stated [77][67]. This is out of the stated working range for this work and therefore secondary nucleation is not found to be present in this system and will not be considered further for modelling purposes.

3.5.2.2 Growth Kinetics

The different models of growth within gFP were assessed to gauge which model provided the best fit for the growth data set being investigated. The growth rate can be described in terms of absolute or relative supersaturation following the combination of Equation 3 and Equation 6. The parameters being assessed with regard to the growth models in question are activation energy, growth constant, effective diffusivity correction factor and supersaturation order. The effective diffusivity correction factor, α, is only considered when estimating parameters within either of the two-step kinetic models via Equation 5 and was fitted from the volume diffusion experiment.

The importance of temperature to the growth of lactose crystals has been described by Wong and Hartel [76]. The effect of temperature has been highlighted in terms of the physical properties of the system as opposed to the growth kinetics of the system. This work highlighted the effect of temperature on the viscosity of the system and the adverse effect this may have on the mass transfer aspects of growth as well as the previously highlighted

impacts of mutarotation. Both of these temperature effects have been accounted for within the basic model equations depicting the state of the system. The other key aspects highlighted within the relationship between temperature and growth rate include consideration of the translation mobility of lactose and the presence of crystal surface distortions. As the literature does not highlight the importance of temperature dependence with respect to the activation energy, the parameter was initially set to zero within Equation 3 for this work.

3.5.2.2.1 Concentration Profile Comparisons

Kinetic Variable	Fitted Value	St. Dev.
$E_{a,g}$ (J/mol)	57329.6	2939.51
k_g (m/s)	19.52	22.41
S^o (-)	1.095	0.106

Table 5 - Fitted kinetic values and the corresponding standard deviation for the developed growth and agglomeration model.

Upon analysing the predicted concentration profiles produced from initial parameter estimation runs two key findings were apparent. Firstly, following a volume diffusion experiment as outlined in section 3.4.2.2.1, the system was found to be surface integration limited with a fitted effective diffusivity value below 0.005. The negligible nature of the volume diffusion step in the case of lactose crystallisation is discussed in the literature and agrees with the preliminary findings here[60][56][57]. Additionally, the initial fitting of the growth kinetics parameters showed a clear dependence for temperature across the tested experiments. Therefore, the growth model was investigated in terms of a power law with activation energy as a considered variable to allow for the temperature effect on growth rate to be incorporated.

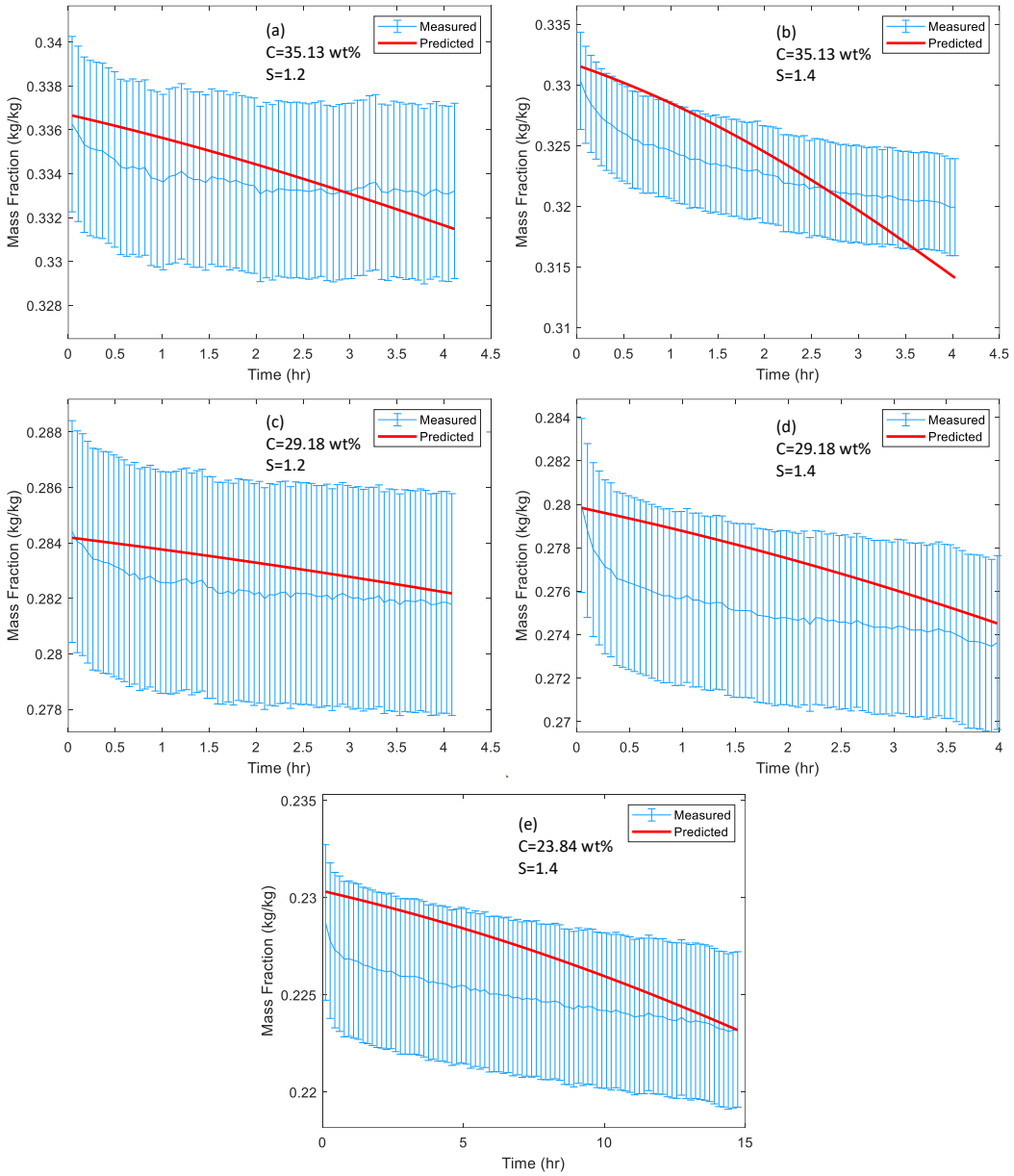

Figure 3-8 - Comparison of the experimental concentration profiles and the predictions from the mechanistic model. Individual plots labelled as per Table 3. The goodness of fit test for this model showed an adequate fit with a χ^2 value lower than the calculated critical value with values of 200.95 and 414.8 respectively.

The fitted kinetic parameters are displayed in Table 5. Figure 3-8 shows the comparisons between the model predicted and the true concentration profiles. The predictions generally fit well within the error bars of the experimental data except for plot (b). However, the model predictions for the higher supersaturation ratio experiments follow a different trend than the

experimental results. The experimental results show an exponential decay with respect to concentration and time which is to be expected following the crystallisation of solute material out from the solution. However, the predicted results follow a very gentle right-hand side bell curve which is particularly clear from plot b. The presence of this suggests an inaccuracy of the model being built. To assess the potential causes for this inaccuracy a look into the PSD predictions is needed. This suggests more work is needed to improve the model going forward.

The slight difference in the slopes of the predicted and experimental trends is minimal within the time frame of these experiments with a maximum range of around 1 wt%. However, as the trends are moving away from each other at the end of the experiment it is important to note that these errors increase over time and could lead to significant errors for longer growth experiments. Secondly, it is also important to notice that the predicted trends follow a more linear trend than the exponential decay seen in all the experiments to different degrees. These differing trends also fall within the error bars of the prediction under the time restraint of these experiments but may lead to errors over the course of longer experiments.

3.5.2.2.2 Particle size analysis

Experiment	(a)	(b)	(c)	(d)	(e)	seed
D10 (µm)	4.01	4.67	1.96	2.18	1.8	1.48
D50 (µm)	12	12.3	8.08	8.7	7.62	4.54
D90 (µm)	23.5	23	16.7	17.2	14.6	9.41

Table 6 – Summary table of the particle sizing based upon the experimentally obtained laser diffraction results following the use of ultrasound (US). Measurements for recovered experimental material are labelled as outlined in Table 3.

A final step to corroborate the growth model is the comparison between particle size prediction and the true PSD obtained via laser diffraction. As previously stated, the size of the seed used is 5 µm.

Focusing on the experimentally recovered results displayed within Figure 3-9 and Table 6, the effects of growth can be seen across the tested conditions. Overall, the measured growth of crystal size displayed is small but considering the mass and number of crystals input to the system as seeds the growth experienced is relatively substantial. With a few exceptions where supersaturation has affected the crystal size recovered, Figure 3-9 shows a trend of greater concentration and temperature producing larger particles. The relationship between increasing concentration and subsequently increasing PSD is well understood as there is more material available for incorporation within the seed particles. The effect of an increasing temperature could also be linked to the increase in recovered particle size directly by the increase of growth rate through the exponential term within Equation 3.

Across all the recovered PSD distributions there is the presence of a second minor peak consistent with the presence of fines. No significant change in particle count was seen from the FBRM results and therefore no nucleation is thought to have taken place. There is also the consideration of the presence of fines in the seeding material as can be seen from the laser diffraction results of the seed material. This could alter the growth rate of the material as there is a substantial increase in the surface area considering the smaller particle sizes. Again, this is something that needs more investigation, especially upon analysing the current prediction capabilities of this model for particle size.

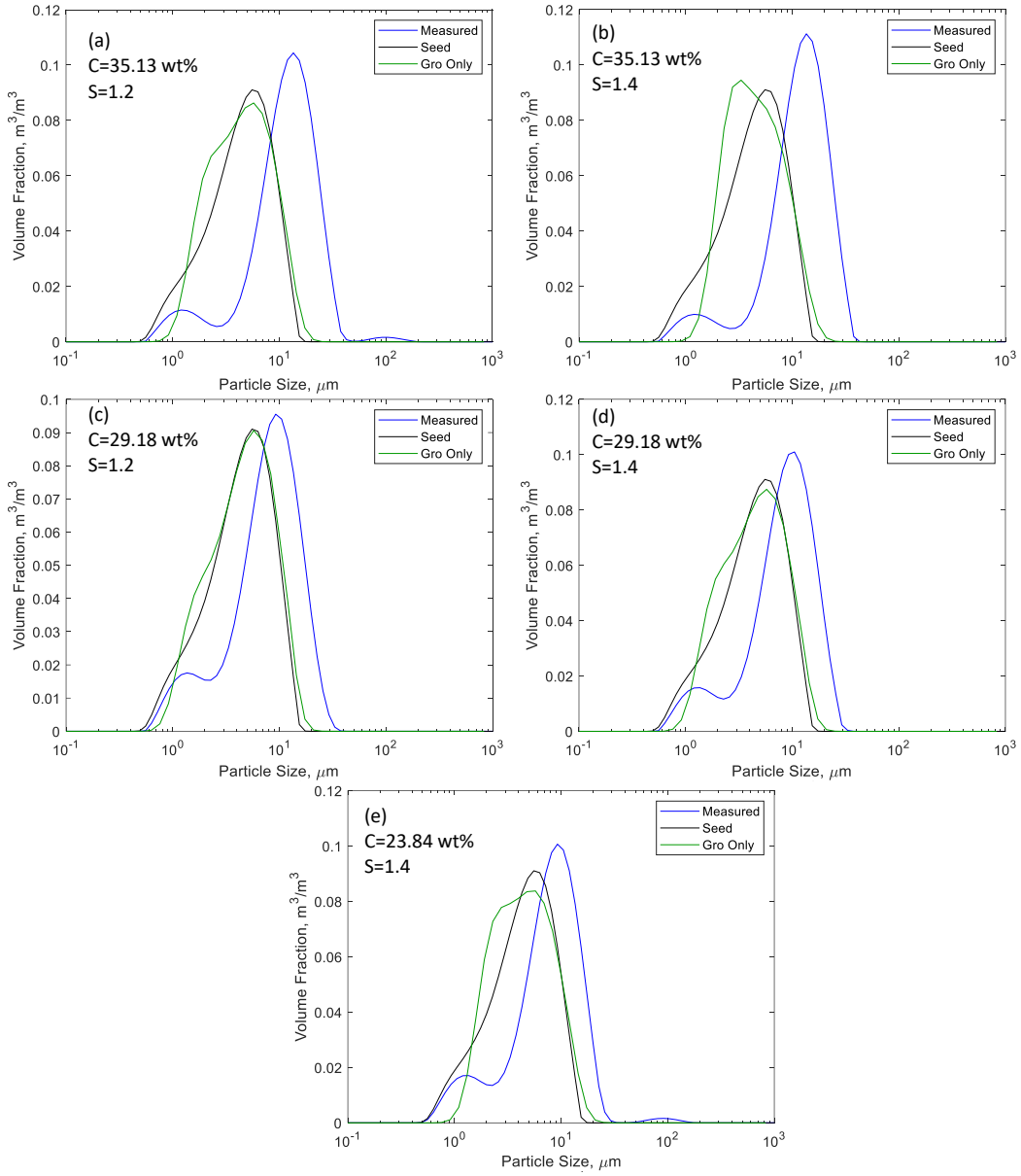

Figure 3-9 – Laser diffraction size analysis results depicting the comparison of recovered experimental material and seeding material as well as the resulting predictions from the current growth-only mechanistic model within gFP. Black – seed material, Blue – experimental recovery, Green – PSD model predictions. Plots labelled as per Table 3.

Comparing the results displayed in Figure 3-9 and Table 6 for experiments (a) and (b) as well as (c) and (d) allows the effect of supersaturation on growth rate to be analysed. The comparison of these PSD plots shows supersaturation to have a minimal effect on particle size. However, the size quantiles displayed in Table 6 shows that increased supersaturation

levels do have positive effect on the PSD of the recovered material. This increase in particle size can be explained due to the increased driving force of the growth mechanism under larger supersaturation ratios.

The predictions are considerably underestimating the size of crystals produced under the specified experimental conditions. When comparing the predicted crystal sizes and the seed material there seems to be a narrowing of the distribution and some removal of the tail discussed previously. This suggests the tail of the left-hand side of the seed distribution is experiencing stronger growth effects than the larger particles. This could be due to the larger surface area of these particles being more susceptible to growth than their larger counterparts. This however is not in agreement with the measured PSD and as such the growth model is inadequately representing the growth processes occurring experimentally.

The reduced growth seen could be linked to the slight differences within the concentration profiles discussed previously. The deviation of particle size prediction within the model from the true PSD is an important issue that could have knock-on effects within the simulation. As the model currently stands there is a need for further development to mitigate the errors producing the unfavourable concentration profile and PSD predictions.

Due to the consistent under-prediction of particle size by the current growth-only model, it was decided to perform SEM on the recovered samples. This analysis provided more information about the produced particulate material. As can be seen in Figure 3-10 the material from the growth experiments is heavily agglomerated across all tested conditions. Agglomeration was not considered during the initial population balance modelling of these experiments however provides a likely explanation for the consistent under-sizing by the

current growth-only model. As a consequence, the inclusion of the agglomeration kernel within gFP to model this set of experiments was decided.

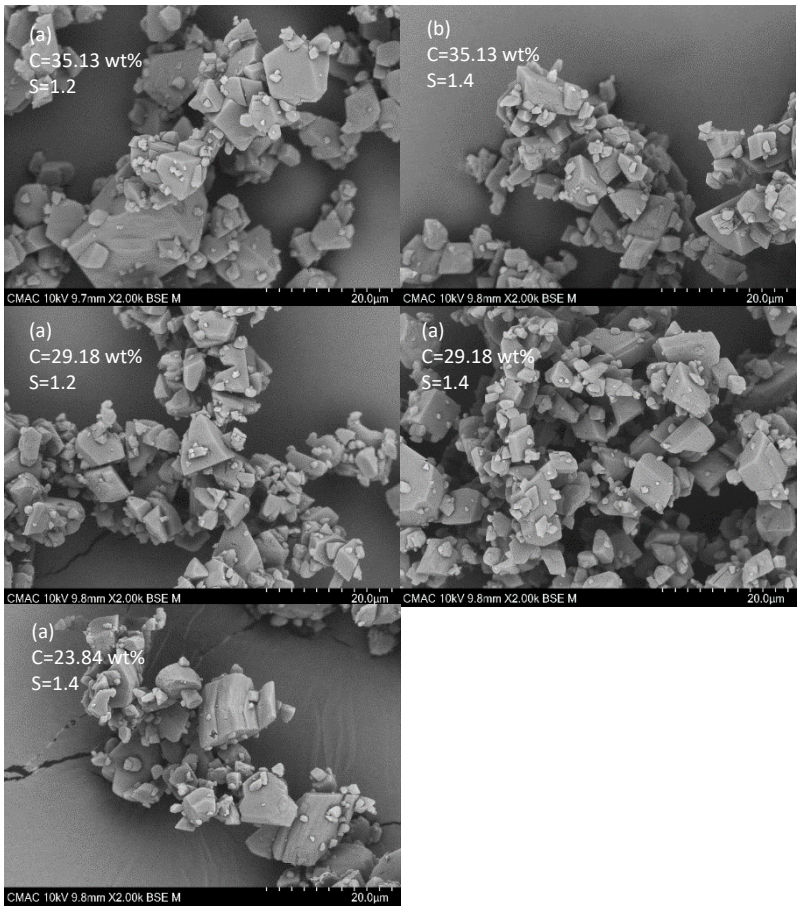

Figure 3-10 Scanning electron microscope (SEM) images of the recovered material from growth investigation experiments. Plots labelled as per Table 3.

Kinetic Variable	Fitted Value	St. Dev.
$E_{a,g}$ (J/mol)	55718.1	2783.7
k_g (m/s)	24.77	27.37
S^o (-)	1.186	0.107
A_{50} (N/m)	0.00187	1.34E-4

Table 7 - Fitted kinetic values and the corresponding standard deviation for the developed growth and agglomeration model.

3.5.2.3 Agglomeration Kinetics

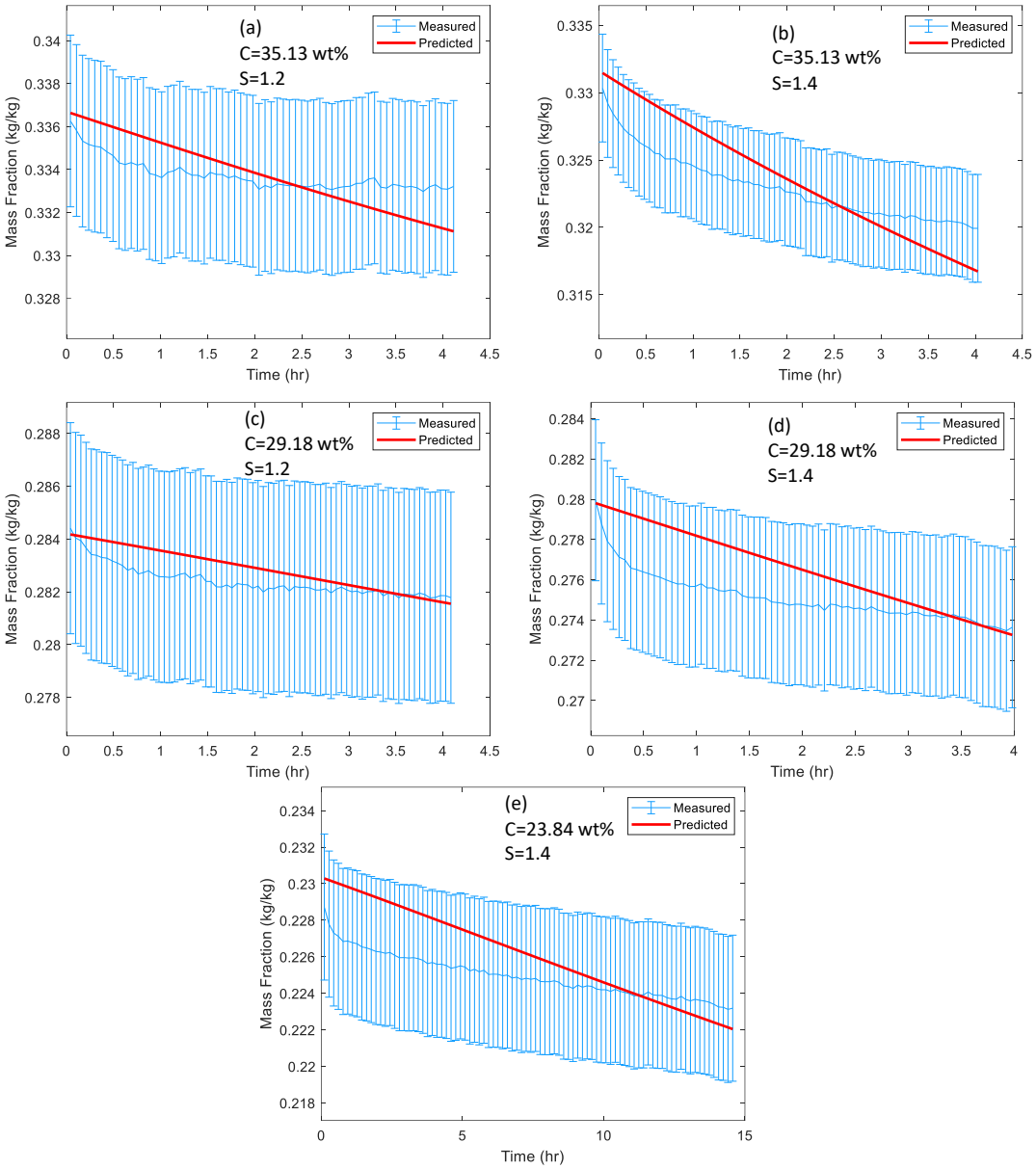

Figure 3-11 - Comparison of the experimental concentration profiles and the predictions from the growth and agglomeration mechanistic model. Individual plots labelled as per Table 3. The goodness of fit results also suggests an acceptable model with overall values of 258.4 and 448.7 for χ^2 and $\chi^2_{critical}$, respectively. More comparably, the concentration-based goodness of fit test resulted in χ^2 value of 106.2 compared to a $\chi^2_{critical}$ value of 413.7.

Estimation of the Mumtaz number has been computed using the following final particle size quantiles: D10, D50 and D90. The constant variance model for D10 and D90 were set to 3µm and D50 only 1µm to allow for focussed fitting of the D50 dataset. The growth kinetics were

initially fixed as per the fitting of the growth-only model. The growth parameters were then subsequently fitted alongside the A_{50} to allow for improved fitting of the experimental data.

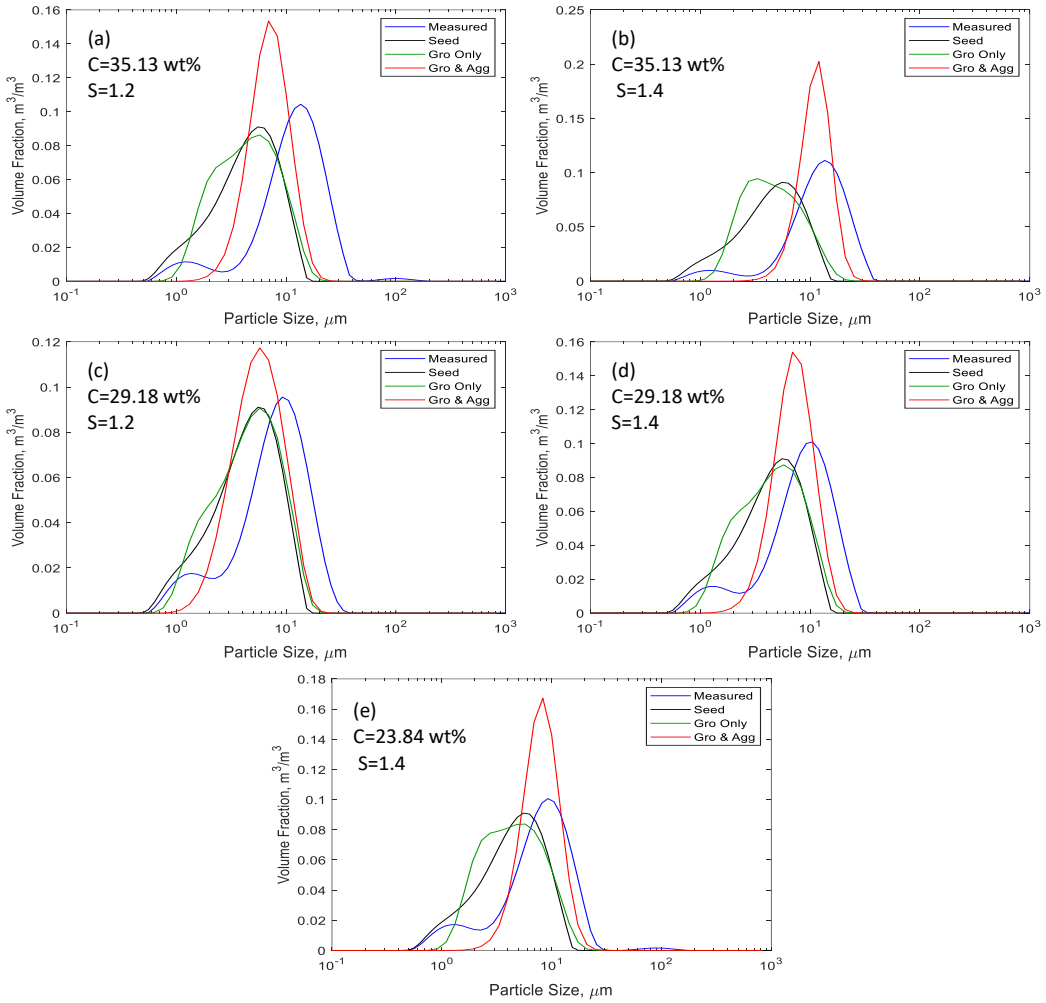

Figure 3-12 Laser diffraction size analysis results depicting the comparison of recovered material and seeding material as well as the resulting predictions from the developed model. Plots labelled as per Table 3.

The current growth-only model built from the growth experiments has been built solely by fitting concentration profiles while estimating only the unknown growth parameters. As such, the growth parameters have been fitted assuming growth upon the supplied seed PSD. With agglomeration now confirmed to be present within this crystallisation system, the sizes modelled during the fitting of the growth terms will have been continually under-predicted.

The expected change in concentration during an isothermal seeded desupersaturation experiment would be minimal as the amount of solute needed to bridge the agglomerated particles is negligible. However, the increase in particle size due to agglomeration through time subsequently results in a reduction in the surface area available for growth to take place. This reduction in surface area consequently results in a smaller rate of change in concentration. Therefore, it was necessary to refit the growth kinetics following the inclusion of agglomeration. The prediction of concentration profiles and PSD can be seen in Figure 3-11 and Figure 3-12 respectively.

The concentration profile predictions have shown a slight improvement upon the predictions from the growth-only model. The presence of the RHS bell curve trends has been removed. However, the trends are still linear as opposed to the exponential decay shown by the experimental results. Overall, the inclusion of the agglomeration term has improved the model's capability to simulate the experiments more accurately. The goodness of fit test, performed as part of the parameter estimation, showed an acceptable fit with χ^2 value lower than $\chi^2_{critical}$. χ^2 values of 258.4 and 200.9 for the growth-agglomeration model and previously discussed growth-only model suggest minimal improvement. However, a direct comparison of the concentration-based statistics of the growth-agglomeration model and the growth-only model shows the model's improved ability to predict concentration for these experiments by a significantly smaller χ^2 value of 106.2 compared to 200.9. This suggests the prediction capability of the PSD from the growth-agglomeration model could be a source of error.

The agglomeration kernel was fit using quantile sizes D10, D50 and D90. This was shown to produce reasonably accurate D50 predictions, but the tail seen in the measured PSD was lost during the simulated experiments. As such, additional quantiles were added to try to improve

the prediction of the overall shape as opposed to the individual quantiles. The seed PSD was also input as a full PSD direct from the laser diffraction analysis to improve the representation of the system and its prediction capability. As can be seen in Figure 3-12, the tail of the seed is lost during the simulated crystallisation process, unlike the true experiments. The tail however is overly dominant in the growth-only model's predictions. As such, the growth and agglomeration model's poor fit of the tail of the PSD is noted as a limitation for the model going forward.

3.6 Global Systems Analysis

3.6.1 Uncertainty Analysis - Fitted Parameters

The acceptability of the fitted parameters is tested using the global systems analysis entity within gFP. In the case of this model, the covariance of the fitted parameters is inputted in terms of a multivariance model utilising the statistical outputs from the parameter estimation. The covariance calculated between the kinetic parameters is input as the bounds for the uncertainty analysis and tested across the two selected outputs of interest: average particle size, $D_{4,3}$ and crystal mass recovery.

The uncertainty in the fitting of the Mumtaz number was found to have no discernible effect on either crystal mass recovery or $D_{4,3}$. However, the fitted growth kinetics were found to have a prominent effect on the recorded outputs of the system as can be seen in Figure 3-13. The uncertainty for the growth rate constant is shown to have an adverse effect on the process outputs. The covariance relationship between the growth rate constant and activation energy is shown in Plot C and is limited by the positive confidence ellipsoid extremes produced from the model validation within gFP. The variation of the activation energy and growth rate constant are shown to have no direct relationship to average particle

size. The relationship between the growth rate constant and crystal mass recovery can be seen in Plot A. The maximal trend is shown around the fitted value of 24.77 m/s. However, the resulting crystal mass recovery values show a broad distribution. The broadness of the resulting crystal mass recoveries was shown to be directly linked to supersaturation order with lower values producing higher yield predictions. This trend is mirrored in the prediction of average particle size, $D_{4,3}$. The positive trend between particle size and yield is shown in Plot B to be directly linked with the supersaturation order. The probability of the variation of supersaturation order is itself rather low and was found to satisfy the t-test for the 95% confidence interval, unlike the growth rate constant. Suggesting that although the variance of the supersaturation order is shown to have the most effect on the process outputs of interest the fitted parameter is still considered to be fitted with statistical accuracy.

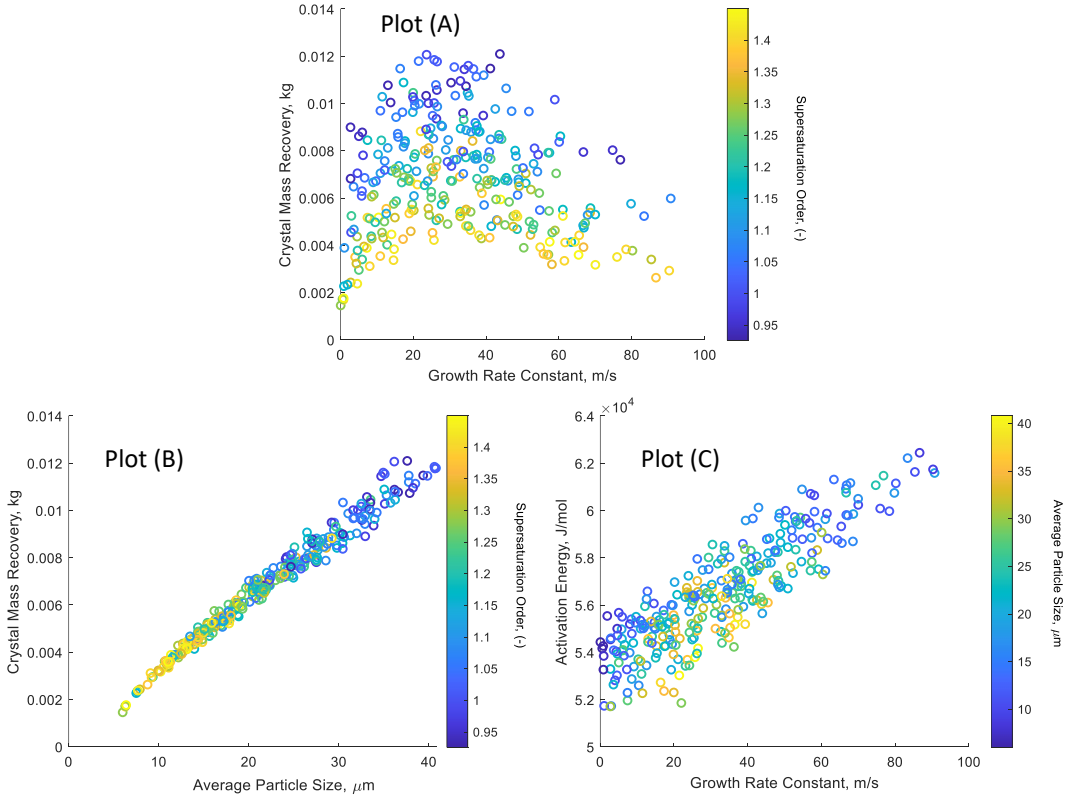

Figure 3-13 - Scatter plots depicting the uncertainty analysis and covariance of chosen fitted kinetic parameters of the developed model. Plot A and B vary by colour with increasing supersaturation from blue to yellow. Plot C varies with colour for increasing average particle size from blue to yellow.

3.6.2 Sensitivity Analysis - Process Conditions

The process conditions of interest, temperature, composition of solution and seed mass, are varied within this sensitivity analysis to investigate the importance of these conditions on the process outputs of interest. The concentration and temperature are input as a multivariate enumerated set to incorporate the mass fraction of all components coinciding with the mutarotation equilibrium at the given temperatures. The positive trend between increasing temperature and both the average particle size and crystal mass recovery can be seen in Figure 3-14 Plot A. The broadness of the plotted data is due to the nature of the enumerated dataset between temperature and concentration. The range produced for both particle size and crystal mass recovery are seen to be very large when varying the process conditions.

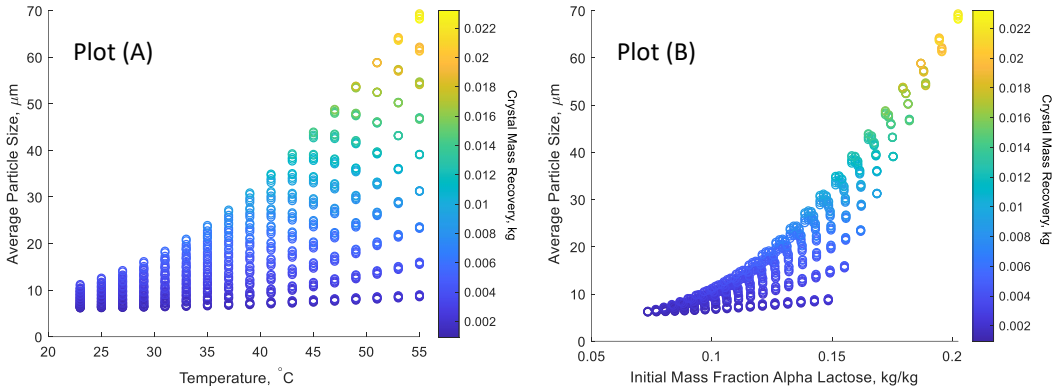

Figure 3-14 - Scatter plots depicting the uncertainty analysis of process outputs predicted upon the variation of the process conditions. Plot A and B vary by colour with increasing crystal mass recovery from blue to yellow.

Plot B shows the effect of increasing the concentration of alpha-lactose in the solution on the process outputs. Figure 3-14 shows the positive trend of both concentration and temperature with yield and average particle size. The increase in temperature would inherently increase the growth rate through Equation 3 and increasing the concentration supplies the system with more material to be crystallised out. Therefore, the increase in temperature or concentration subsequently leads to an increase in both yield and $D_{4,3}$.

Interestingly, there was no trend seen for increasing the mass of seed supplied to the system. An Increase in the mass of the seed would be expected to affect the system in two ways: increase crystal mass and reduce $D_{4,3}$. Firstly, the increase in crystal mass would be due to the increase in initial crystal mass within the system. Secondly, the $D_{4,3}$ will be reduced due to the mass of solute available for crystallisation being spread across more individual particulates resulting in a small extent of growth per particle.

3.7 Optimisation

The global systems analysis has allowed the investigation of the extremes possible for this system based upon manipulation of the process conditions. The outputs from Figure 3-15 act as the initial guide for the optimisation of the process in terms of; reducing batch time, increasing crystal mass recovery and particle size. The process being investigated here was specified as a controlled cooling profile with the key points of interest focusing upon initial temperature, cooling rate and batch time. As can be seen in Figure 3-15, slower and longer cooling paths lead to an increase in particle size and yield. This result is in itself quite intuitive in that a longer batch time with a more gradual cool will allow for more time for the growth of the seed particles. Additionally, Plot A and Plot C also show the effect of initial temperature on particle size and crystal mass recovery, respectively. These show a broad but slightly positive tendency of higher initial temperature relationship to both $D_{4,3}$ and crystal mass recovery. This result is likely due to the increased growth rate seen at higher temperatures. It is clear that cooling rate and batch time have a higher level of influence on process outputs than initial temperature.

Due to the findings from the attainment plots in Figure 3-15, the focus of the optimisation of a controlled cooling profile will be focused upon in the form of initial temperature, cooling

rates and simulation duration based on initial suggestions shown here. It was decided to include hold periods within the cooling profile to increase yield. These holds also allow the supersaturation levels reached within the system to remain below the secondary nucleation threshold corresponding to a ratio of 1.6, as discussed previously[77]. For simplicity, the system was limited to three hold periods; an initial hold following seeding, an intermediate hold and a final hold at the end. The duration of each section of the cooling pathway is open to optimisation as well as the initial temperature and the cooling rate for the cooling section.

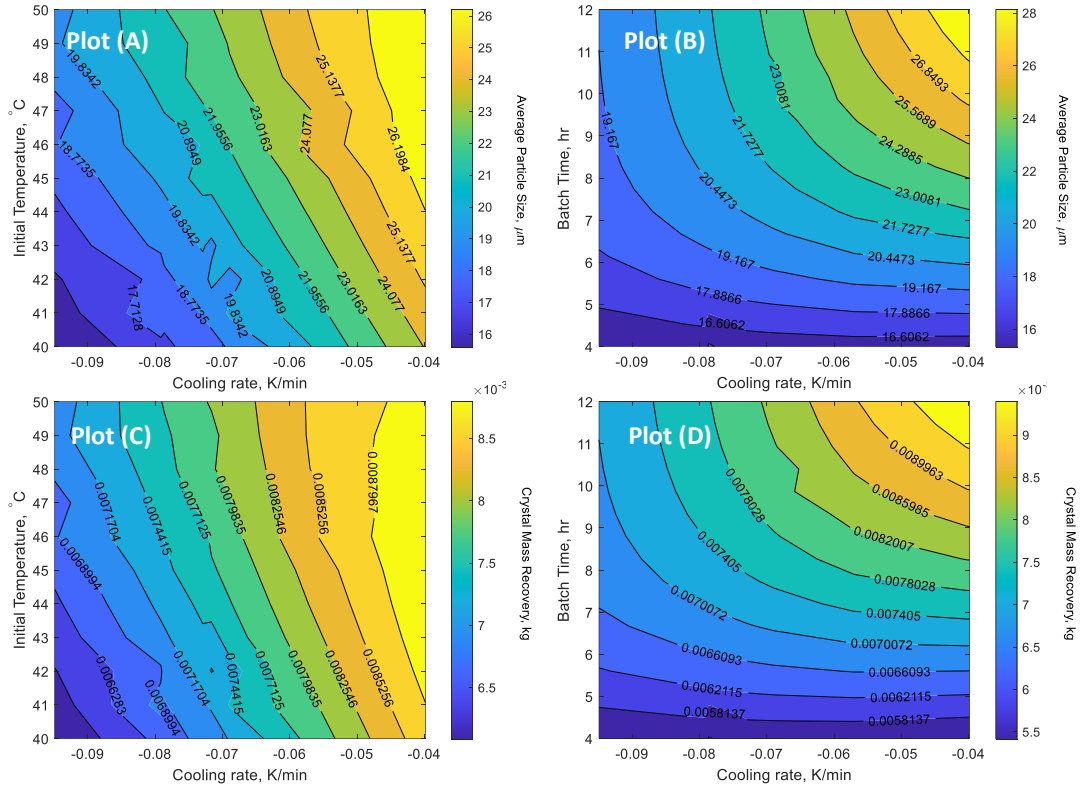

Figure 3-15 - Contour plots showing the effects of selected process conditions on the highlighted process outputs predicted from the developed model. Plot A and B vary by colour with increasing average particle size from blue to yellow. Plot C and D varies with colour for increasing crystal mass recovery from blue to yellow.

3.7.1 Optimising Crystal Mass Recovery

The initial objective for the optimisation was to increase the crystal mass recovered from the system. The optimised time intervals and cooling rates can be seen in Table 8. Additionally,

the outputs from the optimised process can be seen in Figure 3-16. The maximum crystal mass recovered experimentally was 6.58g including the seed mass. The optimised controlled cooling simulated process is predicted to produce 9.6g which is a substantial increase in recovery of over 45%. It should be noted that a controlled cooling experiment is expected to produce a higher yield than an isothermal experiment due to the lower final saturated concentration capable of being reached.

Variable	Final Value (s)	Cooling rate (K/min)	Initial Temperature (°C)
Time interval # 1	3600.0	0.000	40.00
Time interval # 2	15174.3	-0.0198	40.00
Time interval # 3	4660.5	0.000	35.00
Time interval # 4	14949.9	-0.0265	35.00
Time interval # 5	6615.3	0.000	28.39

Table 8 - Table displaying the optimised conditions for the maximising of the crystal mass recovery.

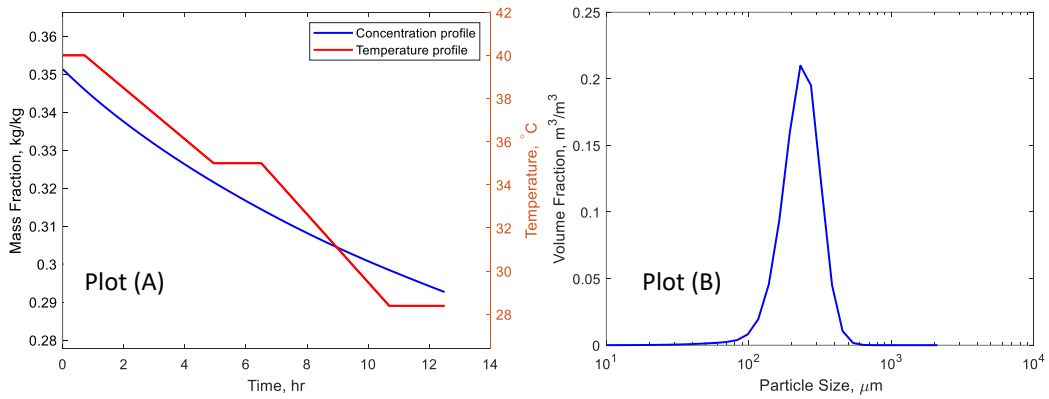

Figure 3-16 - Plots depicting the optimised cooling pathway alongside the resulting concentration profile and subsequent end PSD.

The optimised condition is predicted to produce larger particulates than the experimental results. It should be noted here that the particle size prediction of the resulting particles is a

known limitation of the model as seen by the predictions in Figure 3-12. More specifically, the measured PSD would be expected to be much broader and contain a small peak resulting from fines in the seeding material that is not captured in the narrow predicted PSD. As such, the confidence in the optimised process to produce material following the unimodal PSD shown in Figure 3-16 is rather low and is considered more of a guide than an expected outcome if this process was tested experimentally.

3.7.2 Optimising Average Particle Size

Variable	Final Value (s)	Cooling rate (K/min)	Temperature (°C)
Time interval # 1	3600	0.00	41.28
Time interval # 2	14511.3	-0.0129	41.28
Time interval # 3	7141.89	0	38.15
Time interval # 4	16146.8	-0.03	38.15
Time interval # 5	1800	0.00	30.00

Table 9- Table displaying the optimised conditions for the maximising of the average particle size.

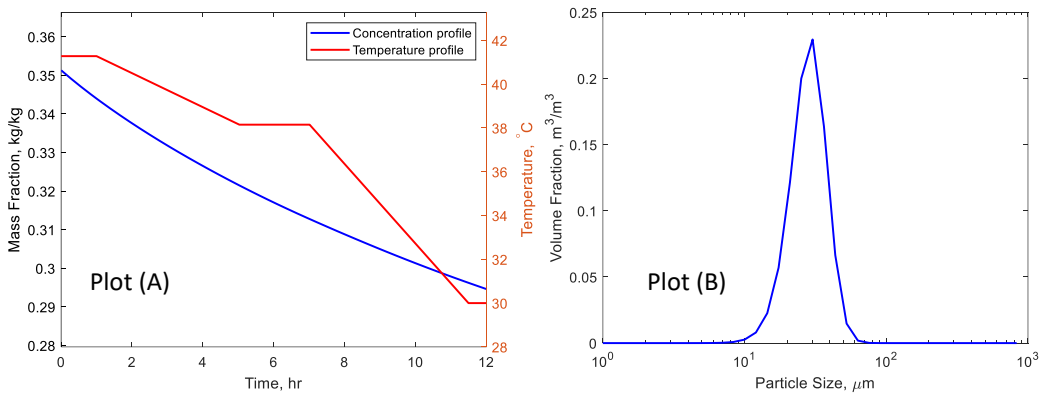

Figure 3-17 - Plots depicting the optimised cooling pathway alongside the resulting concentration profile and subsequent end PSD.

A secondary interest in optimising the cooling crystallisation of lactose is to increase the growth of the seed material as the growth across all conditions was very small as seen in

Table 6. Comparing Plot A of both Figure 3-16 and Figure 3-17, it is clear an initially slower cooling period is seen when optimising for particle size. This initial slower cooling period allows for the particles to grow in a period of higher growth rate due to the increased temperature. Additionally, the intermediate hold is at a higher temperature of 38.15 °C compared to 34.95 °C which again allows the particles more time to experience the increased growth rate from a higher temperature environment. Again, the particle size is a known limitation of the model and the practice of optimising for $D_{4,3}$ is viewed as a guide at this stage. Table 6 shows the particle size quantiles recovered experimentally with a maximum D50 of 12.3 µm which is an order of magnitude smaller than the predicted value for the optimised process. This highlights the potential for a large increase in particle size obtainable from the controlled cooling process compared to the isothermal experiments performed.

3.7.3 Optimising Batch Time

Variable	Final Value (s)	Cooling rate (K/min)	Initial Temperature (°C)
Time interval # 1	2430	0.00	41.46
Time interval # 2	22000	-0.012	41.46
Time interval # 3	7200	0.00	37.03
Time interval # 4	7000	-0.06	37.03
Time interval # 5	1800	0.00	30.00

Table 10 - Table displaying the optimised conditions for minimising the required batch time.

Following the optimisation of the possible particle sizes and crystal mass recovery of the system, an optimisation focusing on reducing batch time while producing similar process outputs was attempted. From Plot A in Figure 3-18, it can be seen that a similarly slow initial cooling period has been selected albeit to a lower intermediate temperature hold. As

discussed previously, this slower cooling allows for larger growth to be seen as well as a larger recovery of crystal mass. The subsequent sharper cooling stage suggests recovery at the lower temperatures has not been deemed efficient through the optimisation process. This preference for slightly higher final temperatures is consistent across all of the optimisations and also aligns with the findings of Visser et al., which show a lower recovery of lactose at lower temperatures due to the shift in the anomer equilibrium [68]. As can be seen from the data in Table 11, the optimisation of the batch time has produced a very comparable $D_{4,3}$ of 30.53 µm compared to 31.68 µm from the optimised process for particle size. It has also maintained a strong crystal mass recovery of 10.00g.

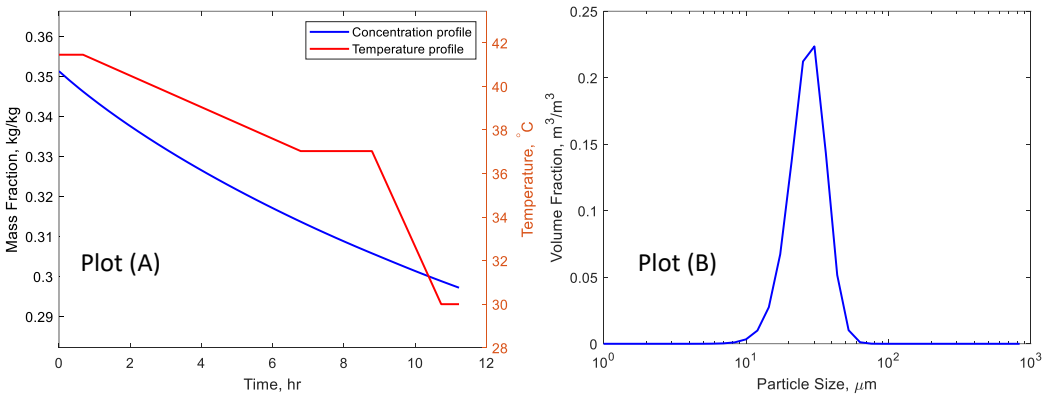

Figure 3-18 - Plots depicting the optimised cooling pathway alongside the resulting concentration profile and subsequent end PSD.

Batch time (hr)	Average Particle Size (µm)	Crystal Mass recovery (g)
11.23	30.53	10.00

Table 11 - Results from the optimisation of the process by means of minimising the batch time while maintaining the desired particle size and crystal mass recovery.

3.8 Conclusion

In this chapter, the development of a mechanistic model of the lactose crystallisation system was developed. This model is capable of handling the mutarotation kinetics of lactose when

in aqueous solution and also specifies the lactose solubility in terms of the mutarotation equilibrium and a correction factor needed to account for the inhibiting effect of the beta-lactose presence in ALM crystallisation. The resulting model was found to be statistically sound through a goodness of fit test. However, the PSD predictions were found to be a known limitation of the model in that the full PSD shape was not captured through simulations. The parameter estimation attempted within this work has allowed for the separation of the individual mechanism of crystallisation taking place for the purpose of fitting kinetic parameters. This ultimately highlighted agglomeration and growth as the defining mechanisms seen experimentally within the working range of interest.

Following the mechanistic model development, the model variance was tested by a global systems analysis on the uncertainties of the fitted kinetic parameters. This highlighted the effects of variance of parameters, particularly k_g and S^o, on process outputs. The model was then used to assess how the process conditions affected the process outputs of interest. This highlighted the strong relationship of concentration with both crystal mass recovery and particle size. Finally, the model allowed for the assessment of attainable regions through contour plots in Figure 3-15 by simulating a large number of processes to assess conditions' effect on resulting process outputs. The model has allowed the optimisation of the system for three main goals without the need for further experimental work: crystal mass recovery, particle size and batch time. The optimisation was focused upon a seeded controlled cooling process and was found capable of increasing the mass recovery from the isothermal experiments of 6.58g to 10g. Similarly, the particle size was also predicted to increase. However, it should be again noted that the prediction of particle size is a known limitation of the model, and the true shape of the PSD is not expected to be well predicted. Finally, the batch time needed to produce comparable results to the two previous optimisations was

undertaken. This resulted in an 11.23 hr batch time with crystal mass again higher than seen experimentally at 10g with a $D_{4,3}$ of 30 µm. The ability to utilise the model to optimise the crystallisation process is the defining advantage of developing the mechanistic model of the lactose cooling process.

This work hopes to firstly show the process to adequately model the crystallisation system from experimental work and secondly show the usefulness of having a mechanistic model of a process of interest. The model itself has allowed the testing of the system under different process conditions to gauge the relationship between process conditions and their effects on the process in the form of yield and particle size.

4 Mechanistic Model Development – Simultaneous Parameter Estimation of an Industrial API

4.1 Introduction

This work aims to use a simultaneous parameter estimation approach to build a mechanistic model of the cooling crystallisation of an API supplied by AstraZeneca (AZ). This work looks to utilise data from previously completed cooling crystallisation experiments to increase the understanding of the system and its kinetics. The utilisation of readily available experimental data shows the ease with which building mechanistic models as part of the development stage of new isolation processes could be undertaken. A key aspect of this work is to highlight the benefits of developing a mechanistic model of processes of interest. Primarily, the utilisation of the model for optimisation purposes in place of copious experiments. The optimisation of this process is focused on increasing the crystal mass recovery by altering the cooling profile and final temperature. The size of the particles produced is not the main focus of this work as the produced material is to be dry-milled to obtain the required particle size distribution.

The crystallisation system modelled within this work is a cooling crystallisation of a proprietary compound, designated for the purposes of this work as Compound-X, from ethanol. The system is known to produce agglomerated plate particles. As such, the focus is for a 1D population balance model of the system to be built that incorporates growth and agglomeration kinetics. The deployment of the model to investigate the optimisation possibilities of this seeded controlled cooling process was intended to increase the recovery of the product by optimising the cooling profile.

4.1.1 Simultaneous Parameter Estimation

The description of multiple crystallisation mechanisms by the fitting of the unknown kinetic parameters is the basis for all mechanistic model development. As discussed previously, there are a number of methods for defining these mechanisms. Chapter 3 shows a sequential method of defining the different crystallisation mechanisms that make up the overall process. This method requires designated experimental work to use the process conditions as a method to decouple the different mechanisms. This work is looking to utilise readily available experimental data from experiments performed during the development stages of the process. As such, the separation of the individual mechanisms for fitting purposes is not directly possible with the experimental data available. Therefore, the fitting of the different mechanisms is completed concurrently not sequentially.

Due to the mechanistic modelling being performed utilising pre-existing data and not a set of designed experiments for the purpose of modelling, the different crystallisation mechanisms are occurring simultaneously. As such, the fitting of the individual mechanisms is interconnected and needs to be decoupled to avoid the correlation of parameters to deliver an unreliable model. The supplied experimental data is from a series of seeded crystallisation experiments with differing cooling profiles. The mechanisms of interest have been highlighted as growth and agglomeration. These mechanisms are inherently linked, however, the consumption of solute molecules for the bridging of particulates to form an agglomerate is negligible. Therefore, concentration profiles can be singularly used as the basis for fitting growth kinetics and subsequently, the agglomeration model can be fitted from the PSD data of the recovered crystalline material.

4.1.2 Model Basis

It is important when beginning the modelling process to incorporate enough detail in the model background to capture the representative physical phenomena to describe the system being investigated. As such, physical properties and solubility relationships are necessary to specify the behaviour of the system. Therefore, prior to assessing the crystallisation kinetics of the system, some expressions were included to improve the model's representation of the true experimental conditions. This required some custom modelling within gFP to allow specified relationships for solubility and physical properties of the solvent to be incorporated. Additionally, the model is discretised following a logarithmic scale with 50 grid points with a minimum and maximum crystal size specified as 0.1 µm to 1500 µm, respectively.

4.1.2.1 Custom Modelling Solubility

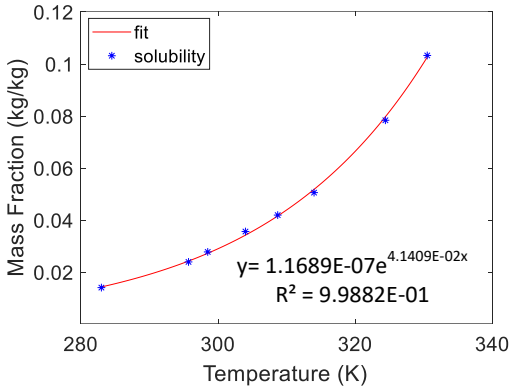

Figure 4-1 - Solubility of Compound-X in ethanol in mass fraction(kg solute/kg solvent) fitted as an exponential. Red – solubility from exponential fit. Blue – Experimental solubility data supplied by AZ.

The solubility of Compound-X in ethanol was investigated previously by AZ and recorded in terms of mass concentration. The calibration of the UV spectra needed for concentration monitoring was not done considering the change in volume due to changes in density with temperature whereas within gFP this would be accounted for. Therefore, the solubility data was converted to mass fraction as this negates the issue with changing density. The solubility

was input as an exponential fit with respect to absolute temperature as can be seen in Figure 4-1. The exponential fit was selected to allow for extrapolation to lower temperatures for use during optimisation calculations.

4.1.2.2 Custom Modelling Physical Properties

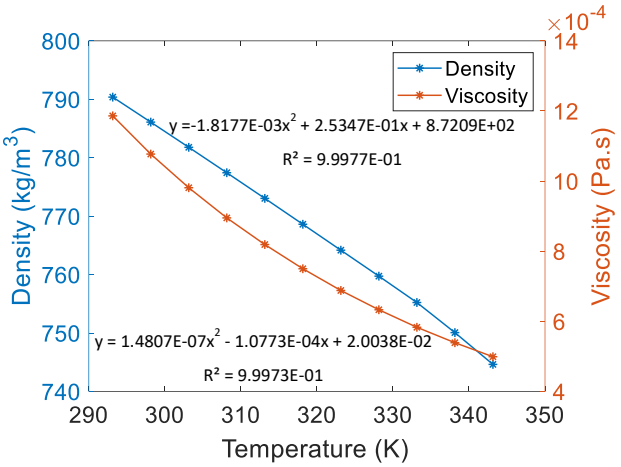

Figure 4-2 - Physical Property temperature polynomials fitted for custom modelling. Red – Polynomial fitted for viscosity data from literature. Blue- Polynomial fitted to density data from literature.

Some physical property expressions were input to the basis of the model to capture their variation with temperature. For this purpose, density and dynamic viscosity were input as custom fits within the model. Data for both terms were found in the literature and temperature polynomials fit were defined as shown in Figure 4-2[16].

4.1.2.3 Fitting Seed Size Parameters

The particle size of the seed used in the experiment has been recorded in terms of PSD quantiles. The availability of PSD quantiles for input into the mechanistic model is limited to three quantile sizes: D10, D50, and D90. Within gFP, it is possible to input seed size data in the form of a full distribution or in terms of location parameters. As the full distribution is not available it was decided to try to fit the quantile data in terms of location parameters and

their standard deviation. This will allow the software to utilise size data in the way that it was designed to. For the fitting of these terms, the flowsheet shown in Figure 4-3 is used as the basis for model validation. In this case, the known experimental quantiles are input and suitable initial guesses for the standard deviation and location parameter, which describe the centre of the distribution are selected. The model validation then allows for the iteration around the location parameter and standard deviation for the best fit of the quantile size data. The resulting best fit found is displayed in Table 12 and is used directly within the flowsheets used for building the mechanistic model. It should be noted that the standard deviation and location parameters of the seed material were refit following the fitting of any crystallisation mechanism based on PSD to improve the resulting fit.

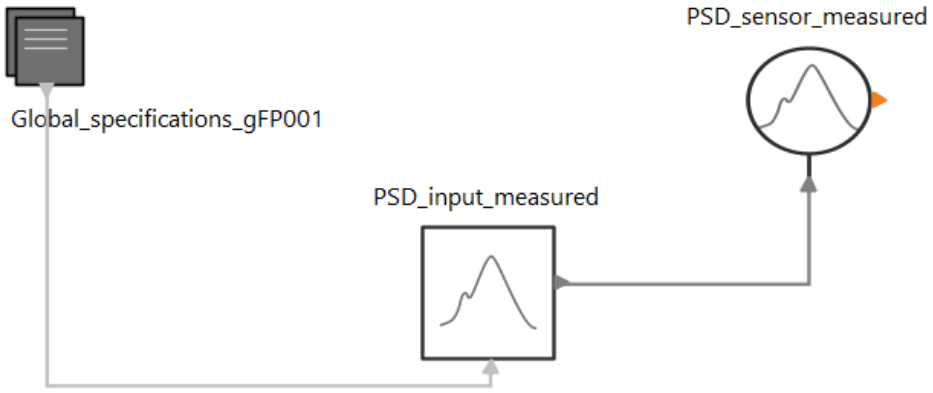

Figure 4-3 - gFP flowsheet used for fitting size parameter for seed material.

Parameter	Measured Values (µm)	Predicted values (µm)
D10	9.35	10.9
D50	31.1	29.9
D90	81.8	82.0
Location Parameter	N/A	29.9
Standard Deviation	N/A	37.6

Table 12 - Model validation results for fitting seed particle size data. Goodness of fit test produced acceptable results with a lower calculated χ^2 of 0.97 compared to a critical value of 3.8.

4.1 Methods

4.1.1 Controlled Cooling Experiments

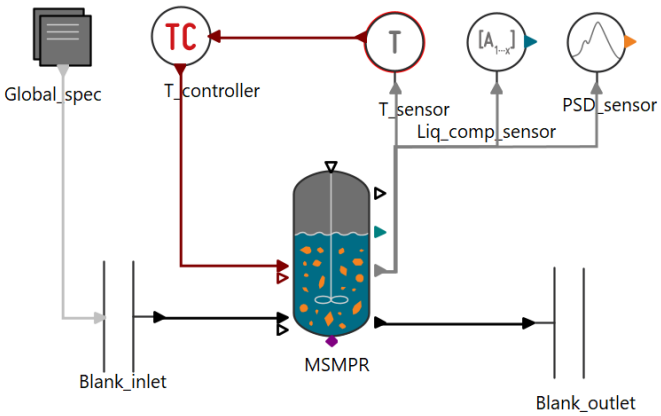

Figure 4-4 - gFP flowsheet used for parameter estimation of systems crystallisation kinetics.

A set of controlled cooling experiments that had previously been completed for this system were made available to build the mechanistic model. The data covers the working range investigated by AZ as part of their development of the process. The differences across the experiments are limited to different cooling profiles and two different initial concentrations. The crystallisation mechanisms the material is known to experience during these experiments are limited to secondary nucleation, agglomeration, and growth based on background information shared for the purpose of this work. The controlled cooling experiments were monitored in situ using a UV probe and an FBRM. This allowed concentration to be monitored continuously alongside the particle count. The recorded FBRM data highlighted only one experiment showing signs of secondary nucleation. This experiment tested the fastest cooling rate within this set of experiments of 0.2 K/min. As there was only one experiment displaying this crystallisation mechanism there was therefore not enough data to fit the secondary nucleation kinetics with any reliability. As such, this

experiment was removed from the model development dataset and the estimation of kinetics was limited to growth and agglomeration only.

The seeded controlled cooling experiments were input into gFP following the flowsheet shown in Figure 4-4 with the point of seeding indicating the start of the simulation. The fitting of the kinetics parameters was achieved by the use of two forms of data: concentration profiles and PSD quantiles. As discussed previously, the primary data used to fit the growth kinetics of the system were the concentration profiles for each experiment. Additionally, the particle size information for the seed material in the form of size quantiles, D10, D50 and D90, was supplied to the flowsheet to ensure an accurate estimate of the surface area over which growth takes place. Following the preliminary fitting of the growth mechanisms, the PSD quantiles of the recovered experimental material were used for the fitting of the agglomeration term. Following model development, the model was assessed and utilised for optimisation purposes following the methods described previously in section 3.4.4-3.4.6.

4.2 Results

Following the customisation for the basis of the model described above, the experimental data was formatted for input into gFP. This formatting requires the truncation of the concentration profiles from the point of seeding. The truncation of data is simply to remove data points prior to seeding as there was no crystallisation taking place at this stage. The concentration profiles are then sampled to reduce the data points inputted to gFP to reduce the computational load. The formatted experimental data was supplied to fit the kinetic parameters of the specified crystallisation mechanism and model validation was begun.

4.2.1 Growth Kinetics

Due to the limitation of the experimental data available and the lack of any volume diffusion experiments fitting a two-step growth model was not appropriate [30]. Therefore, the modelling of the growth mechanism was fitted following a power law model as shown previously and below (Equation 3).

$$G_{Surf}(L) = k_g e^{\frac{-E_{A,g}}{RT}} S^g$$

4.2.1.1 Concentration Profile Comparisons

4.2.1.1.1 Temperature Independent Growth Rate

For the parameter estimation of the data around this model, the activation energy was set to 0 kJ/mol to simplify the model by assuming no temperature dependence on the growth rate. The concentration profiles from the experimental data were used as the basis for fitting the unknown parameters. The resulting fits from the parameter estimation can be seen in Table 13.

Parameter	Unit	Value	St.dev
Growth Rate Constant	m/s	2.206e-5	2.09e-6
Supersaturation Order	-	1.951	0.0193
Location Parameter	µm	29.9	1.62
Standard Deviation	µm	37.6	2.52

Table 13 - Fitted crystallisation parameters from the parameter estimation.

As can be seen in Figure 4-5, the predicted concentration deviates consistently from the measured values. This is particularly evident at lower concentrations. At the lower concentrations and consequently lower temperatures, the growth rate predicted seems to be overestimated with the concentration decrease far sharper than the measured values. Subsequently, the final concentration is consistently under-predicted which is of particular

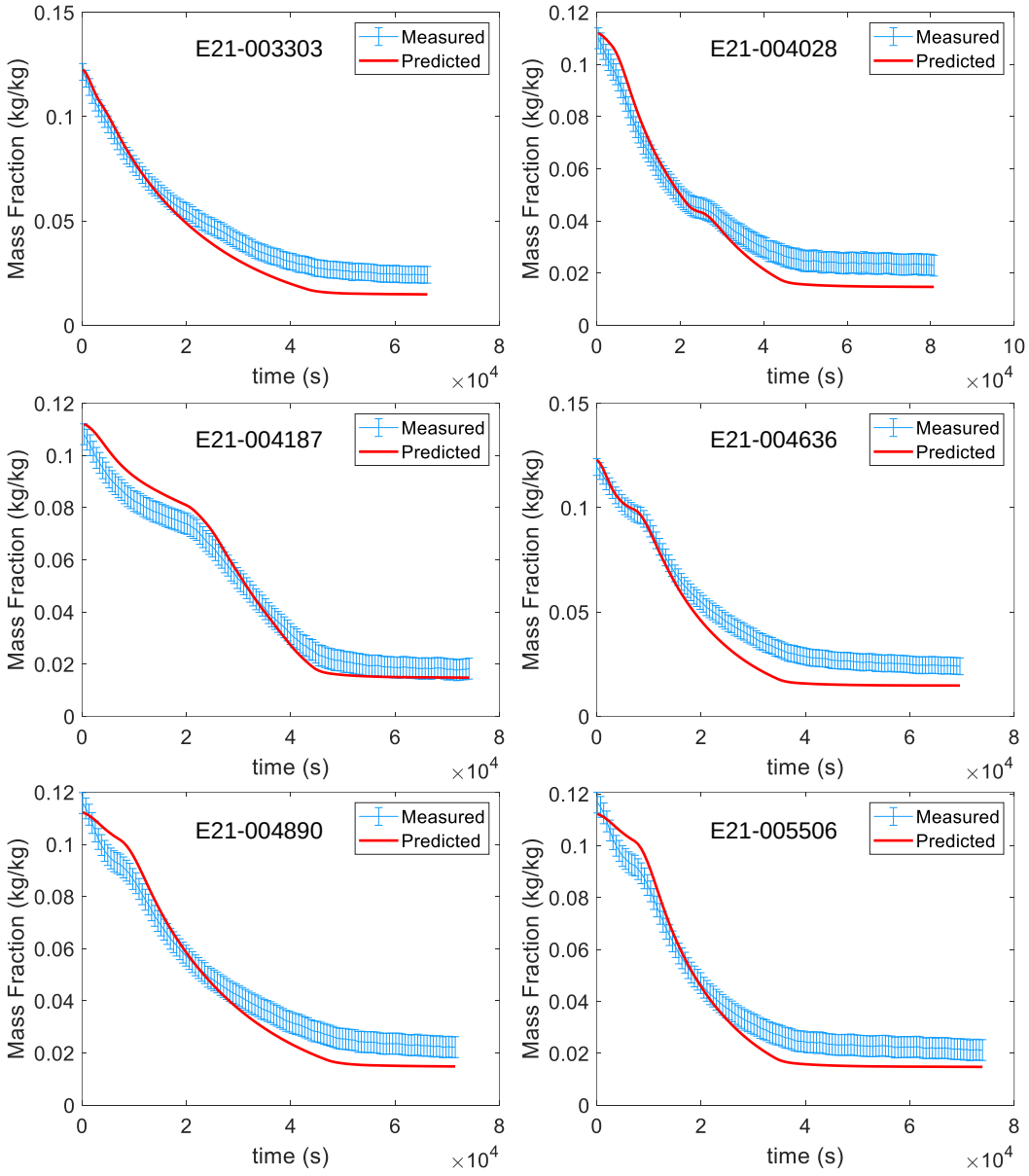

Figure 4-5 - Concentration profile prediction comparisons between measured values and model predictions for a number of experiments. Blue – measured concentrations with an error of 0.004 kg/kg. Red - predictions of concentration from the mechanistic model. The goodness of fit test showed a lack of fit for the current model with χ^2 higher than the critical value with value of 2754.45 and 793.97 respectively.

concern for this work as the aim of the resulting model is to be used as the basis for optimising crystal mass recovery. The concentration predictions also show an under-prediction of the rate of decrease in concentration at the higher temperatures at the beginning of the processes. This trend is particularly evident in experiment E21-004890. This

experiment particularly highlights that at higher temperatures the growth rate predicted is too slow whereas at a lower temperature, the rate is seen to be too fast. This shows the significance of temperature in the lack of fit of the predictions at points within the experiments. The current growth model has no dependence on temperature as the activation energy is set to zero. Therefore, this apparent dependence of temperature in the growth rate seen experimentally has not yet been captured within the current model. From this, it was decided to include activation energy within the parameter estimation to account for the evident temperature dependence of this system. The inclusion of the exponential term of Equation 3 will produce a lower growth rate at lower temperature and vice versa and should allow for a more representative growth model to be produced.

4.2.1.1.2 Temperature Dependent Growth Rate

Parameter	Unit	Value	St Dev
Growth Rate Constant	m/s	10036.7	5616.35
Activation Energy	J/mol	55349.3	1225.18
Supersaturation order	-	1.768	0.0885
Location parameter	µm	29.943	-
Standard deviation	µm	37.584	-

Table 14 - Fitted crystallisation parameters from parameter estimation.

The inclusion of activation energy as an unknown within the parameter estimation allowed for the temperature dependence of this system to be accounted for. The fitted parameters with the inclusion of the activation energy can be seen in Table 14. As can be seen in Figure 4-6, the fits are greatly improved. In particular, the overshoot of under-predicting the final concentration has been removed. Similarly, the over-prediction of concentration at the early stages of the process has been reduced. However, examples of this over-prediction can still

be seen in experiments E21-004187 and E21-005506. At this stage, the fit of the growth model was considered acceptable in terms of the concentration profile and the fitting of the PSD of the final product was focused on.

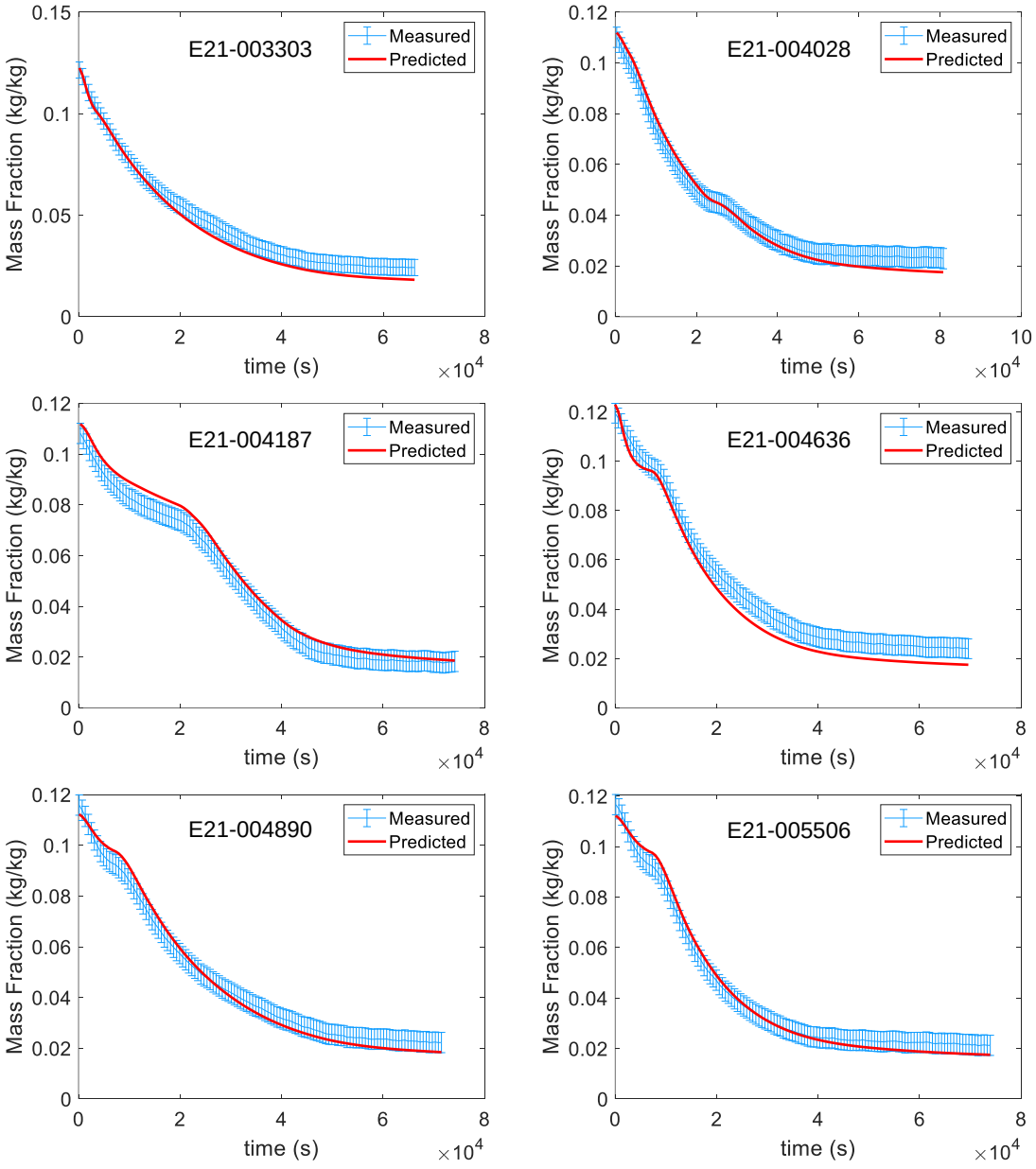

Figure 4-6 - Concentration profile prediction comparisons. Blue – measured concentrations with an error of 0.004 kg/kg. Red - predictions of concentration from mechanistic model. The goodness of fit test showed a much improved fit for this model with χ^2lower than the critical value with value of 631.8 and 799.2 respectively.

4.2.1.2 Particle Size Prediction Comparisons

Exp.	Quantiles of PSD (µm)					
	D10		D50		D90	
	Measured	Predicted	Measured	Predicted	Measured	Predicted
E21-003303	52	39.69	193	62.28	367	100.95
E21-004028	49	39.60	177	62.13	363	100.72
E21-004187	52	39.46	187	61.95	367	100.50
E21-004636	N/A	39.78	N/A	62.40	N/A	101.11
E21-004890	53	39.49	186	61.98	356	100.51
E21-005006	54	39.60	185	62.14	350	100.75

Table 15 - PSD Quantile comparisons from model predictions and measured values.

The full PSD of the recovered material from each experiment is not available for comparison, however, the D10, D50 and D90 quantiles are. Table 15 shows the measured quantile data alongside the predicted values from the growth-only model. It is clear from the comparisons of the quantile data that the growth–only model vastly under-predicts the size of crystals produced from the performed experiments. This is particularly true for quantile sizes D50 and D90. This is unsurprising as the material recovered from these experiments is known to be heavily agglomerated. Therefore, consistent under-prediction of particle size from the growth-only model highlights the need for the agglomeration term to be included for this model to be representative of the system being investigated.

It should be noted that the size data from the performed experiments is very consistent. From the quantile data, there is very little variation in sizes across the experiments. This lack of spread in PSD could lead to a limitation in the model for predicting PSD out of this range.

4.2.2 Agglomeration Kinetics

Parameter	Unit	Value	St Dev
Mumtaz Number (A50)	N/m	0.00457	1.75e-5
Growth Rate Constant	m/s	10047.3	6951.01
Activation Energy	J/mol	53737.8	1692.70
Supersaturation order	-	1.75	0.0098
Location parameter	µm	27.712	50.26
Standard deviation	µm	42.175	163.62

Table 16 - Fitted crystallisation parameters from parameter estimation.

In order to improve the model's representation of the system the inclusion of the agglomeration term needs to be fitted. Equation 7 describes agglomeration efficiency in terms of Mumtaz number. The fitting of the Mumtaz number to experimental data will describe the agglomeration mechanism experienced within this system. Within gFP, the quantile size data, D10, D50 and D90 were supplied for the fitting of the Mumtaz number.The variance for these measurements was set as such to focus the data fitting around the D50 quantile.

4.2.2.1 Concentration Profile Comparisons

When describing agglomeration, the expected effect on concentration is minimal as the uptake of solute molecules in the solution required to form the crystalline bridges between molecules is very small. However, the inclusion of agglomeration within the model will have a significant and continual effect on the size of particles at any given time. This increase in particle size from the formation of agglomerates leads to a decrease in the surface area available for growth to take place upon. The effect of this decrease in available surface area can be seen by comparing Figure 4-6 and Figure 4-7. In some cases, this decrease in the rate of concentration depletion has improved the overall fit of the data. For instance, experiments E21-004028 and E21-004890 can be seen in the growth–only model predictions to have sections that lie on the very outskirts of the error bars of the measured values. The final

model predictions for these experiments lie well within the experimental errors and closely follow the shape of the measured concentration profile suggesting a more physically representative model has been achieved.

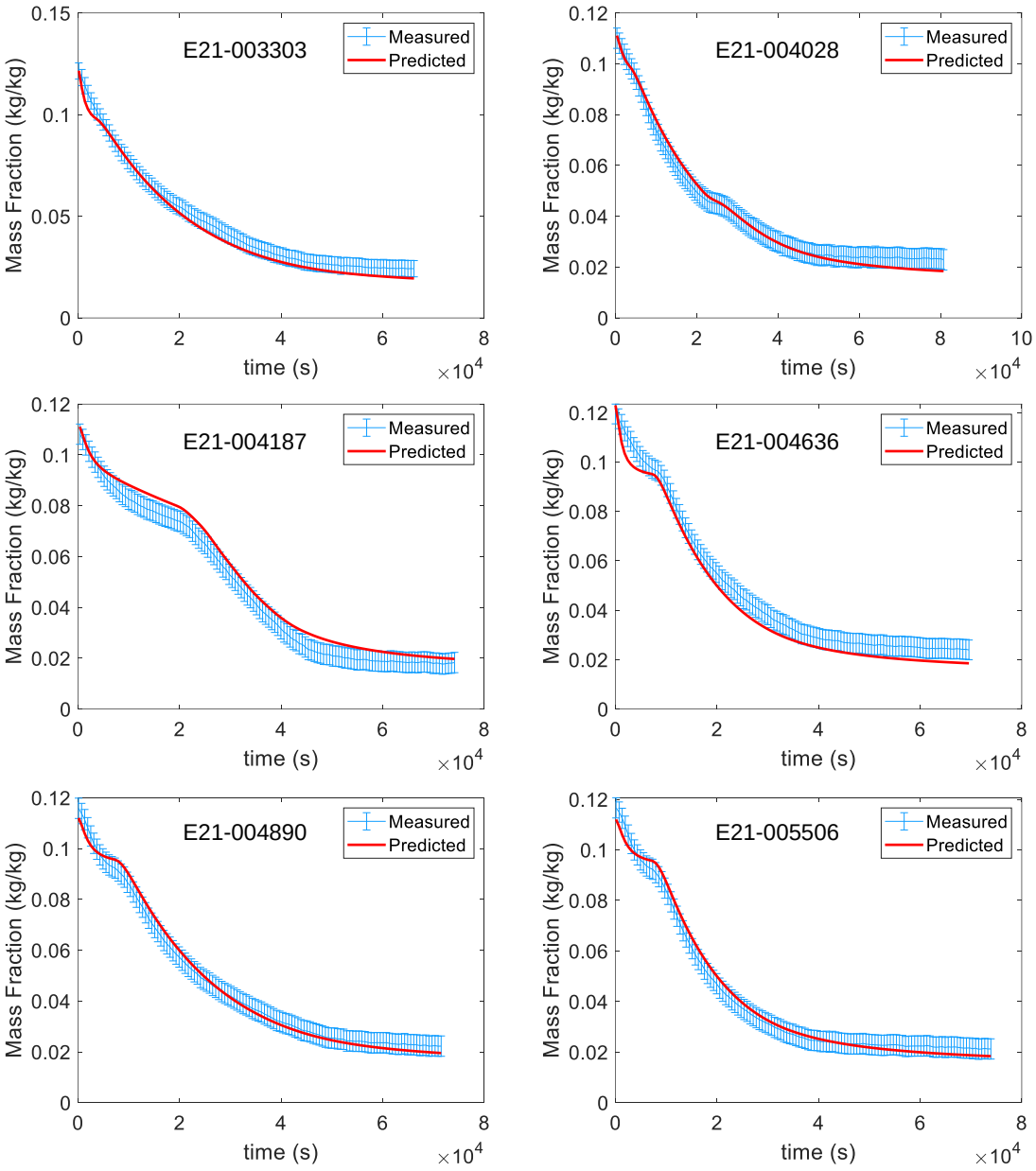

Figure 4-7 - Concentration profile prediction comparisons. Blue–measured concentrations with an error of 0.004 kg/kg. Red - predictions of concentration from the mechanistic model. The goodness of fit test showed a much-improved fit for this model with χ^2 lower than the critical value with the value of 475.2 and 801.3 respectively.

It should also be noted the end concentration predictions are improved with the inclusion of the agglomeration term. A particular improvement in fit is seen for experiment E21-004636.

This was previously predicted outside the acceptable range and now can be seen in Figure 4-7 to lie just at the outskirts of the error bars. The improvement in predictions has some exceptions but is still seen as an overall improvement in the model's abilities. A highlighted experiment with which the predictions are shifted away from the measured values with the inclusion of the agglomeration term is E21-004187. The decrease in surface area, in this case, has pushed the concentration prediction values higher and at times outside the acceptable range. Overall, the shifts in concentration predictions brought on by the inclusion of the agglomeration term have shown improvement and are considered acceptable. The overall goodness of fit is displayed by the weighted residuals and calculated reference, χ and χ^2-critical respectively. All experiments except E21-004187 are calculated to have smaller χ than χ^2-critical and therefore pass the null hypothesis. The total χ^2 for all the experiments combined is found to be 475.2 which is considerably smaller than the total χ^2-critical of 801.267. More directly, the χ^2 values of the growth-only and growth-agglomeration models of 631.8 and 475.2 show the improved prediction capability of the model by including the agglomeration term. The kinetic parameters fitted from parameter estimation and used to define the growth and agglomeration model can be seen in Table 16.

4.2.2.2 Particle Size Prediction Comparisons

Exp. Name	Quantiles of PSD (µm)					
	D10		D50		D90	
	Measured	Predicted	Measured	Predicted	Measured	Predicted
E21-003303	52	122.96	193	188.55	367	275.29
E21-004028	49	117.18	177	179.65	363	262.95
E21-004187	52	115.90	187	177.67	367	260.28
E21-004636	N/A	123.23	N/A	188.98	N/A	275.98
E21-004890	53	116.45	186	178.47	356	261.29
E21-005006	54	116.70	185	178.89	350	261.97

Table 17 – Quantile size comparisons – shows predicted values for growth and agglomerated model.

The focus for fitting the agglomeration term is the improvement of the PSD predictions as the material from these experiments is known to be agglomerated. A comparison between the full PSD of the predictions from both the growth-only model and the final growth and agglomeration model can be seen in Figure 4-8. As expected, the inclusion of the agglomeration term within the model has quite significantly shifted the PSD to larger values.

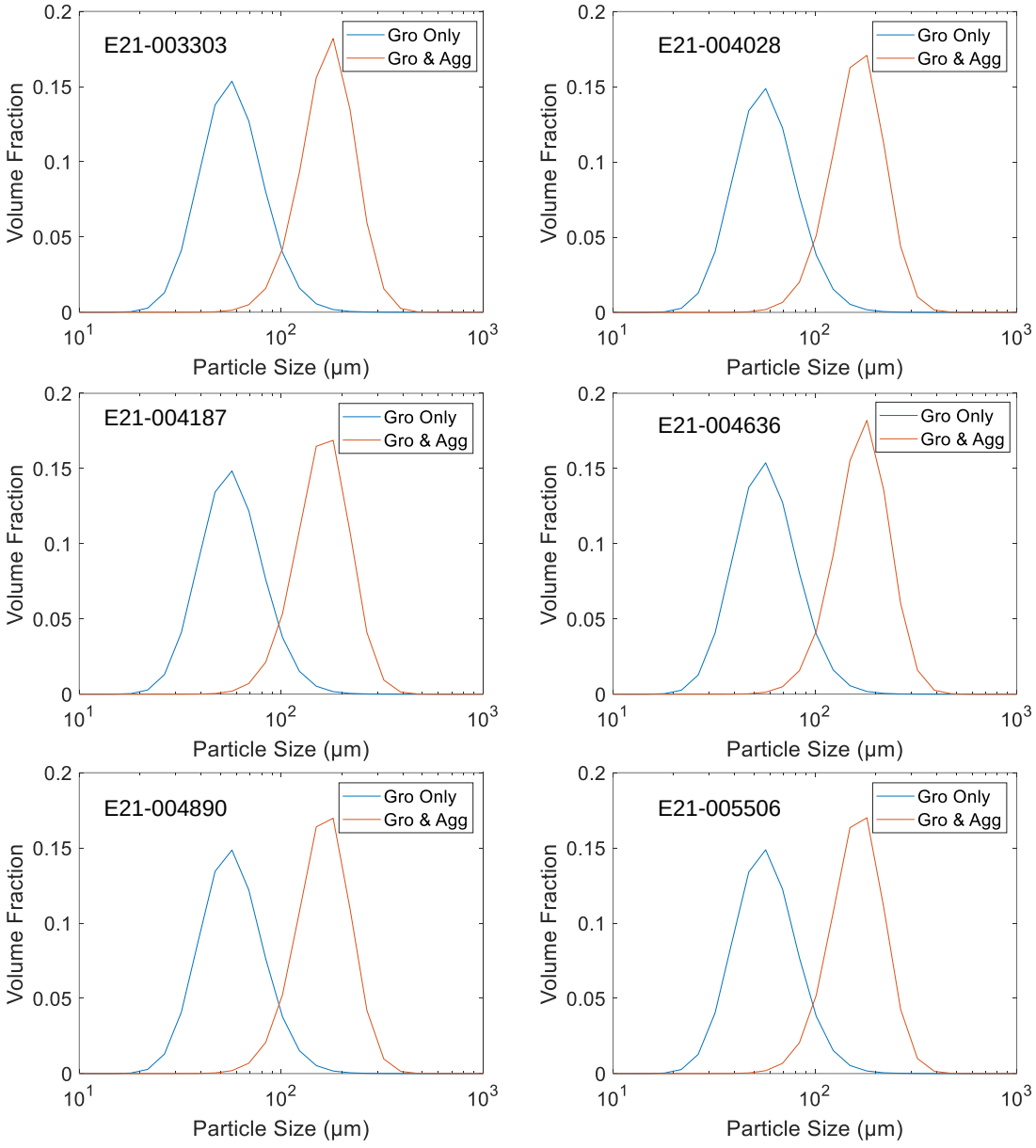

Figure 4-8 - PSD prediction comparisons between both models. Blue - growth only model PSD predictions. Orange - growth and agglomeration model PSD predictions.

A summary of the size data from both models and the true measured values is shown in Table 17. It is clear from the D10 sizes that the final model is heavily over-predicting this quantile with size comparisons over double the true measured value. When comparing the recorded values for D90, the inclusion of the agglomerated term has improved the predictions, however still significantly undersized compared to the measured values. Finally, the D50 predictions show much improvement from the growth-only model. The D50 predictions lie between a few microns and 10 µm from the measured value across all experiments. This accuracy is likely linked to the low variance model input for the D50 dataset and therefore the focus of the parameter estimation to fit these data points over the other quantile data. Overall, the inclusion of the agglomeration term has improved the size prediction of the model, but the broadness of the true PSD is still not being obtained. This is shown by the over-prediction of D10 while under-predicting D90.

The improvement of the size prediction resultant from the inclusion of a suitable agglomeration term could be improved further by using more size quantiles to broaden the information supplied to parameter estimation. The use of the full PSD for final comparison would also aid the fitting of the data as there would be more awareness around the shape of the measured PSD. Knowledge of this shape of the distribution in terms of the presence of tails could help in the selection of appropriate quantiles to best aid the parameter estimation process. Even in light of the limited historical data available to this project, the size predictions are known to be a limitation for this model and should be considered for improvement at a later stage with additional data.

4.3 Global Systems Analysis

4.3.1 Sensitivity Analysis

Factor\Response	Crystal Mass		Size Quantile D50	
	1st order	total effect	1st order	total effect
Seed loading	-0.08061	6.68E-04	-0.01429	0.02817
T set point	-0.08121	2.93E-05	-0.0049	0.03663
Initial Mass fraction of solute	0.5480	0.6163	0.7788	0.8138
Initial Mass fraction of ethanol	-0.07335	0.01037	-0.03503	0.01364
Initial mass saturated solution	0.3840	0.4471	0.1110	0.1456

Table 18 - Factor sensitivity analysis results for different process parameters and their resulting effect on crystal mass and particle size in the form of D50.

Following the finalisation of the growth and agglomeration model, the optimisation of the cooling profile for the increase in the crystal mass recovery is focused upon. Prior to the optimisation, it was necessary to investigate factors of the process that most affect the process outputs. At this stage, it was decided beneficial to investigate factors affecting both crystal mass recovery and D50. The chosen factors of interest were allowed to vary within chosen bounds and the resulting outputs from the process under these conditions were recorded. This dataset of factors and ultimate responses allows for trends to be investigated and visualised.

The factor sensitivity table can be seen in Table 18 and highlights the important factors affecting the crystal mass and the D50. From Table 18, it is clear the deciding factors for the final value of the crystal mass are the initial concentration and the initial mass of saturated solution in a lessening order of importance. These factors' influences on the crystal mass are quite intuitive in that the more solute present within the solution initially, the more material is available to crystallise out. The work of Öner et al [78], discovered the three main factors affecting yield for a batch cooling process were: batch time, cooling profile and concentration. With the tested system within this work limited to an isothermal experiment with a set batch time the initial concentration having this largest effect on process output is

in agreement with Öner et al[78]. The factors found to have the most effect on D50, and in turn particle size, are the initial concentration and mass of saturated solution. This relationship is again intuitive in that the presence of more solute in the solution allows for more growth upon the seed particles. Similarly, Öner et al[78] learned through sensitivity analysis on the batch cooling system the three factors most affecting the average particle size were: seed size, seed mass and initial concentration. This is in overall agreement with the findings of this work except for the seed mass which was found to have a very minimal effect within this study.

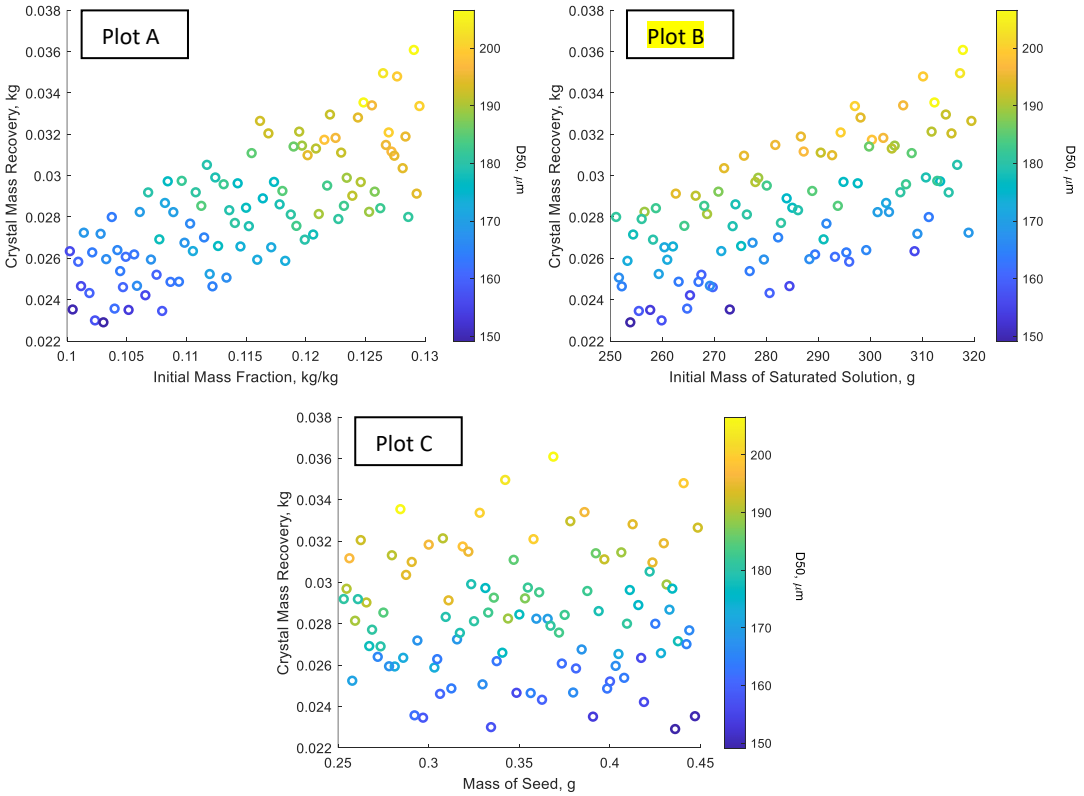

Figure 4-9 - Sensitivity analysis scatter plots highlighting found trends in factors and process outputs. Colour bars trend from blue to yellow denoting the increase of the final particle size in the form of D50.

The scatter plots seen in Figure 4-9 show the relationship between the previously discussed factors and both crystal mass recovery and particle size. As can be seen from Plot A, the initial mass fraction of solute shows a positive trend for the crystal mass as well as the particle size

as would be expected. This positive trend is also seen with regard to the initial mass of saturated solution in Plot B. The positive trend for the initial mass of the solution is quite intuitive in that more material is available to be crystallised out. Finally, the effect of increasing the seed mass surprisingly shows no trend for crystal mass or particle size as shown in Plot C. In this case, the lack of a trend between seed mass and crystal mass could be due to a lack of varied data supplied when building the mechanistic model. From this analysis, the lack of varied seed loading in the supplied experiments is known to have a limiting effect on the model. The two defining variables for optimising crystal mass recovery and particle size are highlighted in Table 18 and Figure 4-9 as the initial mass fraction of solute and the initial mass of the saturated solution.

4.3.2 Uncertainty Analysis

4.3.2.1 Process Conditions

The effects of variation in process conditions are investigated within this section. The small variations in process conditions that could be seen when working experimentally were investigated in terms of their effect on the crystallisation outputs.

Similar to the sensitivity analysis results, the highlighted factor was initial concentration. As can be seen in Figure 4-10, the initial concentration shows a negative trend for the span of crystal size as well as a positive trend for the D50 and the crystal mass recovery. The increase in concentration of around 14% in Plot B leads to an increase in the particle size and the crystal mass of 5% as there is more solute in the solution available to crystallise out. This increase in particle size leads to a reduction in the span of particle size as the increase in particle size is across all particles. However, the span variation is very small only varying from 81.05 to 81.45% which is consistent with the narrow PSD distribution produced during the

parameter estimation in Figure 4-8.The initial mass of the saturated solution showed no trend with crystal mass recovery or particle size, however, the direct relationship between particle size and crystal mass recovery is clear. This positive relationship is intuitive in that the increase in crystal mass recovery is directly linked to the growth of seed material which is fundamental in the increase in particle size alongside agglomeration.

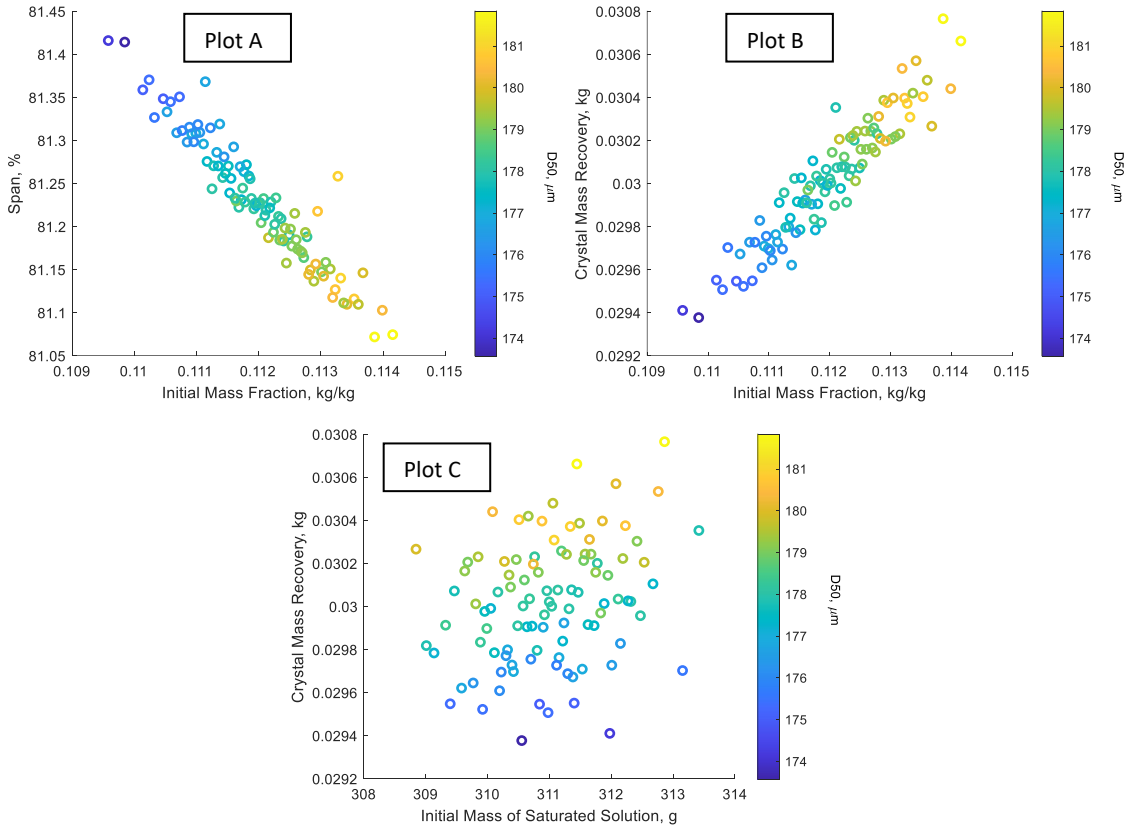

Figure 4-10 - Uncertainty analysis - scatter plots highlighting found trends in process conditions and process outputs. Colour bars trend from blue to yellow denoting the increase of the final particle size in the form of D50.

4.3.2.2 Crystallisation Kinetics

The effect of the uncertainty of the fitted kinetics parameters were investigated in terms of their resulting effect on process outputs. The uncertainty of the fitted parameters on process outputs: D50 and crystal mass recovery, are shown in Figure 4-11. The investigation of the

uncertainty of the crystallisation kinetics was completed by simulating the process with uniform distributions for the kinetic parameters with variations based on the standard deviations found during the model validation stage. Across all plots, it is clear the system holds reasonably consistent in terms of both crystal mass recovery and D50. Plot A shows a broad deviation at lower growth constant values that narrows after following a slow positive trend ending with a plateau with respect to crystal mass recovery. The D50 is also shown in Plot A to vary directly with the growth rate constant, as would be expected and is shown to be directly linked to crystal mass recovery across all subsequent plots. Similarly, in Plot B the trend is shown to broaden in line with D50 and has a very minimal negative trend relating to supersaturation order and crystal mass recovery. This trend is mirrored in Plot C but relates crystal mass to the activation energy. Surprisingly, there is no discernible trend for variation

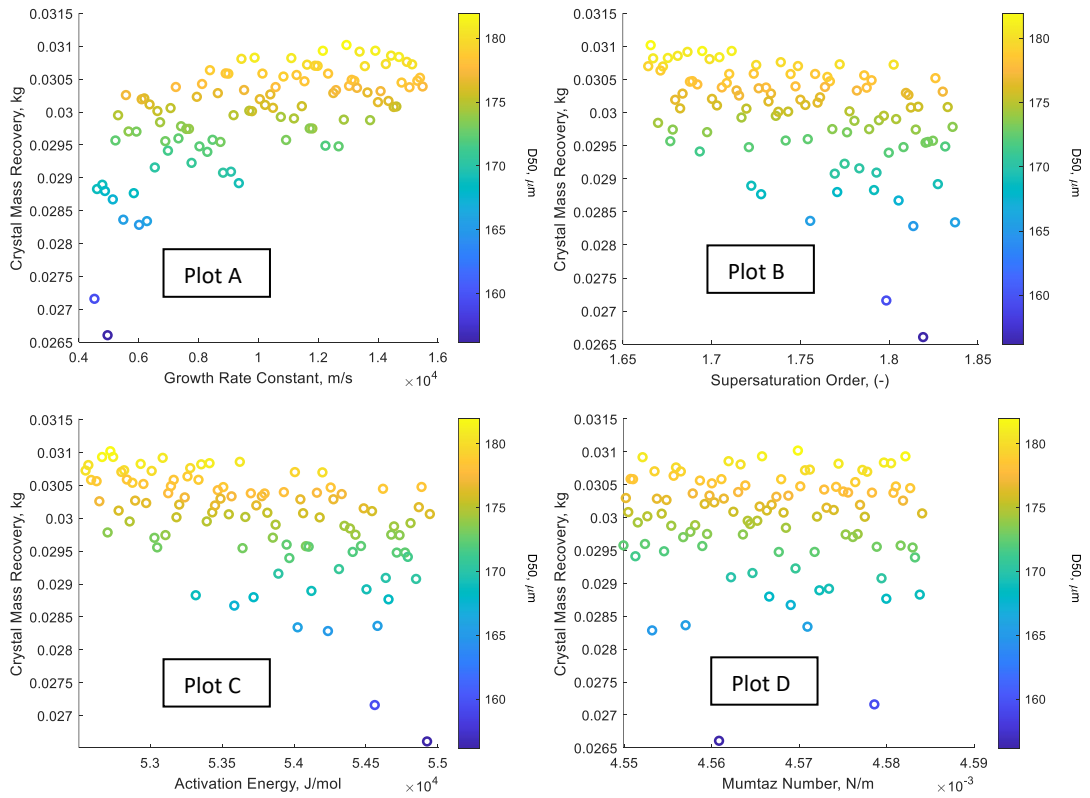

Figure 4-11 - Uncertainty analysis - scatter plots highlighting found trends in kinetics parameters and process outputs. Colour bars trend from blue to yellow denoting the increase of the final particle size in the form of D50.

of the Mumtaz number and can be seen to plot a broad but straight horizontal line in Plot D. The broadness of the trends across all tested kinetic parameters suggests more experiments included in the model validation could be necessary to improve the robustness of the model by reducing the standard deviation of the fitted parameters.

4.4 Optimisation

As stated previously, the focus of this work is to use a mechanistic model to aid in the optimisation of the cooling profile. The goal of the optimisation of the cooling profile is to increase the final mass of crystals recovered. A number of factors were highlighted within Table 18 as possible points for manipulation for optimisation of the process.

4.4.1 Optimising Cooling Profile

Upon optimisation for maximising crystal mass recovery with the highlighted factors from the sensitivity analysis, all were selected for variation, some were shown to tend to the upper bound. These were limited to three factors: initial mass of saturated solution; initial composition of solute and seed loading. The time intervals were also found to push towards the maximum at the higher supersaturation stages of the process. These results are in line with the results from the sensitivity analysis that showed the positive relationship between crystal mass and both: the initial mass of saturated solution and the initial composition of solute. As such, any increase in the two highlighted factors has a resulting increase in the crystal mass produced within the system. The slightly unexpected result is the positive trend for seed mass. This positive trend is quite intuitive that an increase in the mass of the seed would result in a larger recovery due to the larger surface area for growth and the obvious larger mass of crystal at the start of the process. However, the results of the sensitivity

analysis showed no trend between the seed mass and crystal mass recovery. The lack of varied seed data was highlighted previously as a possible limitation of the model and as such, this factor was not studied further for optimisation.

Variable	Units	Conditions
Seed loading	g	0.35
Initial mass of saturated solution	g	311
Initial composition of solute	kg/kg	0.112
Initial composition of ethanol	kg/kg	0.888
Initial temperature	° C	55

Table 19 - Process conditions set for the optimisation of the cooling process.

Variable	Units	Final value	Initial guess	Lower bound	Upper bound
Interval # 1	hr	2.0	2.0	2.0	2.0
Interval # 2	hr	10.94	11.00	7.50	14.00
Interval # 3	hr	12.06	6.50	4.00	12.40
Cooling rate	K/min	-0.077	-0.1	-0.1	-0.03

Table 20 - Time interval and cooling rate optimised values for improved crystal mass recovery.

Due to the factors' tendency to fit towards the maximum bound, it was decided to focus upon the cooling profile as a means of optimising the process. As such, the other process conditions were set as stated in Table 19. As discussed previously, the cooling rate was limited to a maximum of -0.1 K/min as this is the maximum cooling rate used within the experiments that did not show signs of secondary nucleation. The optimised cooling rate of 0.077 K/min is some 10% faster than the current proposed cooling rate of 0.07 K/min with an end temperature of 4.5 °C compared to the proposed method of 10 °C. It should also be highlighted that the time interval for the cooling rate has remained relatively unchanged

during the optimisation process. However, the final hold stage has been considerably increased from the initial value of 6.5 hrs to 12.06 hr as can be seen in Table 20.

Variable		Optimised cooling	Current method
Predicted Recovery (g)		30.69	28.22
Maximum Recovery (g)		32.12	30.56
Theoretical Yield (%)		95.55	92.35
Quantile size	D10	118.34	53
	D50	181.42	186
	D90	265.50	356

Table 21 - Comparison between outputs from the proposed method and the optimised approach.

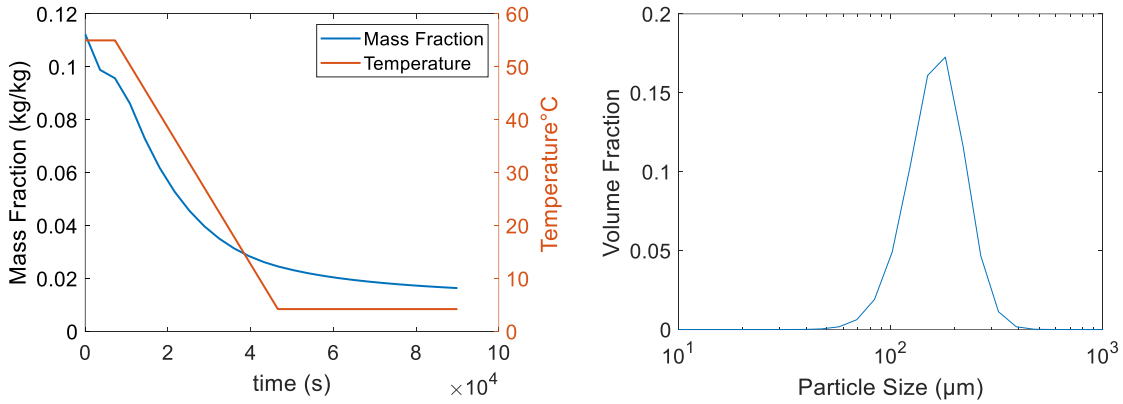

Figure 4-12 – Simulated results of mechanistic modelling using the outputs from the optimisation process.

The optimised process conditions were simulated as shown in Figure 4-12. As can be seen in Table 21, the yield relative to the end solubility from the proposed method is stated as 92.35 wt% whereas the optimised process results in a yield of 95.55%. The mass of crystals recovered has increased from 28.22 g from the proposed method to 30.69 g from the optimised path. The reduced final temperature and subsequent reduction in the endpoint solubility allow for more material to crystallise out of the system. This increase in recovery is also linked to the substantially longer final hold stage of the process. This larger hold period allows more time for the concentration to push towards solubility and ultimately increases

crystal mass recovery. Detailed process economics could determine the effectiveness of this optimised process with respect to relative cost if more details of the specific compound were known and could guide the optimisation towards lucrative avenues.

4.4.2 Optimising Cooling Profile and Starting Concentration

Variable		Units	Final value	Initial guess	Lower bound	Upper bound
Interval # 1		hr	0.80*	1.00	0.80*	2.20
Interval # 2		hr	10.79	11.00	7.50	14.00
Interval # 3		hr	11.41	6.50	4.00	12.40
Initial Composition	solute	kg/kg	0.13*	0.112	0.1	0.13*
	ethanol	kg/kg	0.87*	0.888	0.87*	0.9
Cooling rate		K/min	-0.088	-0.08	-0.1	-0.03

Table 22 - The factors and time intervals of interest in the optimisation of the process. * Depicts values reaching a bound.

Following the optimisation of the cooling profile with set start conditions, it was decided to also open the initial concentration and the first time interval to variation for optimisation. As can be seen in Table 22, the first notable change during the optimisation process was the significantly shorter initial hold stage from 2 hr to 0.8 hr. The shortening of this stage to the lowest allowable bound shows the observed necessity to start the cooling stage as quickly as possible. However, this could raise issues in terms of a secondary nucleation event as the level of supersaturation could exceed a threshold that has not been investigated within this work. If such a threshold could be supplied as a constraint for the optimisation process, there could be an increase in confidence in the optimisation outputs. It should be noted that the two remaining time intervals were similar to the previous optimisation process with an

increase in time for cooling allowing lower temperatures to be reached and a longer final hold time allowing the system to push closer to solubility concentration.

The initial concentration of the saturated solution was also investigated as a possibility for optimisation. As expected from the sensitivity analysis, the initial concentration of Compound-X had a positive effect on crystal mass recovery. The results from the optimisation show the initial concentrations of solute and solvent have reached their respective bounds. As stated previously with regards to the sensitivity analysis, the increase in concentration allows for an increase in crystal mass as there is more material present in the solution to crystallise out onto the seed particles. Finally, the results of optimising the cooling rate showed an increase to 0.088 K/min and the final temperature dropped to -2 °C. The final temperature allows for the system to be pushed towards a lower saturated concentration and in turn larger crystal mass recovery. The faster cooling rate is not considered a point of concern in terms of the level of supersaturation reached throughout the process as previous experiments performed with cooling rates of 0.1 °C/min showed no signs of secondary nucleation.

Variable		Optimised cooling	Current method
Predicted Recovery (g)		36.44	28.22
Maximum Recovery (g)		38.25	30.56
Theoretical Yield (%)		95.22	92.35
Quantile size	D10	130.08	53
	D50	199.26	186
	D90	291.09	356

Table 23 - Comparison between outputs from the proposed method and the optimised approach.

The process outputs from the simulation of the optimised process can be seen in Table 23 and Figure 4-13. The difference in mass of crystal recovery is quite significant from 28.22 g

to 36.44 g for the proposed method and optimised, respectively. This increase is predominantly down to the lower end temperature allowing for a lower final concentration of the solution possible. Upon comparing the theoretical yield of the two processes, a slight increase from 92.35% to 95.22% can be seen. It should also be noted that the resulting PSD from the optimised path shows an increase in size compared to the supplied experiments. As previously discussed, the prediction of size is a limitation of the model due to the limited size data supplied during the building of the model. This prediction of an increased PSD is of interest as previously the predictions, although not fitting the true measured values, have been just as consistent. This increase suggests a shift that could be interesting for future experimental work and could have effects on downstream milling processes.

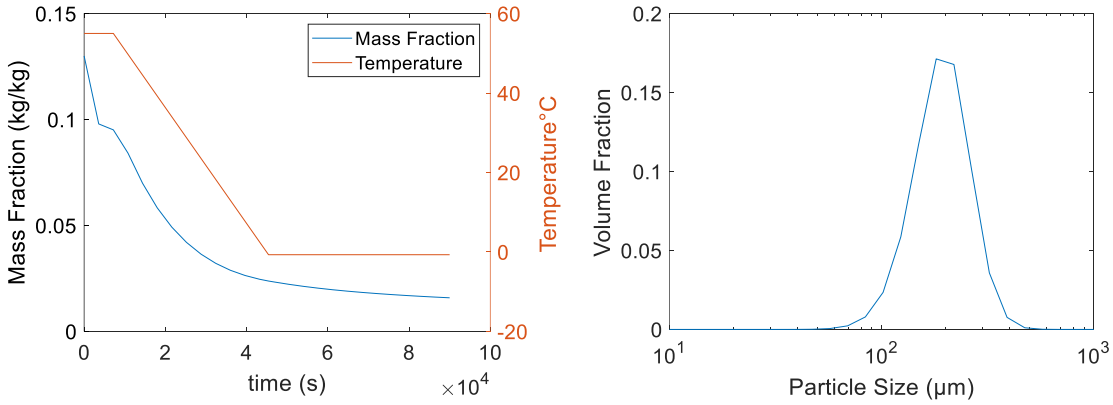

Figure 4-13 - Simulated results of mechanistic modelling using the outputs from the optimisation process.

4.5 Conclusion

Within this work, a mechanistic model depicting the cooling crystallisation of a late-stage development API was achieved by utilising pre-existing experimental data. The experiments were known to undergo growth and agglomeration during the cooling process and as such these mechanisms were investigated for modelling purposes. The fitting of the growth and agglomeration kinetics was achieved by fitting to the concentration profiles and particle size

quantiles for the supplied experiments. The resulting PSD predictions from the experiments show close predictions for the D50 quantile but over-predicted D10 and under-predicted D90. This shows the model does not represent the broadness of the true PSD. Despite the deficiencies in the PSD prediction the overall model is found to be statistically sound by the goodness of fit test.

Sensitivity analysis and uncertainty analysis were performed to highlight the factors most affecting the crystal mass recovery and the particle size in the form of D50. The results from these analyses showed the importance of the initial concentration and initial mass of saturated solution. These factors' influences are expected as the presence of more solute in solution allows for more material to crystallise out and therefore increases particle size as well as the mass of crystals recovered. The surprising result from these analyses was the apparent lack of an effect seeding had on the system. However, this is believed to be due to limited data supplied in terms of varied seed loadings for the building of the model.

Finally, the optimisation of the system was investigated. This investigation was completed across two scenarios with the different factors optimised. Firstly, only the cooling profile was considered and then the cooling profile and initial concentration were investigated for optimisation purposes due to the results from the sensitivity analysis. From this investigation, an increase in the time interval for the cooling stage and the final hold was suggested. This allowed for lower temperatures and lower solubility regions to be reached as well as a longer time interval for the system to push towards the saturated concentration. The cooling rate itself was slightly increased for both investigations, 0.077 K/min and 0.088K/min respectively. However, the suggested cooling rates did not exceed the system's bounds of 0.1K/min and as such, secondary nucleation is not considered an issue with regard to the rate of cooling.

Overall, within this work, a mechanistic model was achieved through the parameter estimation of pre-existing experimental data. This chapter highlights the ability to build a mechanistic model as part of the development stages for a given compound of interest within the industry. Through the limited data available a model was produced that was capable of describing the process well with some discrepancies for particle size predictions. The material from this process was to be milled and therefore the problem of PSD predictions was not considered significant. The resulting growth and agglomeration model then allowed for the optimisation of the process beyond conditions tested experimentally. This particularly highlights the advantages of utilising mechanistic models to aid in the development of the process of late-stage development compounds such as this work focused upon.

5 Mechanistic Model Development of an Evaporative Crystalliser

5.1 Introduction

This section of the work focuses on crystallisation by means of evaporation as a point of interest. This work continues to focus on the crystallisation of alpha lactose monohydrate from water and the benefits of modelling the crystallisation process using population balance modelling. In particular, the defining of the kinetics of the system as well as investigating its capabilities for optimisation and potential for merging different modes of crystallisation. The previous studies into the cooling crystallisation kinetics of lactose highlighted the slow nucleation kinetics and raised interest in studying a system capable of faster recovery. The first method of interest was to utilise supercritical conditions to perform antisolvent crystallisation with the use of supercritical CO_2. The supercritical unit was tested with a model system of paracetamol and API and was found to produce some favourable results. Unfortunately, the system was never successfully run with lactose due to technical problems with the unit itself. Hence evaporative crystallisation was selected as an additional method to investigate the primary nucleation of lactose. The use of an evaporative crystalliser had the added constraint of being capped at 93°C to avoid the crystallisation of the unwanted β-lactose. As such, the development of a vacuum-induced crystalliser was undertaken within this work.

5.1.1 Evaporative Crystallisation

The use of evaporation as a method of isolating lactose was first recorded in 1633 by Bartolettus (Nickerson 1974) and remains a method used in the dairy industry today[79].

However, its use is now primarily reserved for concentrating the whey prior to the cooling crystallisation for the isolation of the ALM crystals. The use of evaporation as a means of introducing supersaturation has the potential to improve yield recovery compared to the standard method of cooling crystallisation. As such, the use of evaporative crystallisation has gained more attention as discussed within the patent of Dinesen and Henningfield [80]. Within this patent the production of ALM is achieved directly from the lactose containing product streams of dairy industries in a continuous process under evaporative and high shear conditions.

There has been some work on modelling the crystallisation of lactose via evaporative methods on both a batch and semi-batch lab scale by Vu et al in 2005[81]. Their work focused on optimising the conditions of both evaporative and cooling crystallisation platforms of relatively small scales of 4L and 2L, respectively. They compared the model simulated conditions to the seeded experiments for both evaporative and cooling with good results. This work found that although the evaporative produced a far greater yield of 30% increase in solid content in only 4 hours, the system itself was difficult to control. Specifically, due to the avoidance of the secondary nucleation threshold. Alternatively, the work completed by Agrawal in 2012 focused specifically on the presence of secondary nucleation within evaporative crystallisers in the industry[82]. This work focused on the development of a mechanistic model for a forced circulation crystalliser (FCC) where the secondary nucleation kinetics are found to be dominant and no primary nucleation was considered prior to start-up. The focus of the work in this chapter is around the evaporative crystallisation on a lab scale and as such limits the crossover with details concerning a FCC.

The work performed by Sowul in 1981 describes a method for assessing different crystallisation kinetics of a sucrose water model by utilising CSD data collected from sampling

a continuous MSMPR system[83]. The running of the continuous platform allowed multiple data points depicting different states of the system prior to reaching a steady state. This method of investigating crystallisation kinetics allowed growth, primary and secondary nucleation kinetics to be defined reliably with minimal experiments performed. The use of continuous platforms for the assessment of the kinetics of a system is an interesting approach to maximise data from minimal experimental work. However, the work within this chapter looks to build a mechanistic model of a semi-batch platform and is not currently looking to utilise the learnings from Sowul et al work directly.

5.2 Designing the Platform

Evaporative crystallisation is dependent upon increasing solute concentration within the system by the removal of the solvent by evaporation. In the case of the lactose-water system, at ambient pressure, the evaporation of water would need to occur at around 100 °C. As the crystallisation would occur above 93 °C, the process would produce beta-lactose crystals and as such, this would not be an effective method to crystallise the desired ALM particles. As such, the design of this crystallisation platform requires the system to be held under vacuum conditions in order to lower the boiling point below 93 °C. As the hope of this work is to develop a mechanistic model of the system, the new crystallisation platform requires in-situ monitoring of the following: concentration, particle count, temperature and pressure. This raised the need for a bespoke 3D-printed lid that allows the vacuum pressure to be maintained in the presence of the probes. The need to maintain constant vacuum pressures resulted in the need for a vacuum controller and vacuum pump. The vacuum controller allows the outlet to be held at a constant pressure set point by controlling a valve connected via the vacuum pump.

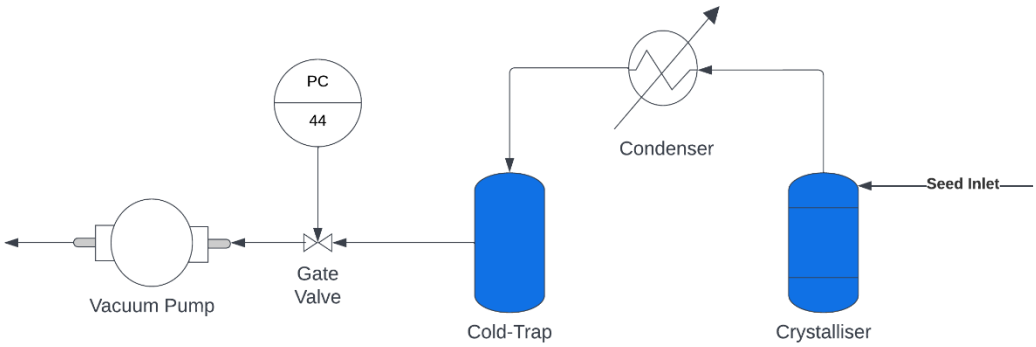

Figure 5-1 - Flowsheet depicting the semi-batch vacuum-induced evaporative crystallisation platform.

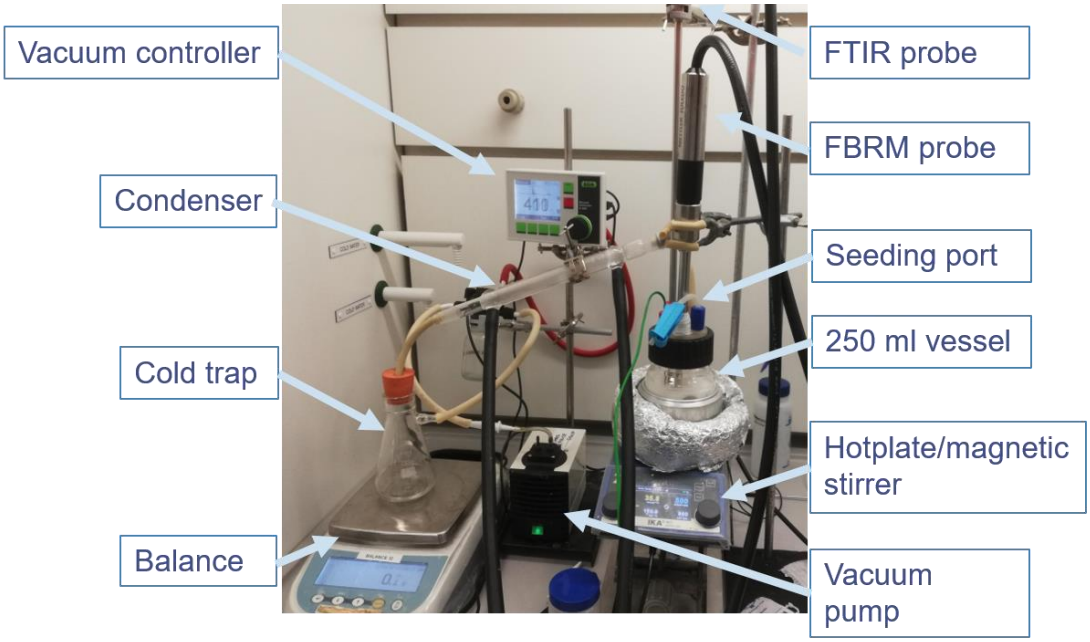

Figure 5-2 - Vacuum-induced evaporative crystallisation platform.

The development of a mechanistic model requires the concentration change across time brought on by the crystallisation process to be recorded. As the concentration of this system will be continually changing due to the evaporation process and not solely the effect of crystallisation, additional consideration is required when modelling this system. As such, the concentration recorded by the IR spectra during this process will not be able to describe the crystallisation process alone and will need the mass of water evaporated to be recorded. This led to the incorporation of a condenser connecting the outlet of the vessel and a cold trap. The mass of water collected in the cold trap can then be recorded using a balance and custom

MATLAB script to record data in real time. The continual measurement of mass evaporated and concentration recorded via the IR spectra allows the solute removed due to crystallisation to be accounted for. Finally, the problem of seeding the system under vacuum conditions had to be assessed. This was solved by utilising a bleeding valve attached to a syringe. This allowed the seed to be added while keeping the system closed. A small pulse in pressure was recorded when testing this method of seeding but it was minimal and deemed not to be significant. The finalised test platform is shown in Figure 5-2 and the corresponding flowsheet in Figure 5-1 allowed the required data to be recorded for developing a mechanistic model of the system in gFP and for adequate control of the system.

5.3 Preliminary Results

The setup of the system was assessed by performing a limited number of seeded and unseeded experiments to ensure the stability and control capabilities of the system. Minor changes were made to the set-up to improve the control of the pressure within the vessel such as new O-rings and tubing. The tubing between sections was found to heat up during experiments and this increase in temperature caused a steady increase in the pressure within the system. As such, smaller sections of tubing were used to connect the different sections of the set-up for better temperature performance. This alteration to the system was found to allow for steady pressure to be maintained during the other preliminary crystallisation experiments. These experiments showed signs of encrustation at the liquid line on both the vessel and the probes. These experiments were run to the extreme to test the system and gauge appropriate times and supersaturation limits to work at for future parameter estimation experiments. The strong presence of fouling highlighted the need to reduce the time before ending the experiment and beginning the recovery of the product material for future experiments. Additionally, the opening and closing of the valve during control resulted

in sharp changes in the cold-trap mass recorded. The resulting very noisy data for the recorded mass of water evaporated was deemed unsuitable for modelling purposes. As such, the mass of water evaporated was calculated based on concentration data collected via the FTIR probe before seeding and before signs of nucleation.

The unseeded experiments were found to nucleate within a few hours. This shows the

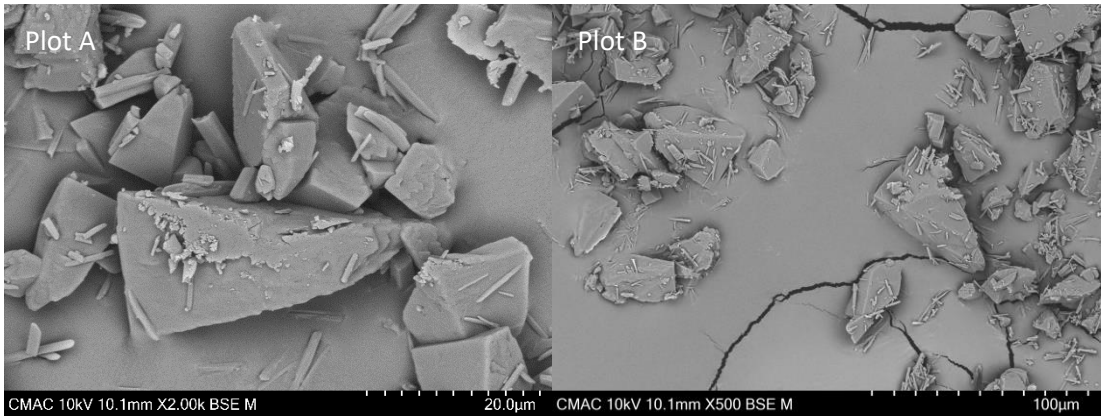

Figure 5-3 - Scanning electron microscopy images of recovered crystalline material from preliminary evaporative crystallisation experiments. Plot A shows a close-up image of the needles adhered to the surface of primary particles. Plot B shows the consistency of the needles present across the sampled crystals.

evaporative system to be a much more suitable platform for the study of primary nucleation kinetics. SEM images were taken of the recovered material from a few of the seeded preliminary experiments as can be seen in Figure 5-3.The SEM images show the presence of small needle particles on the surface of the larger primary particles. The presence of particles of different morphology and smaller sizes raised concerns about the wash solvent protocol and the possibility of antisolvent effects taking place. These small needle particles could be due to uncontrolled nucleation of ALM or potentially beta-lactose during the washing. Therefore, a small investigation into the suitability of the current wash protocol was undertaken.

5.4 Methods

5.4.1 Concentration Calibration Modelling

The monitoring of concentration during the experiments is paramount in the ability to build an accurate mechanistic model of the process. The previously built lactose concentration calibration model developed in section 3.5.1 does not cover the working range of interest for the evaporative work undertaken within this chapter. By nature, the evaporative crystallisation process will run at higher temperatures and concentrations than the cooling crystallisation process the previous calibration model was designed for. As such, an evaporative-based lactose concentration calibration model was built for the working range of interest for the proposed evaporative crystallisation experiments as stated in Table 24. The method for building the calibration model is described in section 3.4.1 was followed for this work.

Component/Mode	Concentration (wt%)	Temperature (°C)
Lactose/Evaporative	30-60	50-90

Table 24 - Working range of interest for the evaporative crystallisation experiments.

5.4.2 Wash Solvent Protocol Investigation

Upon evaluation of the crystals produced from the preliminary growth experiments concerns surrounding the wash protocol were prompted by the presence of crystals on the surface of the primary particulates that displayed a different morphology consistent with the characteristic needle particles of beta-lactose[84]. This is likely due to improper washing methods as the crystallisation of beta-lactose is more common when crystallised using higher antisolvent concentrations[85]. It is key to determine whether the needle crystals are formed during the designated crystallisation space or if the wash protocol is contaminating the recovered sample.

5.4.2.1 Experimental Method

This method is used to assess the presence of nucleation due to both antisolvent effects and the temperature reduction experienced between the crystallisation and wash stages. An intensive method is described by Shahid et al to determine the antisolvent effects of wash solvent choice[86]. The method utilised within this work is simpler and more direct by utilising the multiple reactor vials of the Crystalline (Technobis Crystallization Systems) but does follow a similar approach. Four vials of lactose-water solutions were weighed out and supplied to the Crystalline and heated to a specified temperature. Four additional vials of water-ethanol mixtures were measured out and held at room temperature. Each vial contained a different ratio of ethanol-water, ranging from 40:60 to 70:30, to be assessed for its efficacy as the initial wash solvent. Once the temperature is settled and the lactose-water solution vials are clear, an individual vial of an ethanol-water solution is added directly to the lactose solution vial. The combined solution vial was then re-placed within the Crystalline to be monitored for signs of nucleation. This method was performed for the highest and lowest temperatures seen at the end of the evaporative crystallisation experiments.

Experiment	Concentration (wt%)	Temperature (°C)
Exp-High	47.0	75
Exp-Low	37.0	60

Table 25 -Experimental conditions for the testing of the suitability of different wash solvent ratios. High and Low denotes the extremes of the evaporative crystallisation experiments to be performed. Concentration is set as the saturated concentration for the specified temperature.

5.4.3 Parameter Estimation Experiments

The initial mechanisms of interest for investigation in this work are specified as primary nucleation and growth. In the previous cooling crystallisation work the growth kinetics were assessed, however, the primary nucleation was considered not industrially relevant due to

the exceedingly slow induction times recorded for preliminary experiments. The increased concentration and supersaturation levels within the evaporation platform are expected to speed up the nucleation rate. Due to the nature of the system, the use of heating and cooling cycles to investigate induction time is not possible. As such, the investigation of the primary nucleation kinetics is to be investigated by isothermal experiments with constant evaporation present which ultimately leads to dynamic conditions.

This system will be held at constant temperature and pressure allowing for the continual increase of concentration due to the evaporation of water from the system. The presence of nucleation is recorded by both an FBRM and IR probe. The kinetics will be fitted using the recorded concentration profiles, seed and final PSD collected from a set of isothermal experiments as outlined in Table 26.

Exp.	Concentration (mass %)	Temperature (°C)	Seed Mass (g)	Supersaturation Ratio
GroVac2	36.98	65	0.77	1.2
GroVac4	40.30	70	0.46	1.1
NucVac1	36.98	65	N/A	1.4
NucVac5	43.72	75	N/A	1.4

Table 26 - Parameter estimation experiments for vacuum-induced evaporative crystallisation of lactose.

The required mass of water and ALM were supplied to the 250ml glass Duran vessel used for this process. A 3D-printed lid with dedicated ports was designed to fit the process requirements. This allowed for in-situ monitoring of the process with the use of both FBRM and IR probes. This allowed for the monitoring of particle count to gauge dissolution and nucleation as well as concentration monitoring with a dedicated calibration model. The outlet flows along a condenser to a cold trap vessel. The mass within the cold trap vessel is continually monitored via the scale and a dedicated MATLAB script. The vacuum controller

holds the pressure to the specified set point within the vessel utilising a valve connected to the vacuum pump.

The supersaturation of the system was monitored remotely by the IR and temperature data allowing for a concentration measurement to be made. The mass of the seed was weighed in a beaker and room temperature saturated solution was added to the beaker at a minimum volume required to suspend the seed particles. The seed suspension was then taken up within a syringe. The syringe was then connected to the inlet tubing. The inlet remained closed to the outer environment due to the bleed valve and was opened to allow the inflow of the seed suspension. The bleed valve was then closed, and the syringe was removed allowing the system to remain closed and vacuum pressure maintained.

5.4.4 Modelling

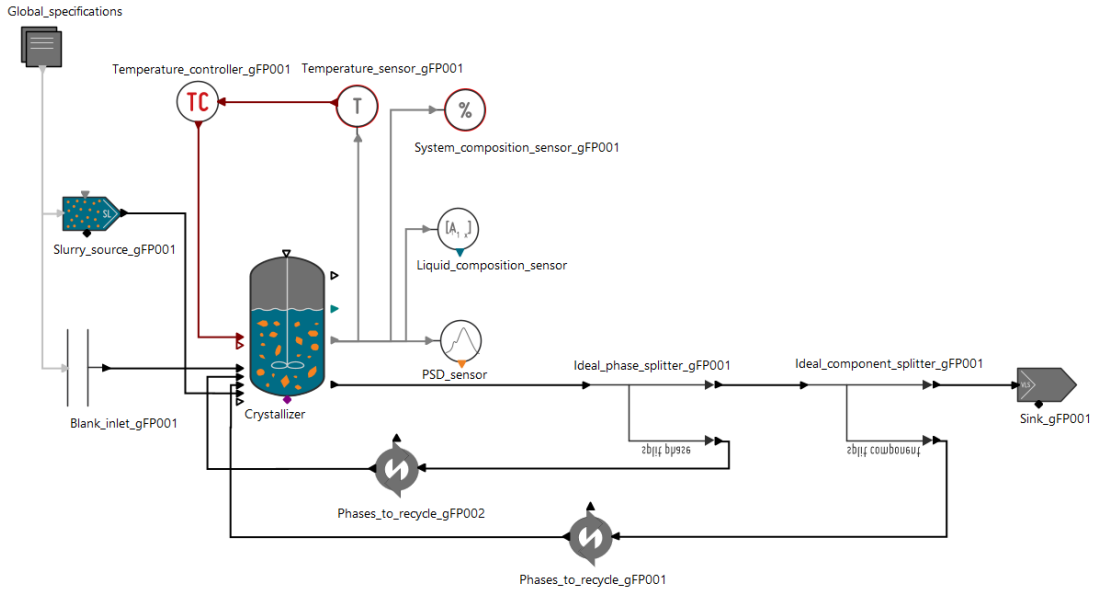

Figure 5-4 - gFP flowsheet depiction of simulated vacuum-induced evaporation crystallisation set-up.

The modelling of the evaporative process is more complex than that of cooling. The modelling of evaporation of the solvent during the process requires the inclusion of the vapour-liquid equilibrium of the system. The fitting of vapour-liquid equilibrium data would allow an

activity model to be defined and evaporation to be modelled. However, the accurate collection of this data would be very intensive and any error in the evaporation rate would have considerable compounding inaccuracies in the fitting of the crystallisation kinetics which is the ultimate goal of this work. As such, it was decided to simplify the modelling requirements and remove the necessity of including an activity model.

The exclusion of an activity model while modelling the evaporation process can only be achieved by not directly modelling the evaporation of the solvent. This was achieved by utilising the splitter components within gFP. The resulting flowsheet can be seen in Figure 5-4. The MSMPR crystalliser is set to have a constant outlet flowrate that is then passed through an ideal phase splitter (ideal_phase_splitter_gFP001) which separates the solid and liquid in the stream. The solid stream is recycled back into the crystalliser while the liquid stream is separated again through an ideal component splitter (ideal_component_splitter_gFP001). This splitter produces a pure water stream and a dissolved solute stream made up of both alpha and beta lactose. The lactose stream is recycled back to the MSMPR whereas the pure water stream is sent to a liquid sink. Utilising the model validation entity within gFP the flowrate set-point for the outflow of the vessel can be fitted to match the measured evaporation rate of pure water to the liquid sink. This was completed for individual experiments to allow for accurate simulation of the measured evaporation rates.

The model for this work is discretised across 50 points following a logarithmic scale ranging from 0.1µm to 1000µ. Finally, the soundness of the model was assessed as described in sections 3.4.4 and 3.4.5. The model was subsequently optimised for different objectives following the methods described previously in section 3.4.6.

5.5 Results

5.5.1 Concentration Calibration Modelling

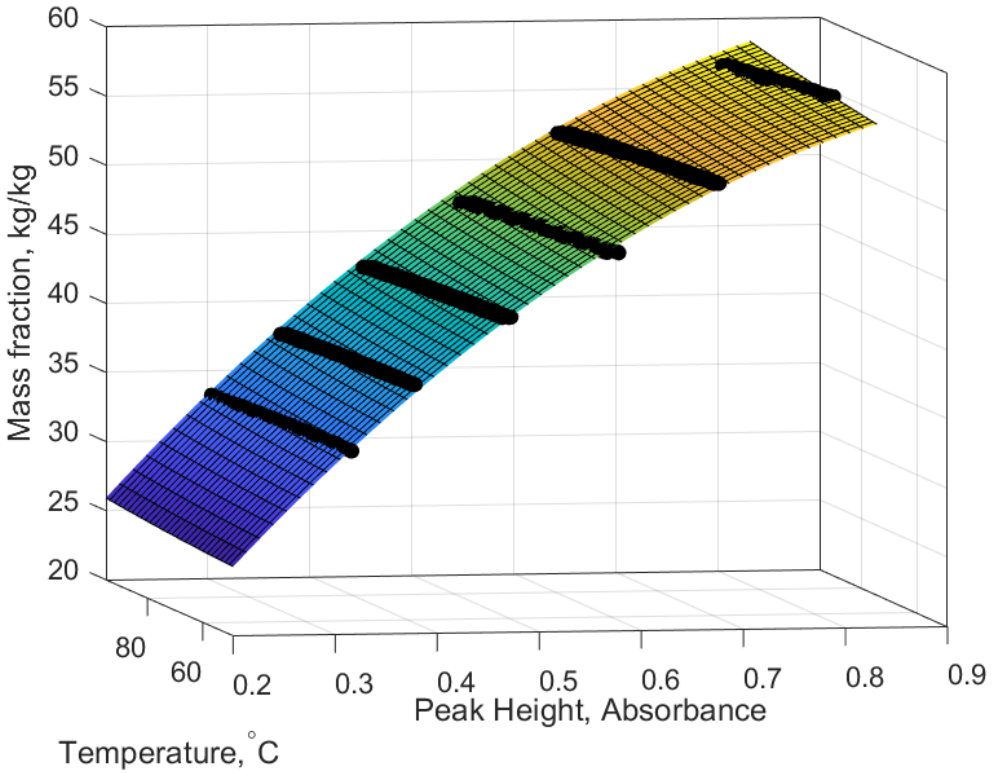

Figure 5-5 - Polynomial surface plot depicting the relationship between temperature peak height and concentration (in $kg_{solute}/kg_{solution}$.) used for prediction purposes. The peak height at 1014 cm^{-1} with respect to the baseline at 1137 cm^{-1} was used for the monitoring of the concentration. Black data points show the collected data from experimental calibration work.

Model	R^2	RMSE	RMSE (validation)
Evap/lactose	0.9976	0.003802	0.002243

Table 27 - Evaporative crystallisation calibration model results.

The combination found to show the least variation brought on by temperature changes for the evaporative working range was identified as 1137 cm^{-1} and 1014 cm^{-1} for baseline and peak positions respectively. Utilising curve-fitting tools within MATLAB, the resulting fit of Equation 21 was defined and displayed in Figure 5-5

The R^2 value for the corresponding fit has been calculated as 0.9976 which again shows the polynomial's ability to describe the calibration data well. The validation experiments for this model were performed over only two concentrations with three corresponding temperatures each. The RMSE calculated for the validation data of 0.002243 kg/kg is very low and highlights the accuracy of the calibration model. Although the RMSE from the calibration data is larger than that of the validation data, the value of 0.003802 kg/kg shown in Table 27 still shows the accurate capability of the polynomial fit.

Equation 21

$$C(H,T) = 0.0815 + 0.928H - 1.39 \times 10^{-4}T - 0.435H^2 + 3.59 \times 10^{-4}HT + 1.78 \times 10^{-6}T^2$$

5.5.2 Wash Solvent Protocol Investigation

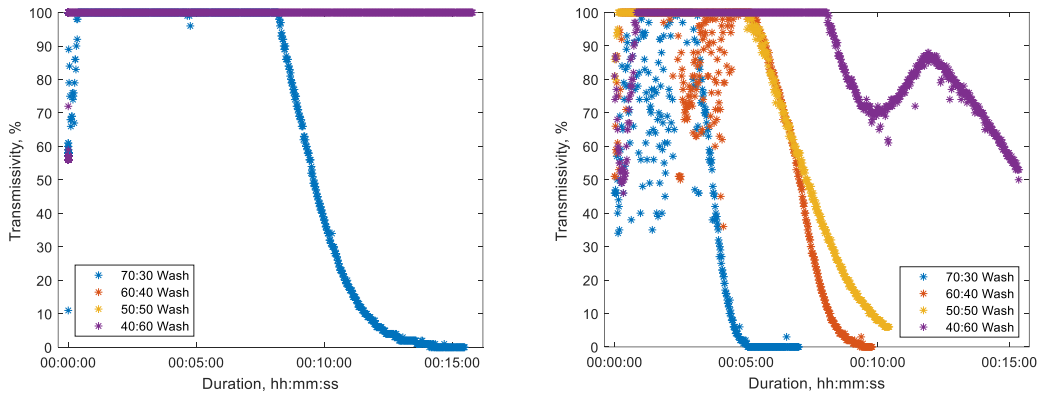

Figure 5-6 - Transmissivity profiles of antisolvent addition experiments for the two tested conditions. Left plot shows results from Exp-Low and the right plot shows results from Exp-High as described in Table 25..

The goal of these experiments is to determine which ratio of ethanol to water is the most suitable for washing the recovered material where the best system shows an absence or minimal nucleation. The trajectory comparisons in Figure 5-6 show the points where nucleation is taking place in the form of a drop in transmissivity. As can be seen from Figure 5-6, the drop in the level of transmissivity brought on by nucleation is very fast when using

the 70:30 solution for both tested conditions. This highlights that the current use of the 70:30 solution as the first wash solvent was unsuitable and the likely cause of the small needle particulates seen from the SEM images in Figure 5-3. Overall, there is a clear trend seen

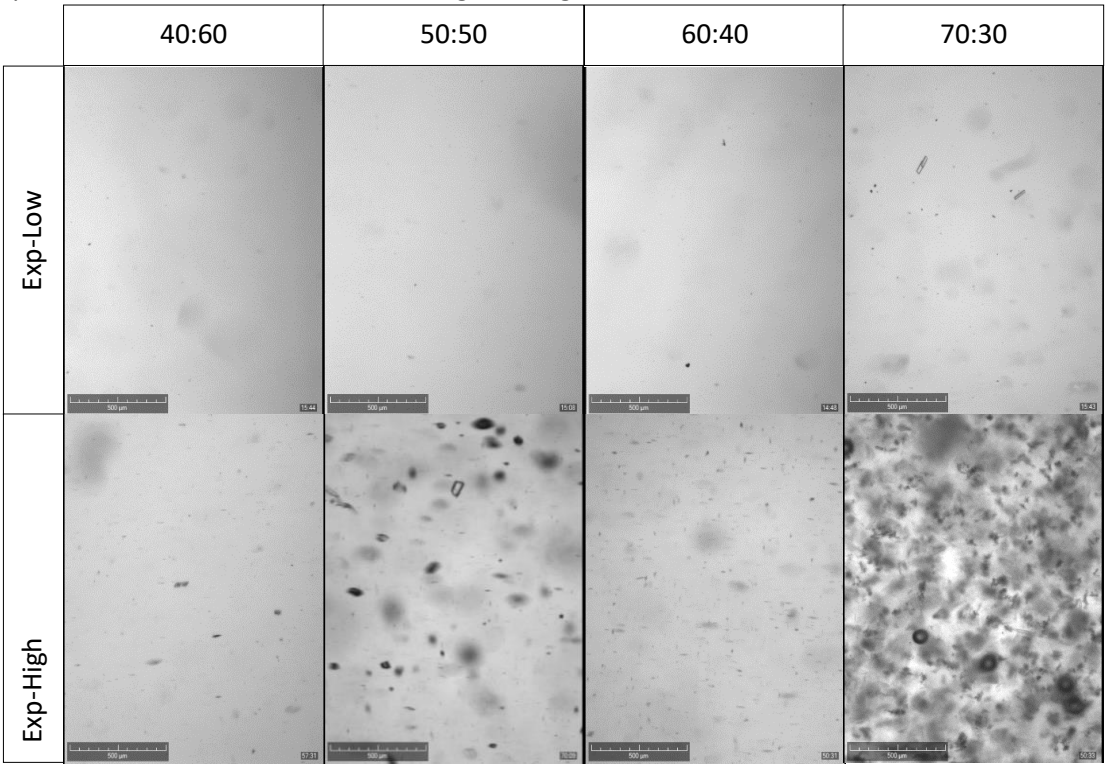

Figure 5-7 - Captured images displaying level of solid content from antisolvent effects from the addition of different wash solvents ratios after 5 minutes. Exp-Low and Exp-High are based on the lactose solution conditions described in Table 25

between higher antisolvent concentration and faster nucleation times.

As stated previously, this method of assessing wash solvent suitability was done for four wash solvent concentrations and two lactose concentrations. The images collected five minutes after the solvent addition can be seen in Figure 5-7. These display the respective level of solid density for each tested wash solvent. There are still some signs of nucleation for the higher temperature experiments using the lowest concentration solvent. The level of solid density is rather low and holds steady for the remainder of the experiment. However, the lower temperature experiments only show nucleation at the highest solvent concentration of

70:30. This is likely due to the lower concentrations of the lactose solution used corresponding to the saturated solution.

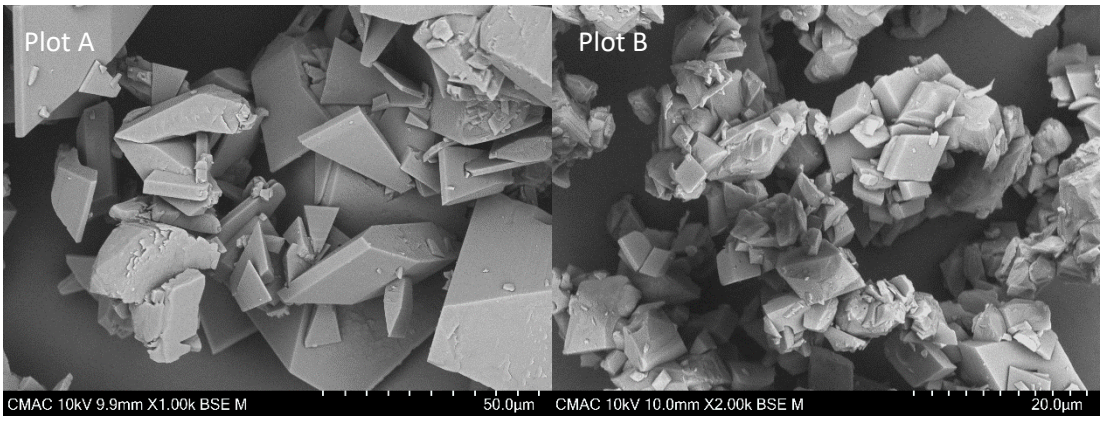

Figure 5-8 - SEM images collected from evaporative crystallisation experiments using the new wash protocol.

From the results of the wash solvent investigation, an improved wash protocol consisting of three washes has been deduced. The initial wash solvent was decided to be the 40:60 solution, as that showed minimal nucleation, followed by 70:30 and finally pure ethanol. This gradual increase in ethanol concentration allows for the antisolvent effects on the present mother liquor to be minimised prior to each wash while thoroughly washing the recovered crystalline material. The effectiveness of the new wash protocol was investigated via SEM images of recovered crystallisation material from additional growth experiments as can be seen in Figure 5-8. These images show there is agglomeration in both experiments but the presence of needle-like particulates on the surface of the crystals has been removed compared to the previous wash method seen in Figure 5-3

Additionally, XRPD patterns of the recovered crystalline material from growth experiments using both wash protocols can be seen in Figure 5-9. All patterns show the distinctive ALM peaks at 20°[87]. However, the beta-lactose peaks at 10.5° can only be seen from the patterns collected from the original wash protocol starting with a high ethanol concentration of 70:30. These results confirm that the needle crystals present in the original results were

beta-lactose as opposed to ALM. Importantly, the new wash protocol starting with a lower ethanol:water ratio of 40:60 has proven to remove the presence of antisolvent effects and uncontrolled nucleation of beta lactose during washing.

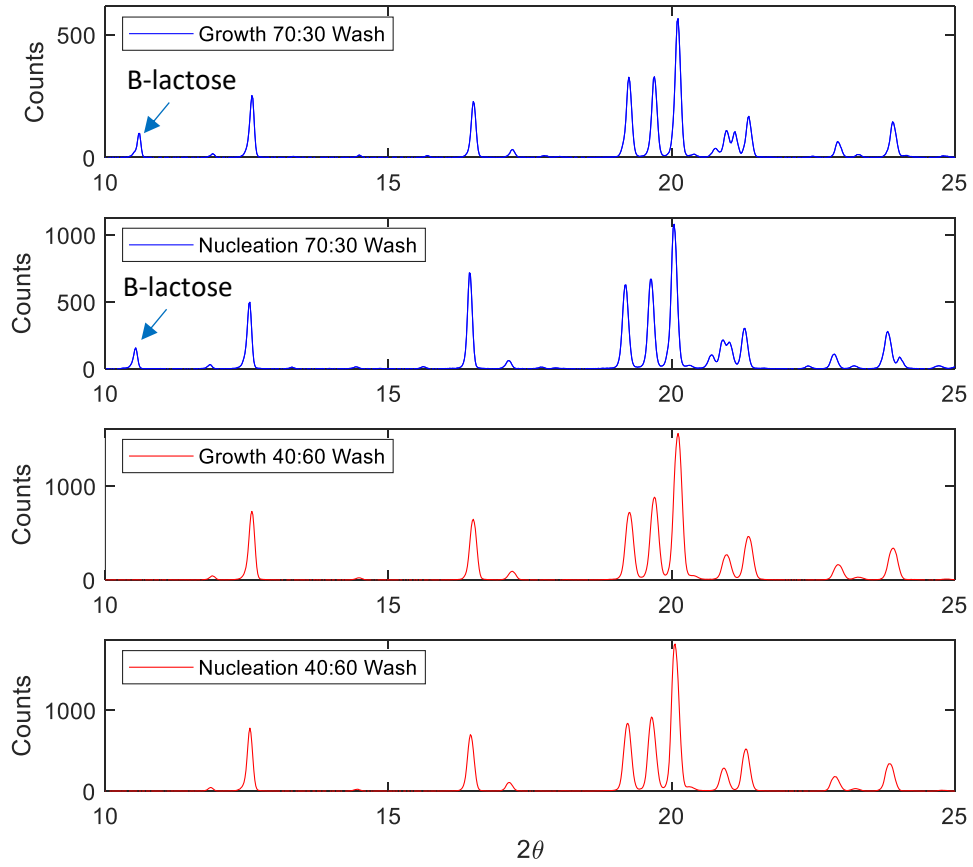

Figure 5-9 - XRPD patterns comparing recovered material from evaporative crystallisation using different wash protocols. Blue – "Old" Wash used. Red – "New" Wash protocol followed.

5.5.3 Growth and Agglomeration Experiments

Due to the high concentration and temperatures being investigated within the evaporative process, there were instances of nucleation detected within the seeded desupersaturation experiments. As such, the experiments known to experience only growth were used for the modelling of the system. This limited the experiments input within the model validation to two growth experiments with different working temperatures and different initial

supersaturation levels. The temperature range investigated within this work varies only between 65 and 80 °C due to the limitation of the vacuum pressures achievable within the system and the maximum temperature of 93°C for α-lactose crystallisation. Due to the small working range of interest, the lower number of experiments is considered sufficient to characterise the crystallisation process's behaviour under these conditions.

The power law, shown in Equation 3, was focused on for the fitting of the growth kinetics of this system. It was investigated in terms of absolute and relative supersaturation. Relative saturation was found to fit the experimental data more closely in terms of concentration trends. Similarly, the inclusion of the exponential term to incorporate temperature dependence of the kinetics was also found to produce a better fitting growth model in agreement with the cooling crystallisation model discussed previously. Following, the initial fitting of the growth terms, the agglomeration model is made active and fitted to account for the agglomeration seen in the SEM images Figure 5-8. Following the learnings of the modelling of the cooling crystallisation, the process of fitting agglomeration and growth kinetics are finalised together.

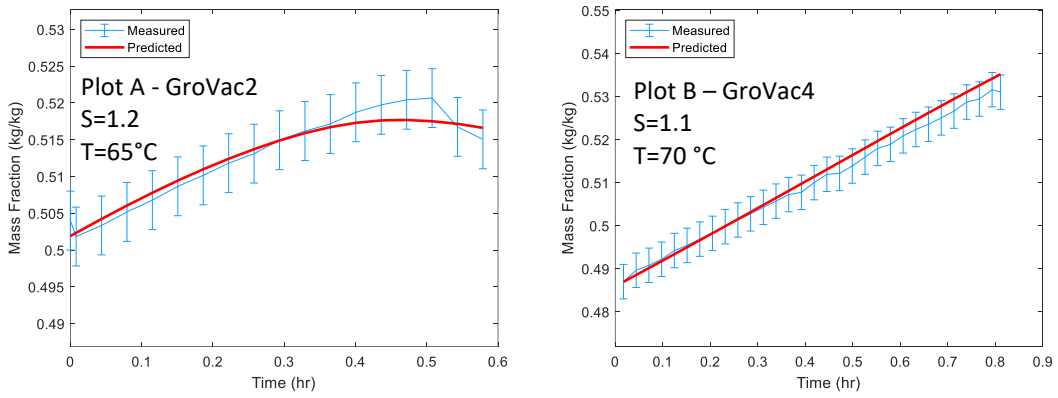

Figure 5-10 – Comparison between the predicted and measured concentration profiles of the growth experiments.

Red- model predictions. Blue – Measured values

As shown in Figure 5-10, the measured concentration profiles follow a steady increase due to the evaporation of water then there is a plateau followed by a drop in concentration. This plateau shows the point at which the dominant mechanism affecting concentration shifts from evaporation to crystallisation in the form of growth. The onset of the plateau, which will be hereby referred to as the 'shift-point', is only just visible in Plot B this is due to the lower level of supersaturation at the point of seeding. The shift-point is more clearly seen in Plot A likely corresponding to the higher supersaturation ratio of 1.2. The prediction of the concentration profiles from the fitted growth and agglomeration model fits the overall trend across both experiments. However, the shift-point seen at the end of Plot B is not currently described by the model and instead, the linear trend is continued to the end of the experiment. Similarly, the shift-point of Plot A is much sharper following the measured value compared to the more gradual curve predicted by the model. The deviation across these experiments is, however, within 1% relative variance of the measured values and as such considered acceptable.

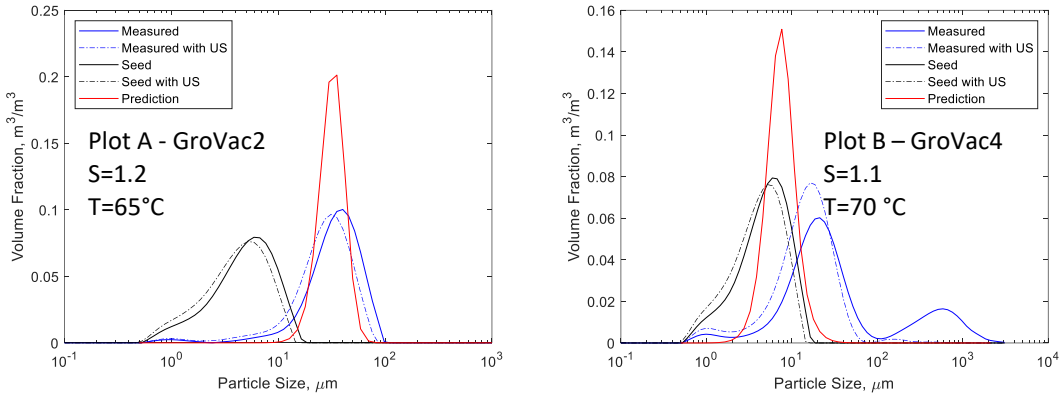

Figure 5-11 - Particle size distribution comparisons between the measured values and the predictions from the developed model.

The necessity of fitting the agglomeration kinetics in the form of the Mumtaz number was highlighted during the preliminary experiments. Following the fitting of the growth kinetics initially, the Mumtaz number was then investigated in parallel with the growth terms. This

was necessary as the previous fitting of growth and agglomeration kinetics found the presence of agglomeration had a significant effect on the concentration profiles when using such small seed particles. The resulting particle size predictions from the growth and agglomeration model can be seen in Figure 5-11. The prediction for the quantile sizes is consistently undersized across all experiments. Particularly the D90 predictions, which show the model's lack of fit for the agglomeration seen experimentally. The measured size quantiles are quite broad when considering the very small D10 values seen in Table 29. As such, the broadness is difficult for the agglomeration kernel to capture as it tends to produce narrow distributions.

5.5.4 Primary Nucleation Experiments

Following the fitting of the growth and agglomeration kinetic parameters, the model validation is focused upon fitting the primary nucleation kinetics. The main advantage of using evaporative crystallisation over cooling is the faster inducement of nucleation due to the higher temperature and supersaturation values reached by the system. As such, the fitting of the primary nucleation parameters is key for the usefulness of the resulting model.

Parameter	Units	Fitted Value	St Dev
Growth rate constant	m/s	0.00437	8.58E-03
Supersaturation order	(-)	5.911	1.663E-01
Activation energy	J/mol	20804	5.568E+03
Mumtaz Number	N/m	0.003223	2.994E-04
Primary nucleation rate constant	Ln(#/m^3.s)	60.562	1.695E+01
Supersaturation order	(-)	2.907	4.448E-01
Activation Energy	J/mol	93605	4.670E+04

Table 28 - Fitted kinetics parameters for the evaporative crystallisation model. The goodness of fit for this model found that concentration was predicted very well by the model with a χ^2 0f 39.5 compared to a higher $\chi^2_{critical}$ of 177.4. However, the PSD has not been captured well by the model with a χ^2 significantly greater than $\chi^2_{critical}$ of 338.4 compared to 25.0.

The concentration profiles are supplied to the model validation for the estimation of the primary nucleation kinetics and as such only points following the onset of nucleation are included. Across the primary nucleation experiments, the shift-point is very clear and occurs significantly later than the point of nucleation recorded by the FBRM data. The broadness of the plateau in Plot B of Figure 5-12 is due to a drop in temperature from 75°C to 63°C resulting in the drop of evaporation rate hence the steady concentration between 1.75 and 2 hrs. This drop in evaporation was included in the performed experiment within gFP allowing the experiment to be used for the fitting of the kinetic parameters.

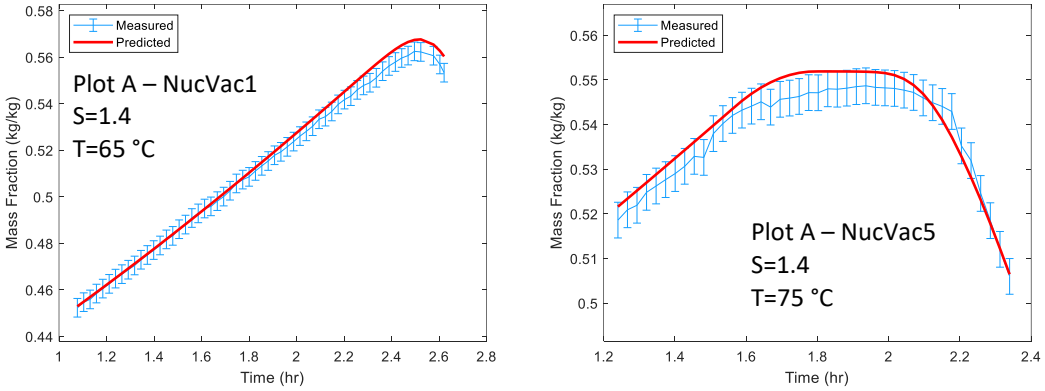

Figure 5-12 - Concentration profile comparisons between the measured values and the predictions of the developed mechanistic model. Red- model predictions. Blue – Measured values

Exp.	PSD Quantile					
	D10		D50		D90	
	Measured	Predicted	Measured	Predicted	Measured	Predicted
GroVac2	11.6	22.0	29.9	33.2	54.7	47.1
GroVac4	4.54	3.5	15.8	6.4	34.3	11.9
NucVac1	35	48.2	74.8	75.7	139	112.9
NucVac5	15.3	37.9	57.7	59.2	151	88.8

Table 29- PSD quantile comparison between measured values and the predicted values from the mechanistic model.

The power law was chosen for the fitting of the primary nucleation kinetics. As can be seen in Figure 5-12 the resulting predictions for the concentration profiles fit the recorded

concentrations within a reasonable error. The error is inputted as a constant relative variance of 1%. It should be stated at this stage the growth and agglomeration kinetics were also opened for variation to improve the fitting of the kinetics to a greater set of experiments. This resulted in a very acceptable model with a χ^2 value of 39.5 which is notably lower than the critical value of 177.4 when considering the concentration predictions. The PSD data was also supplied for the fitting of the resulting kinetic data. The model's ability to predict the curvatures seen as both the experiments cross the shift-point is considered very encouraging. The prediction of PSD comparisons can be seen in Figure 5-13 and Table 29. The D50 predictions for the primary nucleation experiments are seen to be very accurate. Again, the broadness of the full PSD is not quite captured by the model. This poor ability to predict the overall distribution is captured by the failed goodness of fit test with respect to PSD with a significantly higher χ^2 value compared to the critical value as seen in Table 28. This ultimately highlights a failure in the model to adequately describe the evaporative crystallisation process as a whole despite the promising concentration predictions. This limitation in the model is likely due to the agglomeration parameter as this would have no direct effect on concentration but would ultimately hinder the effectiveness of the model to predict PSD. The overall narrowing of the PSD when modelling agglomeration was also seen for the cooling

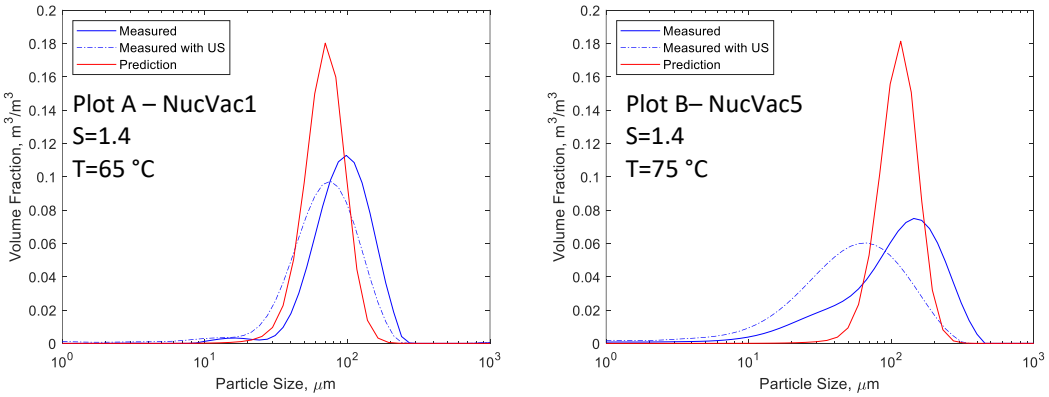

Figure 5-13 - Particle size distribution comparisons between the measured values and the predicted values from the mechanistic model.

model developed in section 3. The D50 predictions are very encouraging as shown in Table 29 and suggest that although the shape of the PSD is predicted poorly the D50 is an accurate guide to the size of the material produced experimentally.

5.6 Global Systems Analysis

5.6.1 Kinetics

The resulting effects of the uncertainty of the fitted kinetic parameters on the predicted outputs of the system are investigated within this section. In the case of this work, the kinetics have been fitted using a very small set of experiments due to the difficulty in controlling the crystallisation platform as such the error with the fitting of the parameters is of keen interest.

Response	Expected Value	Std	range
Crystal mass (g)	0.0561	0.0025	0.0201
$D_{4,3}$ (µm)	355.86	43.79	313.42

Table 30 - Distribution statistics for process outputs due to the variance of the fitted kinetic parameters of the mechanistic model.

The process outputs of interest from the model were highlighted as crystal mass and $D_{4,3}$. These were decided upon for two reasons: the use of evaporative crystallisation for seed generation and the improved yield compared to cooling crystallisation. As can be seen from Table 30, the uncertainty of the fitted kinetic parameters is found to maintain fairly consistent crystal mass recoveries and the standard deviation is relatively small. Conversely, the recorded range seen for the crystal mass recovery is rather large. Additionally, the effect of the uncertainties on the average particle size is found to be much greater with a standard deviation of 43.79 µm and a range of 313.42 µm which is equatable to the expected value of

355.86 µm. The uncertainty of the fitted parameters is shown to lead to a very strong deviation in average particle size, suggesting a need for greater validation of the mechanistic model.

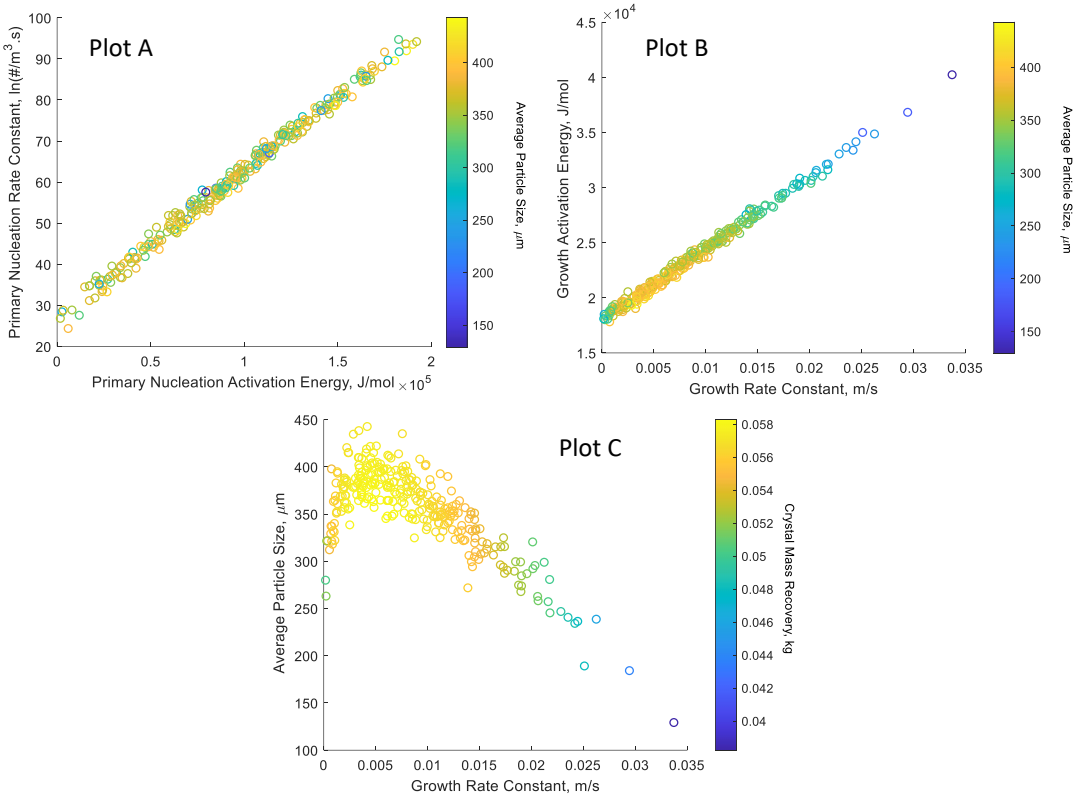

Figure 5-14 - plots depicting the variance of selected fitting kinetic parameters and their resulting effect on process outputs. Plot A and Plot B - Colour bars trend from blue to yellow denoting the increase of the final average particle size. Plot C - Colour bars trend from blue to yellow denoting the increase in crystal mass recovery.

The primary nucleation kinetic parameters were found to have no direct relationship with average particle size or crystal mass recovery. The covariance relationship between primary nucleation activation energy and rate constant is displayed in Plot A and clearly shows the lack of trend for average particle size. Similarly, the covariance relationship between the growth activation energy and the growth constant is shown in Plot B. However, there is a clear relationship with regard to average particle size as shown by the clustering of the larger particle sizes at lower growth rate constant values. This effect is more clearly seen in Plot C

with a maximum for both particle size and crystal mass recovery around the fitted growth rate constant value of 0.00437 m/s.

5.6.2 Process Conditions

This section identifies the important process conditions affecting the outputs of the process. This can be used as the starting guide for the optimisation of the process and more generally the capabilities of the system. The optimisation has been approached from two possible objectives: increasing yield and increasing $D_{4,3}$. Due to the complicated nature of the set-up, the factors that are readily controllable are limited to temperature via pressure control, initial concentration and batch time. The importance of all three variables on process outputs is highly correlated in that the time to nucleate would depend on the supersaturation levels within the experiment which are directly dependent on initial concentration and temperature. As such, for the purposes of investigating the effect of process conditions on the yield and particle size it was decided to link the initial concentration and temperature inputs. This allowed the initial concentrations to always coincide with an initial supersaturation ratio of 0.9 for all corresponding temperatures. It should also be noted that the evaporation rate was set constant for the purposes of the uncertainty analysis. This is simply due to the inability to directly control the evaporation rate during the experiments. The recorded evaporation rates for a number of different experiments were examined and no discernible link between evaporation rate, temperature or concentration was seen. As such, there is no credible way to assess the effect of the evaporation rate on the process outputs. This is a known limitation of the model at this stage that can only be aided by the inclusion of evaporation kinetics that were not considered for this work.

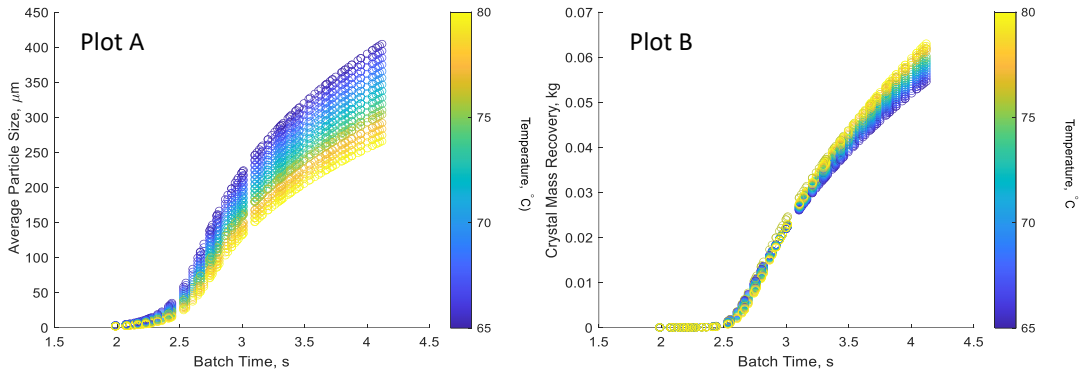

Figure 5-15 - The effect on selected process outputs from the variance of the process conditions. Colour bars trend from blue to yellow denoting the increase in temperature of the vessel.

The relationship between process outputs and the controlled variable of temperature and batch time is displayed in Figure 5-15. The increase in temperature is shown to have a positive effect on the crystal mass recovery of the system. This is likely due to the increase in growth rate seen at higher temperatures. Surprisingly, the larger temperatures are shown to have the opposite effect on average particle size. As discussed previously, the growth rate would be expected to be increased at higher temperatures. This effect is linked to the lower temperature simulations reaching higher supersaturation values than the higher temperature counterparts. Therefore, the higher supersaturation ratios increased the growth rate experienced by lower temperatures simulations leading to larger-sized particulates.

5.7 Optimisation

The clear advantage of the evaporation process, as opposed to cooling crystallisation, is the increase in crystal mass recovery and as such it is of keen interest to investigate the capabilities of this system through the use of simulations. Consideration of the level of solid content within the system at any given time is key for the suitability of the tested process

conditions. As such, the inclusion of an interior constraint, based on Equation 22, has been made to ensure the process is practicable in real life.

Equation 22

$$solid\ content\ \% = \frac{100 * Mass\ of\ solids}{Mass\ of\ solids + Mass\ of\ liquid}$$

For simplicity, the initial concentration was held constant and only temperature and batch time were investigated for optimisation purposes. As discussed previously, the evaporation rate of water from the system is not directly controllable or modelled and is an inherent inaccuracy in the model.

The two goals of optimising this process are to increase yield and particle size. Figure 5-16 shows the attainment capabilities of this system and as such guides the inputs for the process variables for the optimisation of the system. Plot A shows that to maximise the average particle size produced within the system large batch times and lower temperature values are favourable. Alternatively, Plot B shows large batch time and higher temperature values to increase yield. However, the temperature effect is very minimal and not expected to play a large role in the optimisation of the crystal mass recovery. It should also be noted that $D_{4,3}$ and mass recovery are highly correlated due to the fast kinetics of the system as can be seen in Plot C and Plot D of Figure 5-16.

The optimisation of the process is centred around the manipulation of temperature and batch time. The initial concentration is held constant at a supersaturation ratio of 0.9 for the lowest temperature of 65 °C assessed within this work. This allows for the testing of all initial temperatures as the saturation concentration for any given temperature will be reached given sufficient time for adequate evaporation to take place. The optimisation of this process

is focused upon the two different uses for the evaporative process: seed generation, and high recovery batch crystalliser. The optimisation of the developed model allows for different evaporative crystallisation setups to be investigated digitally without the need for physical set-up and experimentation.

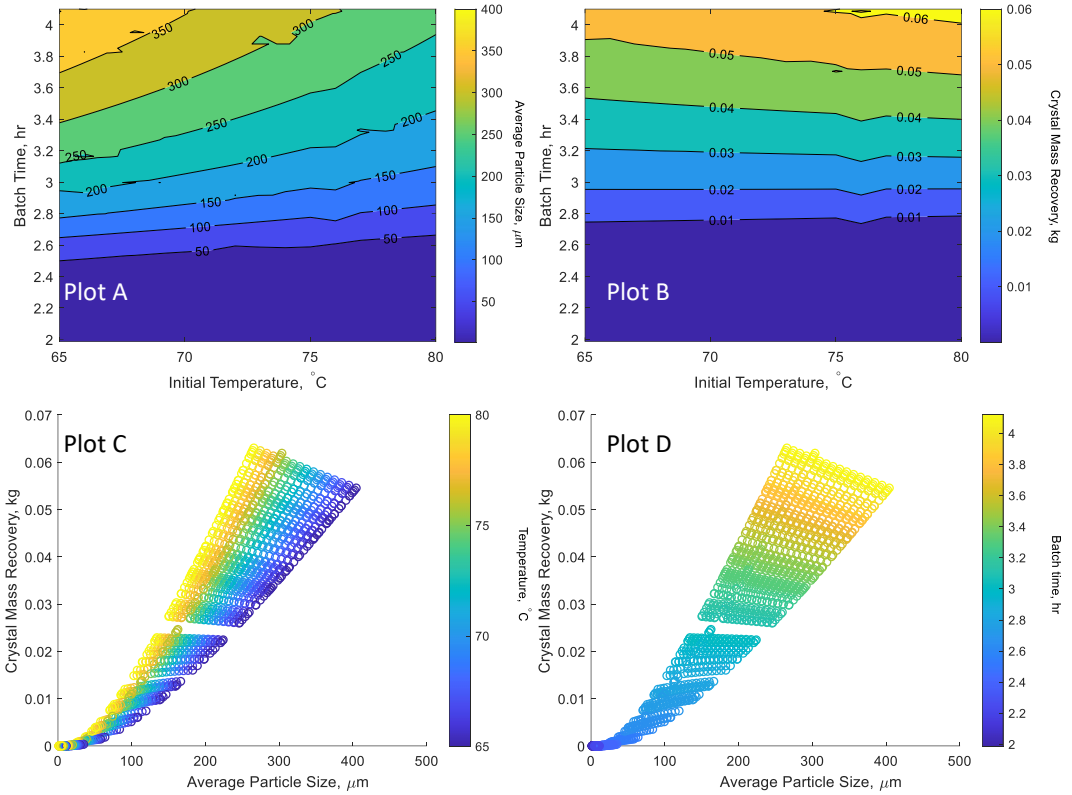

Figure 5-16 - Contour plots showing the attainable regions of process outputs of interest in relation to process conditions.

5.7.1 Batch Optimisation

Batch time (hr)	Temp (°C)	Average Particle Size (μm)	Crystal Mass (kg)
4.06	65	386	0.052

Table 31 - Optimised conditions and the resulting process outputs.

The simplest method of investigating the system is the optimisation of the batch crystalliser that was tested for the development of the model. In this case, the focus is to optimise the

crystal mass recovery and the size of particles produced. The only constraints imposed for the optimised pathway are a maximum solid content of 40% and a maximum supersaturation of 1.55. The optimised conditions and outputs can be seen in Table 31 and Figure 5-16. As expected, there was a preference for lower temperatures for the increasing particle size. The operating temperature of 65°C is the lower bound of interest and is also the lowest temperature tested on the experimental setup. The final average particle size of 386 µm is considered very large for a batch time of only just over 4 hours. Comparing the recovered L_{50} of 360 µm from an industrial cooling crystalliser with a batch time of 13 hours from the work of Wong et al the prediction of a comparable L_{50} of 377 µm from a 4-hour evaporative crystallisation is impressive [88]. Evidently, direct comparisons between an industrial plant experiment and a small batch experiment are impossible due to the added consideration of scale. However, the promise of evaporative crystallisation as a method of producing large lactose crystals fast is clear.

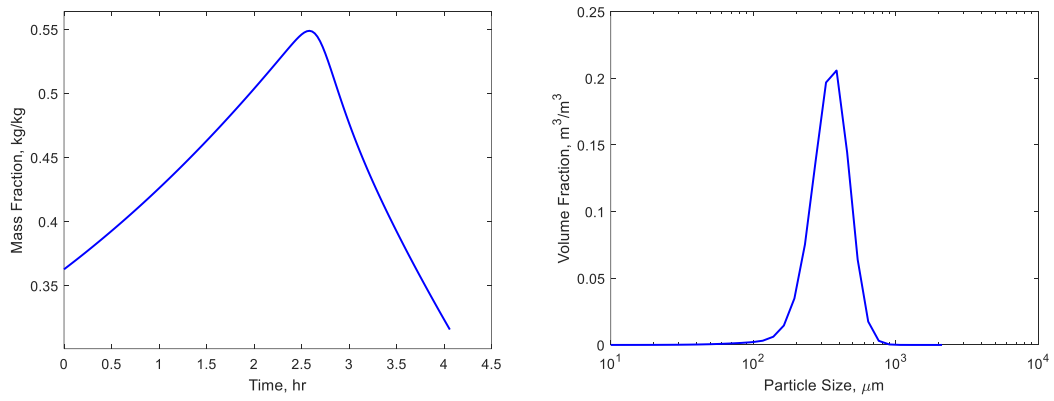

Figure 5-17 - Concentration profile and final PSD of simulated optimised batch process.

5.7.2 Optimising a Potential Seed Generation

The unique attribute of the evaporative process compared to the cooling is the ability to nucleate material in short time frames. Therefore, the investigation of using the evaporative

crystallisation platform as a fast seed generation unit is desired. The goals of such a platform are very different from the previous optimisation of the crystal mass recovery from batch processing in that small sizes are desirable for the purpose of seeding. As such, interior constraints were set to obtain an average particle size between 50 µm and 100 µm similar to Wong et al 2012[88]. Additionally, the maximum solid content was maintained at 40% to ensure realistic and desirable working conditions within the vessel.

Batch time (hr)	Temp (°C)	Average Particle Size (µm)	Crystal Mass (g)
3.79 (2.37)	80	99.02	12.07

Table 32 - Optimised conditions and the resulting process outputs.

Due to the fast nature of the crystallisation process under evaporative conditions, the production of small particles is inherently linked to a low yield. As can be seen from Table 32, the desired particle size of below 100 µm has been captured with a value of 99 µm and a subsequent mass recovery of 12g. Unlike the optimisation of the batch recovery, the optimisation of the seed generation unit favours a higher temperature of 80°C and slightly shorter batch times. This predilection for higher temperatures is in agreement with Plot A in Figure 5-16.

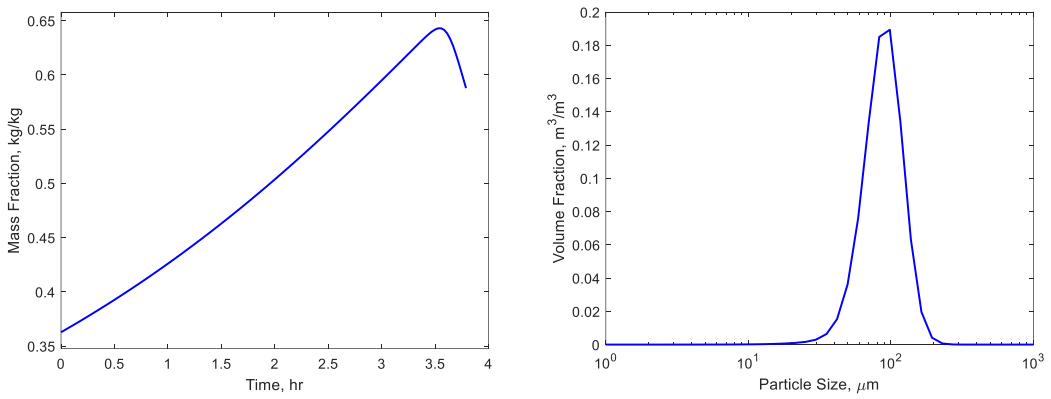

Figure 5-18 - Concentration profile and final PSD of optimised seed generation process.

The main variable controlling this process is the batch time as the goal is to stop the growth of the particle from growing beyond the desired size range. This subsequently limits the crystal mass recovery possible for the given particle size. However, a mass of 12 g from one batch run of fewer than 4 hours would be sufficient for seeding purposes for many experiments depending on scale. A potential problem with the proposed optimised processes is the lack of control of process outputs as they are fundamentally linked to batch time. The changes in concentration and particle size are quite sharp as can be seen in Figure 5-18 and the ability to control these outputs is likely to be difficult and open to variance.

5.7.3 Limitation of Model

Unfortunately, due to the nature of the evaporative process, there is no other method of controlling the system with the current level of characterisation of the platform other than temperature and batch time. As the model is currently defined without the inclusion of the pressure and temperature relationship the system is forced to work under isothermal conditions. If the evaporation kinetics were considered, then an additional control variable of pressure could be manipulated to alter the evaporation rate through temperature. Additionally, the current model is assumed to have a constant flowrate out of the vessel of 0.017 g/s with the corresponding mass of water removed to mimic the evaporation of water of around 0.0065 g/s to 0.0085 g/s. As such, the evaporation rate has no defined relationship with temperature. These limitations in the defined model have a direct restrictive effect on the ability to optimise the platform for given parameters.

5.8 Conclusion

A vacuum-induced evaporative crystallisation platform was developed for the investigation of the crystallisation kinetics of the system. The use of vacuum conditions allowed for the

evaporation of water from a lactose-water solution in a temperature range suitable for the crystallisation of alpha-lactose monohydrate. The platform itself was developed to ensure pressure was maintained throughout the experiments including during the addition of seed. Preliminary results of seeded evaporative experiments were found to be unsuitable using the current wash protocol followed for lactose crystallisation. As such, an investigation into suitable wash solutions was tested and a new wash protocol for the expected recovery concentrations from the evaporative process was designed and implemented.

Following the development of the platform, the investigation into the crystallisation kinetics of the system was focused upon. This system was investigated with the aim of fitting the agglomeration, growth and primary nucleation kinetics for the development of a mechanistic model. Minimal experiments were used for the development of this model due to the difficult nature of controlling the platform. The concentration profiles for all experiments are shown to pass the goodness of fit test. However, the prediction of the particle size quantiles does not pass the test as was expected from the comparison of the predicted PSD and the recovered experimental values as shown in Figure 5-11 and Figure 5-13. Two of the fitted kinetic parameters were calculated to have high standard deviations and the corresponding effects on the process outputs were shown to be prevalent. The variation in predicted process outputs based on the variance of the fitted kinetic parameters is particularly evident with regard to the particle size resulting in a large range of predictions but a much smaller standard deviation of 43 μm. The high standard deviation and the resulting effect on process outputs highlight the benefits to the model that could be made with more experimental data to fit the parameters. Unfortunately, due to the unsteady nature of the platform, this was not suitable at this stage.

The investigation into the effect of varying the process conditions was limited to temperature and batch time. This highlighted the capabilities of the system in terms of particle size and crystal mass recovery. The ability to utilise the model in the place of experiments for the optimisation of the process for a range of goals was shown. The developed mechanistic model allowed the optimisation of a batch evaporative crystalliser to be investigated. The result showed an optimised process producing particles of 370 µm within 4 hrs and a crystal mass recovery of over 52 g. This far exceeds the capabilities seen experimentally from either the cooling or evaporative processes within this work. Additionally, the process was optimised focusing on the production of suitable-sized particles for seeding other processes. This showed the capability of the platform to produce 12g of material with an average particle size of 99µm. The clear advantage of this mechanistic model is that it has allowed for the testing of extremes the evaporative platform could be used for.

The developed model for the evaporative crystallisation of lactose was found to accurately describe the concentration profiles but did not capture the overall PSD shape despite good predictions for D50. The resulting errors on the fitted parameters were found to be quite high which is likely due to the limited number of experiments performed and used for model development. The potential for a vastly improved yield has been found through the optimisation of the process suggesting a significant improvement in both the cooling crystallisation work in chapter 3 and the evaporative experiments performed within this chapter.

6 Multimode Continuous Crystallisation Configuration

6.1 Introduction

With mechanistic models of both the evaporative and the cooling crystallisation of lactose from water defined previously, a unique opportunity to test configurations for continuous multimode crystallisation platforms is made possible. As such, this chapter will implement a theoretical assessment of the suitability of different configurations of continuous platforms for the recovery of lactose. As discussed previously in section 5.1.1, the use of evaporative crystallisation has been studied at both laboratory and industrial scales. The typical method of evaporative crystallisation on an industrial scale is the FCC but within this chapter, the focus will be MSMPR due to the capabilities of studying on a small scale and the previously built mechanistic model.

6.2 Continuous Evaporative Crystallisation

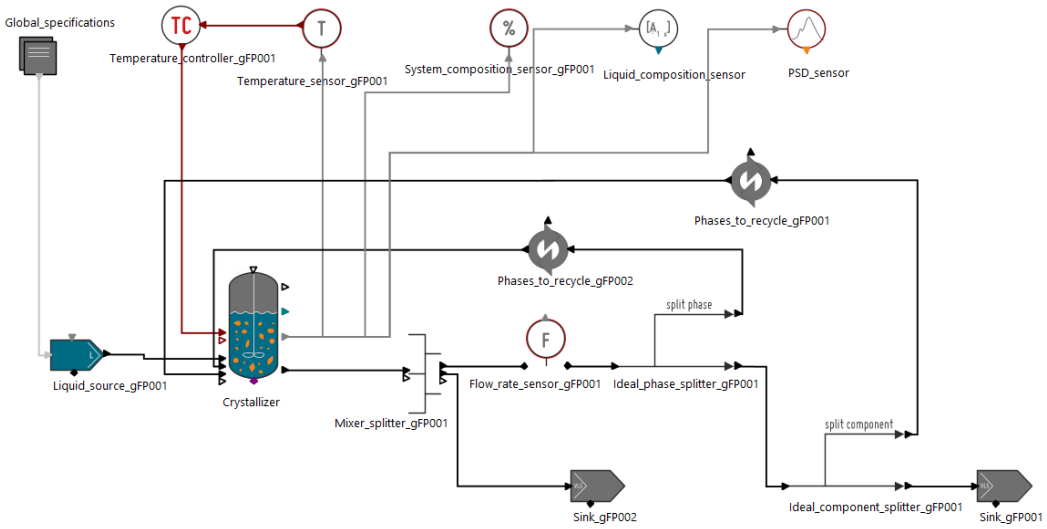

Figure 6-1 - gFP flowsheet depicting the continuous evaporative crystallisation process.

The conditions used for the crystalliser were set to the tested conditions experimentally to allow for confidence in the evaporation rate. This allows the flow rate used to mimic the evaporation rate to be from experimental tested conditions. As such, the temperature is set at 67.5 °C and the flow rate to pass through the ideal splitter sections is set to 0.017g/s. The continuous configuration is shown in Figure 6-1.

Manual mass balance calculations were done across this system with assumed concentrations and solid content recovery to allow for initial guesses during the optimisation of the process. The system was optimised over a longer simulation time than necessary to ensure a steady state was reached. The optimisation was based on the variation of the feed flowrate, flowrate leaving the vessel and the mixer-splitter fraction. As the consideration for an evaporation rate recorded experimentally the flowrate passing through the ideal splitter sections was constrained to the measured value of 0.017 g/s. The only other constraint imposed on the optimisation was the limitation of a supersaturation ratio below 1.6 to avoid the secondary nucleation threshold as this has not been covered within the model.

6.3 Methods

This chapter focuses on the utilisation of pre-existing mechanistic models to allow for investigation into continuous and multimode platforms through digital means. The potential for these hypothetical crystallisation configurations is achieved through the use of global systems analysis and optimisation capabilities within gFP. The methods utilised for these techniques have been discussed previously in sections 3.4.5 and 3.4.6.

6.3.1 Continuous Unseeded Evaporative Crystalliser

The first configuration of interest is taking the model developed from batch evaporative crystallisation processes, in the previous chapter (5) and converting it to continuous mode.

This continuous evaporative crystalliser model can then be used to find the steady-state conditions needed for producing sought-after particulates. The capabilities of the evaporative crystalliser in terms of continuous manufacture are investigated by utilising the modelled kinetics of the system without further experimentation. The batch evaporative crystalliser was optimised in the previous chapter (5) for PSD and crystal mass, however, the continuous configuration will allow greater control by obtaining desirable attributes at steady-state conditions. The ability to utilise the evaporative model to design a theoretical continuous evaporative crystalliser has the potential to offer a dynamic solution to the slow nucleation kinetics of the lactose system being studied.

Optimised Variable	Unit	Final Value	Initial Guess
Crystalliser → mass fraction (lactose, liquid phase)	[kg/kg]	0.4045	0.5039
Crystalliser → mass fraction (water, liquid phase)	[kg/kg]	0.5955	0.5961
Crystalliser → Flow rate set point	[g/s]	0.1241	0.1363
Feed→ Mass flow rate set point	[g/s]	0.1140	0.1262
Feed→ Mass fraction (lactose)	[kg/kg]	0.5569	0.5613
Feed→ Mass fraction (water)	[kg/kg]	0.4431	0.4377
Mixer splitter → Split fraction	[-]	0.1362	0.1240

Table 33 - Optimised process conditions for maximised recovery from the continuous evaporative crystallisation.

Optimisation of the continuous evaporative crystalliser for solid content in the product stream was focused upon. The introduction of the continuous mode allows for more control of the process outputs as the previous batch mode shows sharp changes in PSD and solid mass recovery due to increasing supersaturation levels within the vessel. However, the continuous mode allows process outputs to be maintained at steady-state conditions and subsequently allows for easier and more consistent product recovery. The process conditions

found to maximise the solid content in the product stream are shown in Table 33. These process conditions allowed for the recovery of ALM particles with a $D_{4,3}$ of 401 µm with a product stream solid content of 7.97 %. The particle size allowed for this optimised process was limited to below 400 µm due to considerations for downstream processing which has only been slightly eluded.

The time for steady-state to be reached is found to be relatively short for this process at around 5.5 hrs. The optimised conditions produce a solid product flowrate of 30.8 g/hr which is not considered high. The increase in control of particle size and solid content due to the continuous configuration has resulted in a loss of recovery. This is an unfortunate disadvantage of the continuous platform. However, comparing the particle size and solid content profiles for the continuous platform to the optimised batch process the control that is offered through continuous manufacturing for this system is very clear. It should also be noted that although 30.8g/hr is not a large solid recovery, the largest recovery from the batch process seen experimentally was roughly 40 g for a 4-hour batch time. Therefore, comparing the batch and continuous processes in terms of crystal mass recovery would favour the continuous when considering larger running times.

6.3.1.1 Sensitivity Analysis

Due to the continuous nature of the proposed process, the effect of the variation in flowrates on the process outcomes is key to the suitability of the proposed configuration. Therefore, the robustness of the continuous evaporative crystalliser was investigated by allowing variation of the flowrate setpoint within the system. The advantage of the continuous platform is the consistency in the produced material in terms of size and yield. As such, the effects of the variation of the flowrates away from the setpoints due to disturbances and

other minor unavoidable variations on the process outputs are key to the robustness and suitability of the proposed process.

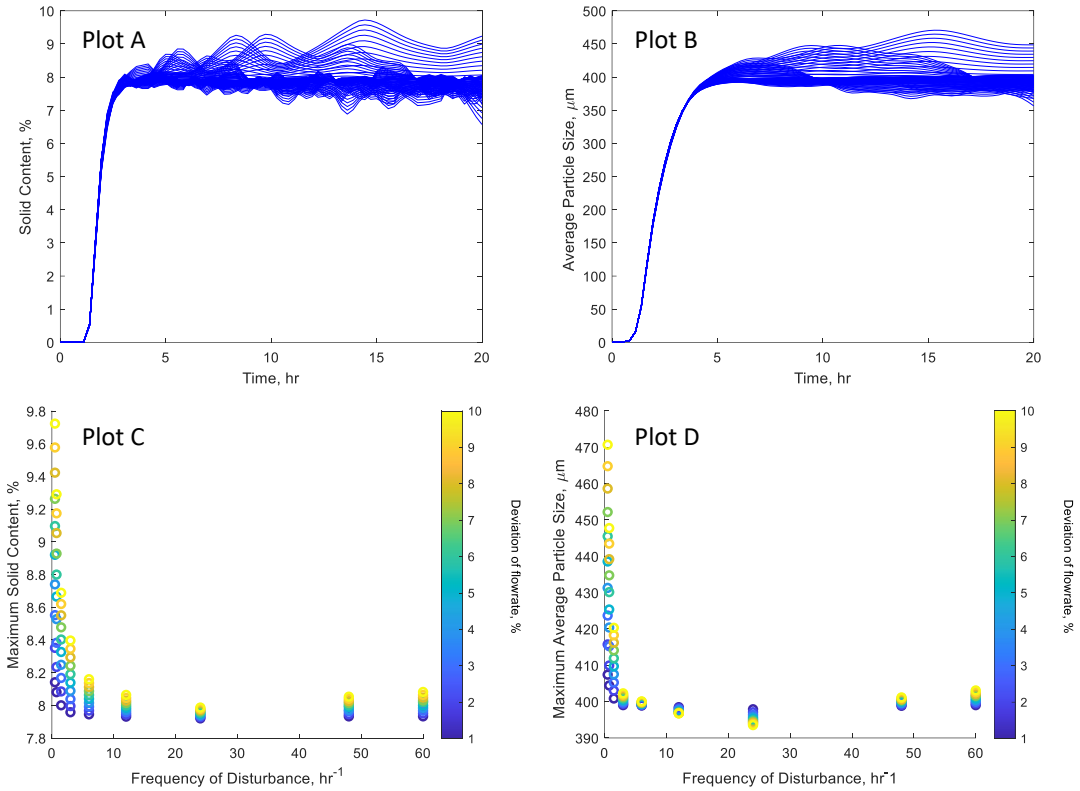

Figure 6-2 - Sensitivity analysis of feed flowrate disturbances. Plots A and B show disturbance effects over time. Plots C and D show the maximum effect seen due to disturbances of different frequencies and magnitudes.

The variation of the feed flowrate and the flowrate leaving the vessel was allowed to vary via uniform distribution with limits of +/- 10% of the optimised value discussed previously. Some of the tested conditions resulted in the vessel emptying and as such the failure of the process. Additionally, solid content in the recovery stream and the particle size were shown to vary across a large range. The consistent error of a flowrate exceeding or undershooting for the whole process is an unusual problem only seen if there were problems with the pump calibration. However, the onset of sharp changes in flowrates such as surges can be caused by upstream processing conditions or control settings. Therefore, it was decided that testing the system's ability to handle fluctuations in the feed flowrate in terms of disturbances would

give an insight into the robustness of the configuration. The disturbances were investigated in terms of frequency and level of deviation from the setpoint value. As can be seen from Figure 6-2, the presence of disturbances was only seen to greatly affect the process outputs for frequency values below 1 hr^{-1}. This is due to the slowness to correct for such low frequencies. The ability of the system to remain steady with the presence of these disturbances highlight the system's robustness to flowrate changes. It should also be noted that with adequate controls and monitoring, the correction of disturbances would be quick enough to avoid the high variance seen within Figure 6-2.

Value	Process Output	Unit	Exp. Value	St.Dev	Min	Max	Median
Max	Average particle size	µm	403.63	13.299	393.54	470.71	399.64
	Solid content	%	8.12	0.33	7.92	9.72	8.01
	Liquid mass	kg	0.255	0.0170	0.250	0.364	0.250
Final	Average particle size	µm	393.52	13.434	352.98	448.63	395.97
	Solid content	%	7.79	0.37	6.40	9.24	7.88
Min	Liquid mass	kg	0.203	0.0179	0.140	0.244	0.207

Table 34 - Sensitivity analysis distribution statistics.

The recovered distribution statistics of the process outputs shown in Table 34 upon the variation of the simulated disturbances to the feed flowrate shows the presence of broad ranges for the minimum and maximum values predicted for the final solid content and the particle size. These broad ranges would suggest a lack of stability in the process when dealing with fluctuations in the feed flowrate. However, combining the results in Table 34 and Figure 6-2 it is clear the large variations are all seen for low frequency and high variation percentage and as discussed previously, the use of adequate control and process monitoring would negate such persistent runoff of process conditions. Additionally, the median value for both particle size and crystal mass recovery is quite consistent for both the final and maximum values suggesting an overall consistency to the process outputs.

6.3.2 Seed Generation Unit

Optimised Variable	Unit	Final Value	Initial Guess
Crystalliser → mass fraction (lactose, liquid phase)	[kg/kg]	0.5044	0.4860
Crystalliser → mass fraction (water, liquid phase)	[kg/kg]	0.5956	0.6140
Crystalliser → Flow rate set point	[g/s]	0.0584	0.0585
Feed→ Mass flow rate set point	[g/s]	0.0495	0.0496
Feed→ Mass fraction (lactose)	[kg/kg]	0.450	0.450
Feed→ Mass fraction (water)	[kg/kg]	0.550	0.550
Mixer splitter → Split fraction	[-]	0.289	0.289

Table 35 - Optimised conditions for the production of a seed product stream from a continuous evaporative crystallisation.

An advantage of the evaporative process over the cooling crystallisation of lactose is the faster onset of primary nucleation. As such, the use of a continuous evaporative crystalliser for use as a first-stage crystalliser, with continuous seed generation, would be considered very beneficial for use in the continuous manufacturing of lactose. Therefore, the evaporative process needs to be optimised in a manner to allows the product stream to be suitable for use as a seed stream for a separate crystallisation process.

In this instance, the chosen point of interest Is the development of a continuous evaporative crystalliser capable of producing material suitable for use as seed. The limitation of the process is therefore small seed size while producing an outlet stream with a solid content between 0.5-5%. Additionally, the $D_{4,3}$ was limited to a maximum of 150 µm to ensure suitability as seeding material. The optimisation aim was to maximise the solid content of the recovery. Again, the solid content was aimed to be above 1% to ensure suitability for the outflow of the process for use as 1st stage in a multimode crystallisation platform or as a seed stream to any continuous system.

This optimisation resulted in an average particle size of 150µm with a seed loading of 1.4%. This is considered a low seed loading for a continuous process, especially considering the slow kinetics of lactose crystallisation. However, the crystal mass recovery of the evaporative process and seed size are directly linked. Therefore, there is a trade-off between a suitable particle size and a sufficient solid content level for use as an inlet seed stream.

6.3.2.1 Sensitivity Analysis – Seed Generation Unit

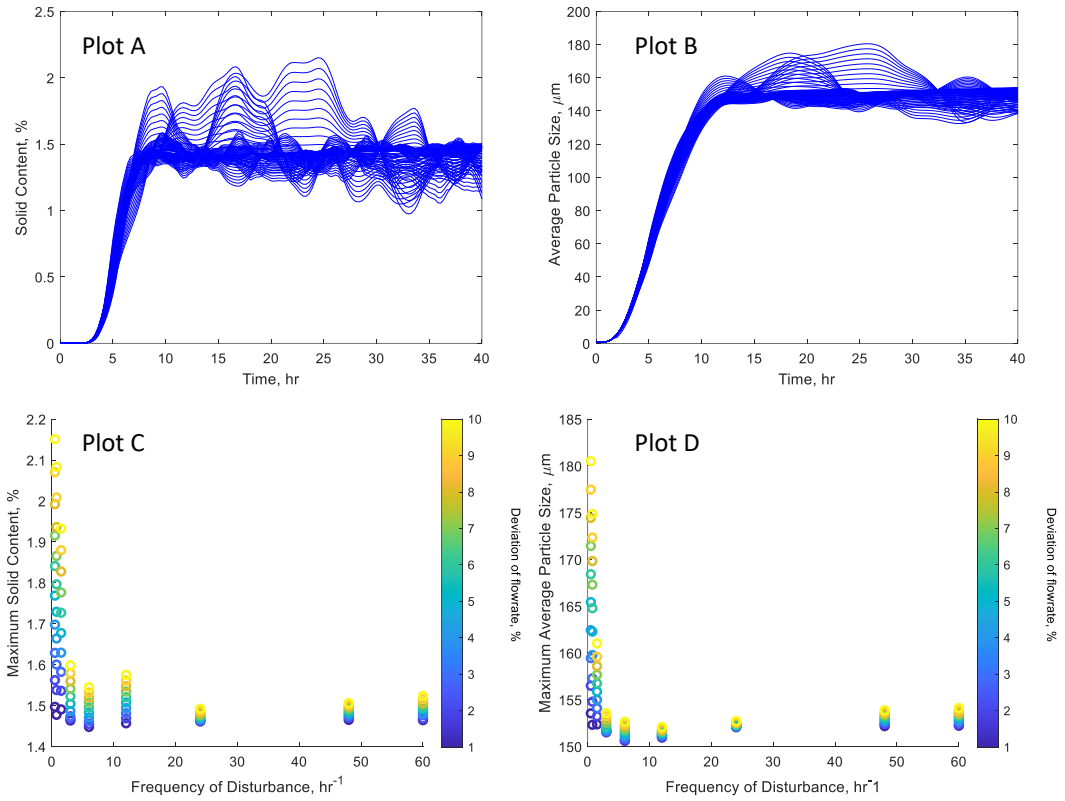

Figure 6-3 - Sensitivity analysis results for the presence of disturbances to feed flowrates for the seed generation unit. Plots A and B show disturbance effects over time. Plots C and D show the maximum effect seen due to disturbances of different frequencies and magnitudes.

Similar to the previous sensitivity analysis performed on the maximised evaporative crystallisation platform, the effect of disturbances to the system in the form of flowrates is also investigated with regard to the proposed seed generation unit. The variation of the feed

flowrate is performed again with a variation of 10% of the setpoint value. The effects of the disturbances on the process outputs can be seen in Figure 6-3 and Table 36. Plot A and Plot C show the largest effect on the solid content recovery is seen at lower frequencies with higher frequencies shown to have minimal effect. There is a similar but less obvious trend between the frequency of the disturbances and the $D_{4,3}$ as can be seen in Plot B. The overall learnings from this sensitivity analysis are that disturbances to feed flowrate need to be large and low frequency before the system significantly deviates from the optimised process outputs. Also, it should be stated that Plot C and Plot D display the maximum values, not the end values. Therefore, the consistency capable of this process with the presence of disturbance is clear within Plot C and Plot D for frequency values lower than 1 hr^{-1}.

As previously stated, a large deviation and a low frequency are required to shift the system away from the desired output variables. Therefore, the system is considered fairly robust. However, as the output from this process is to be used as the feed source for a subsequent process any variations could have an effect on the succeeding processes. Therefore, the resulting variation of the product PSD and solid content per cent are to be used as part of the basis for the sensitivity analysis of the cooling cascade process.

Value	Process Output	Unit	Exp. Value	St.Dev	Min	Max	Median
Max	Average particle size	µm	149.51	0.71	147.65	152.64	149.61
	Solid content	%	1.455	0.023	1.423	1.547	1.451
	Liquid mass	kg	0.250	5.05E-4	0.250	0.255	0.250
Final	Average particle size	µm	148.61	1.77	142.23	150.85	149.46
	Solid content	%	1.401	0.050	1.223	1.512	1.417
Min	Liquid mass	kg	0.237	0.0038	0.2235	0.2420	0.2372

Table 36 - Sensitivity analysis distribution statistics of selected process outputs.

6.4 Continuous Multimode Crystallisation

6.4.1 Cooling Cascade

Following the optimisation of the continuous evaporative seed generation unit, the use of a multimode crystallisation process was investigated. Figure 6-4 shows the flowsheet configuration for a 5-stage cooling crystallisation platform. For simplicity and reduced computational time, a slurry source has been used in replace of the continuous evaporative crystalliser. The concentration, flowrate and particle size set within the slurry source module are all finalised in agreement with the previously optimised continuous seed generation unit. The simulated particle size quantiles were used to set the standard deviation and location parameter values within the slurry source module to accurately represent the output from the evaporative crystalliser. This greatly reduced the computation time to run simulations, optimisations and other analyses on the proposed multimode crystallisation process.

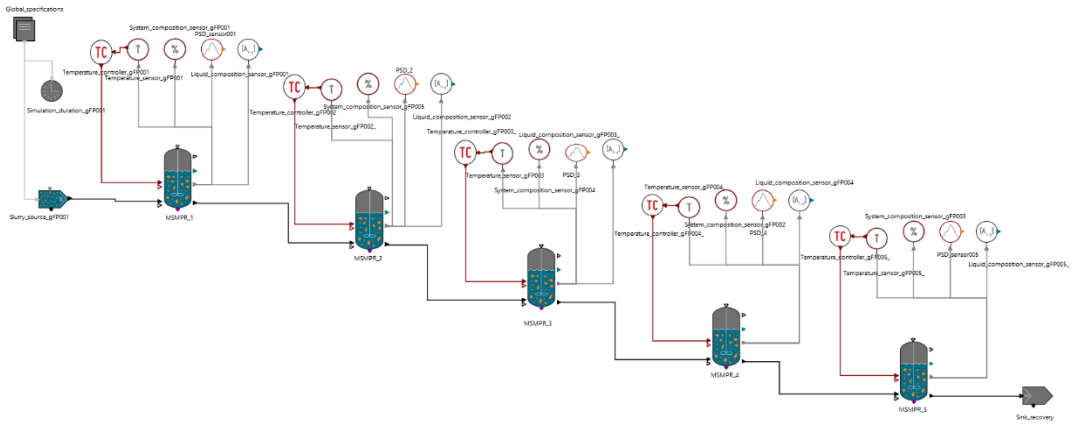

Figure 6-4 - Flowsheet depicting a 5-stage cooling cascade with seed pot representing the stream produced from the continuous seed generation unit.

The output of the optimised continuous evaporative crystallisation process also sets the product flowrate and conversely the inlet stream for the cooling cascade. The inlet stream for the cooling cascade is a limiting and defining factor for the multimode platform as it will

directly dictate the residence time and subsequently, the time to reach steady-state. The slow kinetics and low flowrates are a consideration for the applicability of the proposed multimode platform due to the time required to reach steady-state conditions for desired process outputs. Therefore, a defining factor of reaching a steady-state is only possible to manipulate through the vessel size. Due to the slow kinetics of the system being studied, there is a trade-off between minimising time to reach a steady-state and suitable residence time to allow for sufficient growth. Figure 6-5 shows an uncertainty analysis performed on a single-stage MSMPR connected to the previously discussed slurry source module. Temperature, concentration, and vessel volume were allowed to vary to gauge the effects on the process output. Plot A and Plot B show the progression of the solid content % and the average particle size for the tested simulations, respectively. The effect of the mass of solution within the vessel has been highlighted as a determining factor in the capabilities of the process. The mass of solution within the vessel is a direct representative of the vessel volumes that are being investigated. As discussed previously, the slow flowrates and slow kinetics of the system being tested are known limitations of the process and heavily limit its capabilities. Figure 6-5 shows that greater crystal mass recovery and larger particle size recoveries are capable through the proposed process, however, the system either takes a very long time to reach a steady-state or not at all under the tested time frame. The consideration of the time to reach steady-state is particularly important considering the proposed use of a cascade will multiply the time per stage. As such, the second lowest vessel size investigated is proposed at 250ml and subsequently 250 g initial mass within the vessel. This vessel size had a shorter time to reach a steady-state of around 10 hours. This vessel size was fixed upon for all future stage additions.

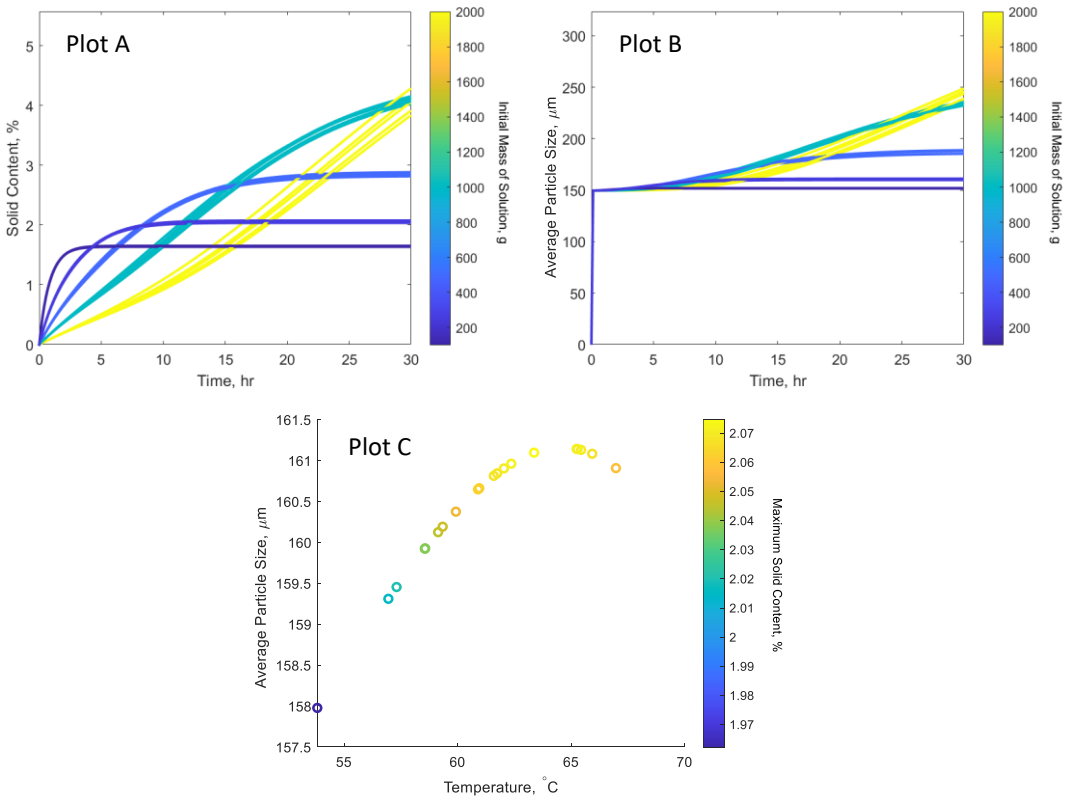

Figure 6-5 - Sensitivity analysis of a single stage cool vessel for variation in temperature and vessel size. Plots A and B vary in colour with increasing initial mass of solution from blue to yellow. Plot C also varies in colour form blue to yellow for increasing maximum solid content produced.

As can be seen from Plot C in Figure 6-5, the temperature of the vessel has a significant effect on the solid content recovered from the process. Across the tested temperatures between 67.5 °C and 53.8 °C, there is a variance of 0.1% which may be considered insignificant. However, if this 0.1% reduction is viewed in relation to the increase of the solid content from the seed stream of 1.4%, the solid content is increased by between 36% and 44% across the cooling stage. It is interesting to note that the maximum recovery and particle size are not recovered at the lowest temperature and therefore the highest supersaturation ratio. This highlights, that the growth rate within this temperature region is more affected by temperature than the level of supersaturation.

Following the sensitivity analysis of a one-stage continuous cooling crystallisation process, an initial attempt at optimising this process was carried out to gauge the optimal temperature for the first stage of a cascade. This optimisation focused upon increasing solid content in the vessel by varying temperature setpoints. The temperature of the seed stream is held constant at 67.5 °C. The optimisation showed a reasonable increase in $D_{4,3}$ from 149 to 161µm when the stage was held at 63.8C as shown in Table 37. The optimisation of the process was constrained by the supersaturation ratio limit of 1.6 to avoid conditions that could induce secondary nucleation if repeated experimentally. The temperature difference across the seed generation unit and the 1st stage is less than 4 °C according to the optimisation results. This highlights the potential limit in the cooling that is possible for this configuration when considering real-life considerations in the form of a number of stages and time for the process to reach a steady-state with desirable outputs.

Variables	Temperature	$D_{4,3}$	Solid Content %	S ratio
End Values	63.8	161	2.075	1.33

Table 37 - Optimisation of continuous single-stage cooling crystallisation process.

To aid the optimisation of the proposed 5-stage cooling cascade, a sensitivity analysis was performed with varying degrees of cooling between vessels. As was shown in the analysis of the single-stage crystallisation process the optimal temperature was found to be 63.8C, however, this does not appear to be optimal when considering the full cascade. For this analysis, four temperatures were trialled for the first vessel and the subsequent vessel temperatures were investigated considering equal drops in temperature between vessels. Three sets of temperature changes across the cascade were tested: 2, 3 and 4 °C. This allowed different cooling rates to be considered across the whole cascade but did not allow for

variation in temperature changes between different vessels. This analysis was primarily used for an initial understanding of how the cooling cascade is likely to behave and to further aid in the optimisation of the process.

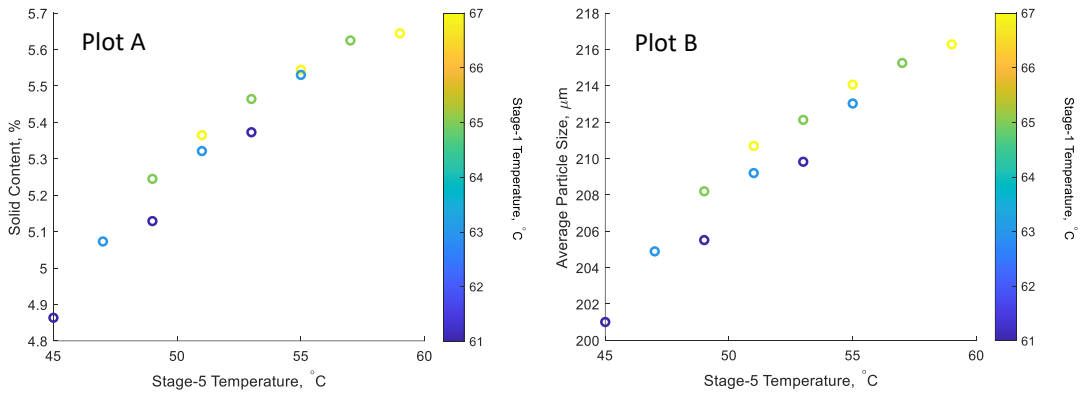

Figure 6-6 - Sensitivity Analysis of 5-stage cooling cascade temperature relationship between vessels and process outputs. Colour bar varies from blue to yellow with increasing Stage 1 temperature.

The temperatures of preceding vessels directly affect the recovery of the latter vessels in two ways: the concentration and the mass of solid present in the succeeding vessel outlet streams. The solid content and concentration of the inlet streams affect the amount of material available to be crystallised upon and the amount available to be crystallised out. As the solid content is relatively low, the effect of solid content from preceding vessels is not expected to have a determinant effect. However, the temperature of a vessel affects the growth rate and the resulting concentration of the outlet stream. As such, the temperature of each vessel is paramount in the optimisation of the process. Figure 6-6 shows the relationship between the temperature of the 5th stage and the chosen process outputs in relation to the temperature of the 1st stage. It is clear from Figure 6-6 that there is a positive relationship for both solid content recovery and average particle size with respect to the temperature of the 5th stage. This again, highlights that the growth rate is shown to have a stronger dependence on temperature than supersaturation. However, there is the beginning

of a plateau at the maximum temperature range, suggesting there may be a point where supersaturation is the dominant factor in growth over temperature. It should also be noted that the temperature of the 1st stage was previously optimised to 63.8 °C and is now shown to vary from 63 °C to 67 °C with favourable results in the maximising of both solid content recovery and average particle size. This increase in potential temperatures of the 1st stage was unexpected and has highlighted the usefulness of performing sensitivity analysis prior to attempting the optimisation of the 5-stage cascade.

Variable	Temperature set point (°C)				
	Stage 1	Stage	Stage 3	Stage 4	Stage 5
Optimised Value	63.4	63.6	62.8	61*	60*
Initial guess	63	61	59	57	55

Table 38 - Optimised temperature setpoint values for each vessel in the multi-mode 5-stage cooling cascade.

** indicates values that hit the upper bound.*

Process Output	Solid content (%)	Final $D_{4,3}$ (µm)	Supersaturation ratio (-)		
			Stage 3	Stage 4	Stage 5
Final Value	5.69	216.7	1.336	1.367	1.379

Table 39 Process outputs from the optimised multi-mode 5-stage cooling cascade.

Initial attempts to optimise the 5-stage cooling cascade are shown in Table 38 and Table 39.There is an evident restriction with the proposed process with respect to temperature. The initial guesses for the temperature values were for the most gradual cool between vessels investigated within the previous sensitivity analysis. The result of the optimisation showed a preference for an even more gradual cool. The favouring for higher temperatures was seen in earlier sensitivity analysis but the lack of cooling across the stages suggests the unsuitability of the proposed process with the current conditions. The proposed process conditions were predicted to produce an increase of over 400% in the solid content and a

final average particle size of 217 µm. The growth of particles from the seed value of 149 µm to 217 µm is quite small considering there are five vessels within the process. Additionally, a larger recovery of solid content would also be desired for this proposed process. This current optimised process is not producing favourable results that would warrant the investigation of this multimode continuous process experimentally.

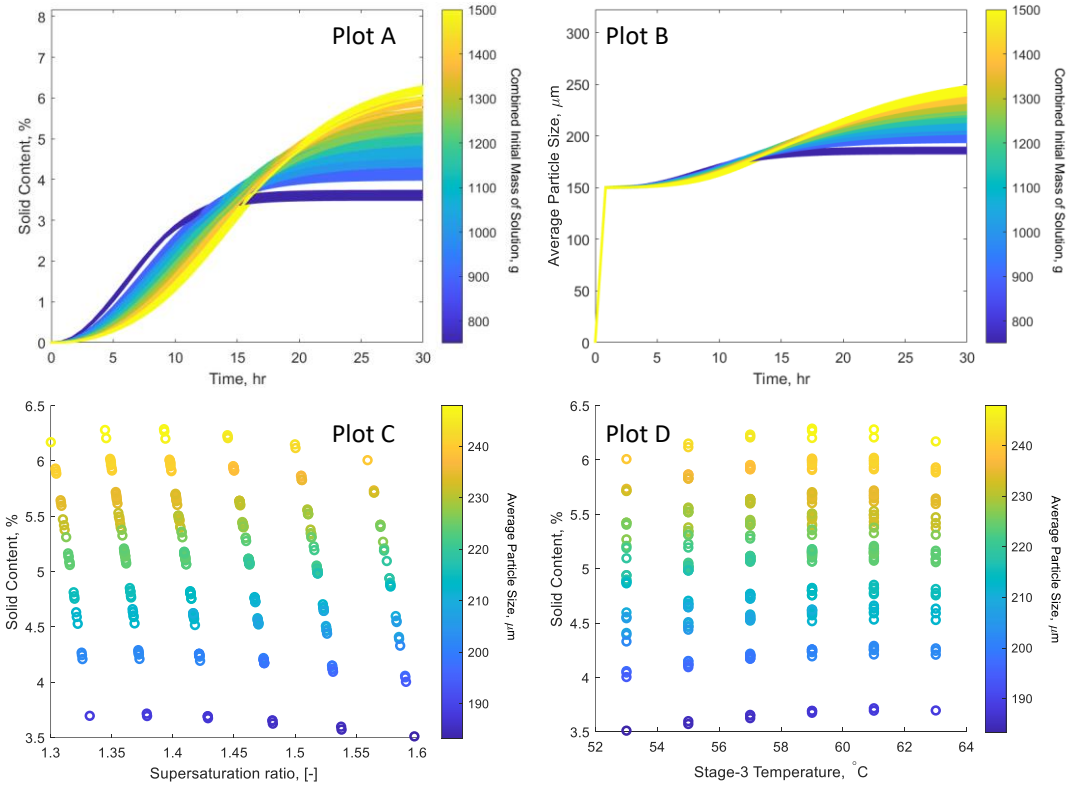

Figure 6-7 - Sensitivity Analysis for the 3-stage cooling cascade with variation in temperature and vessel sizes. Colour bar varies from blue to yellow with increasing combined initial mass of solution (Plot A and B) and average particle size (plot C and D).

Due to the stagnation of temperature when attempting the optimisation for a 5-stage cooling cascade. A 3-stage cascade was investigated within a sensitivity analysis for variation in temperature and vessel size. This investigation allowed for different-sized vessels within the same cascade to be tested. The tested vessel sizes were limited to 250ml, 400ml and 500ml. Larger vessel sizes would allow for a longer time for the material to remain within the vessel

and therefore more significant changes in the concentration within each stage. This larger change would allow for larger cooling steps between the stages and overall greater crystal mass recovery. Plot A and Plot B within Figure 6-7 show the increase in solid content and average particle size for increasing the overall mass of solution in the vessels. This is in agreement with the previous investigation into the effect of vessel size where larger sizes increase recovery but the time to reach steady state is prohibitively slow. The effect of temperature is still consistent with a maximum of around 60 °C as can be seen in Plot D. Interestingly, Plot C shows a maximum in terms of recovery for all tested vessel sizes at supersaturation ratio values between 1.35 and 1.37. This is consistent with the optimisation results for the 5-stage cascade discussed previously and displayed in Table 39. This analysis showed that the variation of vessel size was prohibited by the time taken to reach a steady state and that the effect of temperature was not removed by the use of larger vessels anyway. Therefore, the use of the cooling cascade alongside the continuous seed generation unit was still not producing favourable results.

With the consideration of temperature and vessel size not sufficient enough to improve recovery in a reasonable timeframe, the evaporative seed generation unit is likely the limiting factor. The development of the continuous seed generation unit was discussed previously and was shown to have a low solid content and low flowrate. These are two considerations that have a direct effect on the potential of the multimode process in question. The low solid content means there is less material available to be crystallised upon and could be limiting the potential output of the cooling cascade. Additionally, the low flowrate directly affects the residence time within the vessel and subsequently the suitability of different vessel sizes for adequate recovery time frames. Simulations investigating the effect of feed flowrate and the

solid content from the seed generation unit on the recovery of the cooling cascade were tested to find the limiting factor of the recovery of the multimode process.

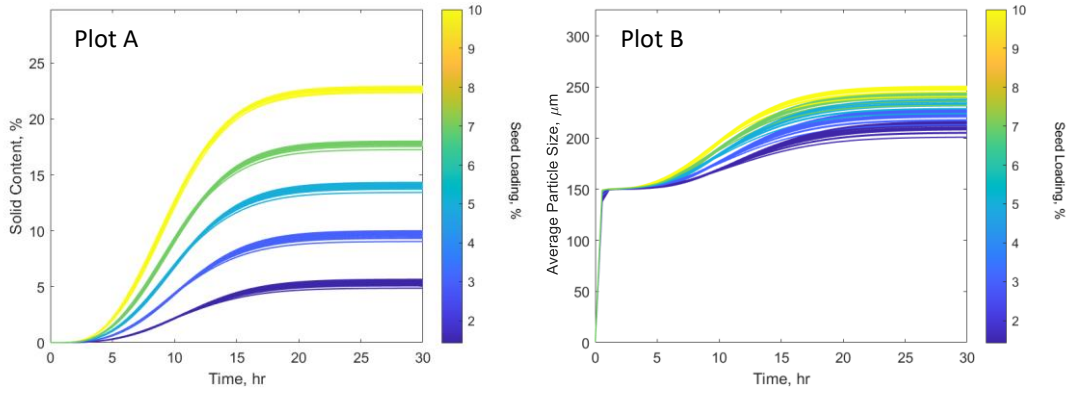

Figure 6-8 - Sensitivity analysis for 3-stage cascade with a constant flowrate of 0.1495 kg/hr. Variations for temperature and seed loading. Colour bar varies from blue to yellow with increasing solid loading.

The effect of seed loading is evident in Figure 6-8. Increasing the solid content of the feed stream to the 5-stage cooling cascade was shown to increase the solid content recovery of the process as well as the average particle size. This highlights the low solid content produced from the seed generation unit as a limiting factor in the proposed multimode process. The positive effect of seed loading on the process outputs is linked to the greater reduction in concentration within each vessel. It should be noted that although the solid content has greatly increased, in relative terms the recovery using smaller seed loading is larger. A feed stream with 1.4% solids results in an increase in solids of over 400% but a feed stream of 10% is currently showing a relative increase of only 220%.

The sensitivity analysis also investigated the effect of flowrates within the cascade and two different vessel volumes. The effect of larger vessel volume was found to increase the amount of time to reach a steady state for set flowrate values. However, the end values recovered for both average particle size and solid content have increased. This suggests through the variation of the flowrate from the seed generation unit, larger vessel volumes

may be necessary to improve the yield recovery from the proposed multi-mode platform. Larger flowrates are shown to decrease the time to reach steady state but also produce smaller particles and lower solid content values. The effects of flowrate and vessel volume are directly linked in terms of their suitability and are restricted by the slow kinetics of the lactose crystallisation system.

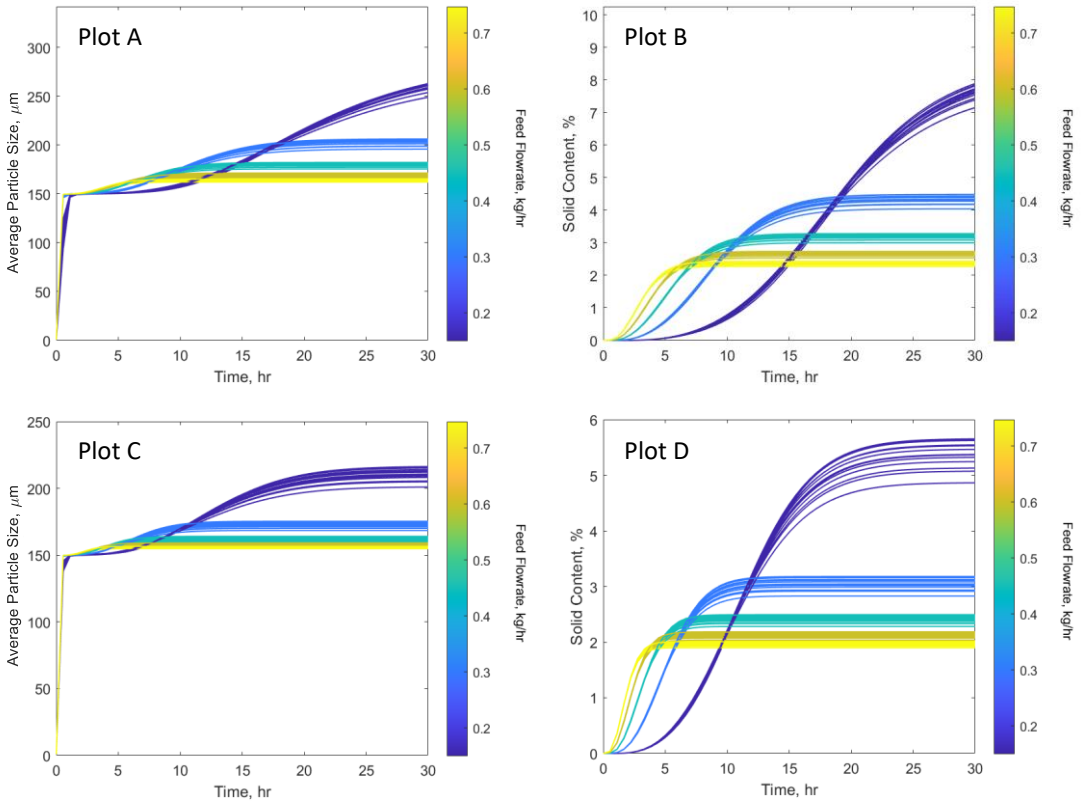

Figure 6-9 - Sensitivity analysis for 3-stage cascade with a constant seed loading of 1.4%.. Variations for flowrate shown by colour bar. Top graphs tested on 500 ml system. Bottom graphs tested on 250 ml system. Colour bar varies from blue to yellow with increasing feed flowrate.

It is clear from the investigation into the variation of flowrate and seed loading that the current outputs of the seed generation unit are not suited for the proposed multimode MSMPR cascade. Due to the current evaporative crystallisation being limited to 250ml experiments and therefore limited data on the evaporation rate out with these conditions it

was decided not to attempt scale-up of the seed generation unit. As such, the proposed multimode cascade is deemed not suitable for further work at this stage.

6.4.2 Plug Flow Reactor

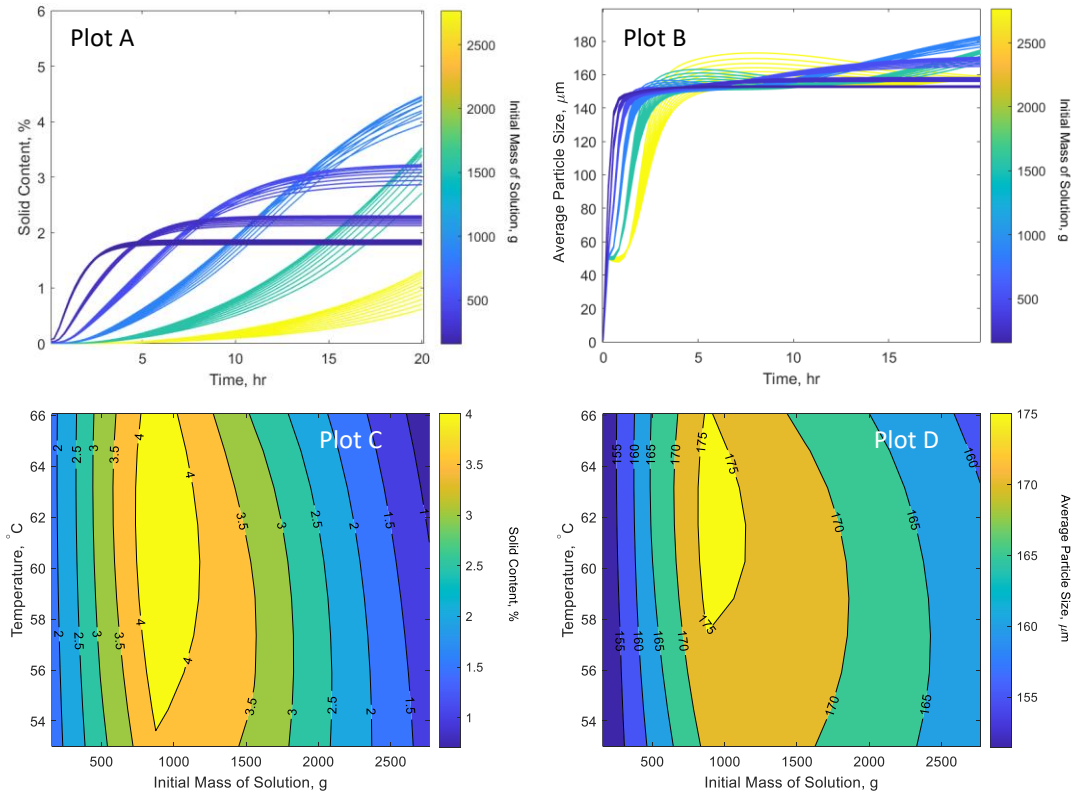

Figure 6-10 Sensitivity analysis of PFR cooling crystalliser with seed generation unit. Colour bar varies from blue to yellow with increasing: Initial mass of solution (Plot A and B); solid content (Plot C) and average particle size (plot D).

As the MSMPR cooling cascade was not found to produce favourable results when connected with the seed generation unit, a plug flow reactor (PFR) was investigated. The PFR system was considered as four separate modules with separate temperatures that would allow for a controlled cool across the overall vessel. This framework of a four-module reactor follows the Rattlesnake from Cambridge Reactor Designs. The feed flowrate is rather low due to the seed generation unit's output and as such different vessel sizes are considered for this

potential PFR set-up. The ratio between the cross-sectional area and the length of each module is kept consistent with the measurements of a single module from the rattlesnake to keep the set-up relative in nature.

Sensitivity analysis was done for the PFR multimode set-up to investigate the possibilities of the proposed process. The vessel size and dimensions of the PFR were all varied in connection with each other and the temperature was also varied to investigate the degree of cooling capable over the PFR since this was highlighted as a limiting effect of the multimode MSMPR cascade previously investigated. Plot A in Figure 6-10 shows at least two initial masses of saturated solution that reach a steady state in a reasonable time. However, the solid content value of 2.3 % for an initial mass of 0.277 kg is very similar to that recovered for the single-stage MSMPR vessel with 250g in the previous section of 2.08%. This suggests the limitations of the previous MSMPR cascade may be also seen with the cooling PFR multimode platform. Plot B shows the particle size leaving the vessels through time for different initial masses of solution. It is clear from this that there is a limitation in the growth capability due to realistic times for the running of the set-up. It is also clear from Figure 6-10 that the particle size outputs from the 1st module are very minimal with the current conditions of the seed generation unit. Again, this is similar to the findings of the multi-mode cooling cascade in that the flowrate and solid content of the seed generation unit are the limiting factors in the optimisation of the platform.

From initial investigations into the first module of a cooling PFR system, it is clear that the problems seen in the multimode MSMPR platform are still prevalent in the multimode PFR system. As such, the optimisation of the multimode PFR platform is not investigated further as the limiting factor has already been highlighted as the process outputs from the seed generation unit.

6.5 Conclusion

The simulation capabilities of gFP were utilised in this chapter to investigate the capabilities and robustness of proposed crystallisation processes that had not been investigated experimentally. Initially, the focus of this work was to investigate the transfer of the semi-batch evaporative crystallisation process investigated in the previous chapter to continuous operation. This evaporative crystalliser was focused upon in terms of two different output goals. An optimised continuous evaporative crystalliser for solid product flowrate was developed and the optimised process conditions have been highlighted in Table 33. This optimised process is predicted to produce particulates with an average size of 401 µm and a solid content of 7.97%. The size of particles predicted to be produced from this process is quite impressive for only 5.5 hrs to reach steady-state. The optimised continuous process was then tested under the presence of disturbances to feed flowrate to test the robustness of the proposed platform. The proposed continuous process was found to only deviate strongly from the optimum process outputs with the presence of low frequency and high deviation disturbances.

The evaporative crystalliser was also used as the basis for the development of a continuous seed generation unit. The hope of this process was to have a process with a continual output stream with suitable properties to be used as the seeded feed stream to a cooling platform. The limitations of 150 µm particles and a solid content of above 1% were set for the optimisation of the continuous evaporative process. These constraints were set to ensure the suitability of the process as a seed generation unit. The particle size and solid content are directly linked and therefore the optimised process was found to produce a low solid content of 1.4% and a large $D_{4,3}$ of 149 µm. This process was also tested for its ability to handle

disturbances of the feed flowrate stream. Again, the system was only strongly seen to deviate from process outputs for low frequency and high deviation disturbances. However, due to the lower values of solid content and particle size, the deviations are large when considered relative to the optimised values.

The optimised seed generation unit process outputs are used as the feed values for two different cooling crystallisation processes. The first investigated was the use of a 5-stage cooling cascade. The optimisation and sensitivity analysis of the use of cooling cascades found the current conditions of the seed generation unit limited the level of recovery possible. This was due to the low level of solid content in the feed stream resulting in a slow depletion of the concentration in individual stages and therefore minimal cooling across stages was seen. The slow kinetics and the low process outputs from the seed generation unit are direct limits on the proposed multimode crystallisation platform with a cooling cascade. Additionally, the seed generation unit was connected with a cooling crystallisation PFR. Through sensitivity analysis, the multimode PFR system was also found to be limited by the current outputs of the seed generation unit.

The seed generation unit is found to be the limiting factor of the proposed continuous multimode crystallisation platforms. Unfortunately, the specific problem with the seed generation unit is the outlet flowrate and solid content when producing material of a suitable size for seeding purposes. As discussed previously, the solid content is directly linked to the size of particles produced and therefore cannot be separated to allow for higher solid content values. The scaling of the evaporative seed generation unit would require a knowledge of the evaporation rates seen experimentally at larger vessel volumes which are not available at this stage.

In conclusion, this work has allowed for the investigation of continuous evaporative crystallisation processes from the development of the batch mechanistic model developed in the previous chapter. Additionally, proposed continuous multimode crystallisation platforms were investigated through the use of mechanistic models. However, due to the limitations of the continuous evaporative seed generation unit, the proposed multimode crystallisation platforms were not found to be feasible at this time.

7 Conclusions and Future Work

This work has centred on the use of mechanistic models to describe different crystallisation processes and the use of such models to aid in the optimisation of crystalline recovery processes. The use of sequential parameters estimation has been used for both cooling and evaporative crystallisation of ALM from water. The design of experiments for the different platforms was slightly modified to allow for the intricacies of the semi-continuous vacuum-induced evaporative crystalliser compared to the batch cooling set-up. The parameter estimation methods allowed for the building of mechanistic models of both platforms that describe the crystallisation kinetics of the systems. The cooling crystallisation model in particular was shown to accurately represent the system with only some variation in the PSD prediction not fully capturing the shape of the recovered material. The evaporative model, however, did pass the goodness of fit test but the uncertainties on the fitted kinetics were shown to have quite large effects on the process outputs. In particular, the PSD was greatly affected by the uncertainty of the growth rate constant. The evaporative crystalliser model was built using minimal experiments and as such the error is higher than the cooling model.

The building of mechanistic models for a late stage development API was also endeavoured to utilise pre-existing experimental data from controlled cooling experiments. This required the decoupling of the growth and agglomeration kinetics similar to the previous modelling work. The resulting model was found to accurately describe the process in terms of concentration prediction. However, the PSD predictions were again too narrow and not fully capturing the broadness of the recovered PSD. The D50 quantile was accurately captured by the model and as such the model was found to accurately describe the chosen process.

The developed mechanistic models were then all used for optimisation purposes to gauge the possible outputs of the tested system. The lactose cooling crystallisation was optimised for recovery due to the low recovery seen experimentally. A large increase in recovery was seen from the batch-seeded desupersaturation experiments compared to the batch-controlled cooling platform that was focused on for optimisation. The cooling profile was the focus of the optimisation and was found to produce a crystal mass recovery of 10 g with a predicted particle size of 30.53 µm for a reduced batch time of 11.23 hrs. The mechanistic model allowed for these different process conditions to be investigated without the need for additional experimentation.

The crystallisation of Compound-X was also focused on in terms of optimisation and found to be influenced by the initial concentration and the cooling profile. The model allowed for extrapolation down to lower temperatures than were tested experimentally and was found to be useful in the increase in crystal mass recovery. The optimisation of the Compound-X crystallisation process was found to rely on faster cooling time and longer final hold period to allow for lower temperatures to be reached and added time for the system to push towards the saturated concentration for the tested temperature.

Finally, the evaporative process was investigated in terms of optimising for crystal mass recovery in both batch and continuous mode. The continuous mode optimisation of crystal mass was attempted for two goals: producing large particulates and small particulates for seeding purposes. The conditions for the running of the continuous evaporative crystallisation process were found to maximise the capabilities of the process and for use as a seed generation unit. The robustness of the proposed continuous processes was found to hold for disturbances with a frequency greater than 1 hr^{-1}. The seed generation unit was then tested as the first stage of a multimode crystallisation process. This looked to link the

evaporative crystalliser to a cooling crystalliser in order to utilise both lactose mechanistic models. A cooling MSMPR cascade and a PFR were both trialled within a multimode platform. Both processes were found to be limited by the process outputs of the seed generation unit. The testing of the proposed multimode platform was achieved through entirely computational means and was capable of ruling out the use of such processes at this stage.

The future work that would be proposed based on the results of this thesis would be to expand the working range of interest for the cooling lactose crystallisation model to allow for a more dynamic model to be built. Greater temperature and supersaturation regions would allow for additional mechanisms of interest to be included within the model such as secondary nucleation. Additionally, it would also produce larger concentration changes across the experiments and would likely improve the accuracy of the model being built. In terms of the Compound-X model, there are limits to the improvements that can be made due to available data but it would be recommended to include the full PSD for fitting where possible to improve the model's PSD predictions. The developed evaporative crystallisation model could be greatly improved through further experimentation. This is however limited by the current platform and the recommendations would be to improve the control of the pressure in the vessel to reduce the noise from the valve. Additionally, the inclusion of evaporation kinetics through a VLE model would give a more complete look into the evaporative crystallisation process being studied. Finally, the hypothetical process proposed for the multi-mode crystallisation platform was directly limited by the results of the evaporative crystallisation model and as such could benefit from more work into the evaporative crystallisation model.

A limit of the usefulness of the models built within this thesis has been consistently highlighted as the size prediction inaccuracy. A key area of focus would be to endeavour to

improve the PSD prediction and uncertainty by the inclusion of additional PSD data during the development of the model. This could be achieved by PSD data produced from image analysis of images taken in-situ during the experiments. This would rely on a relatively new piece of technology and its accuracy would have a direct link to the robustness of the model produced. Alternatively, sampling during experiments could also supply the required additional PSD information but it would also increase the complexity of the flowsheet used for modelling.

The key takeaway from this thesis is the usefulness of mechanistic models and their ability to aid process design and ultimately increase understanding of processes while reducing waste. An innovative approach to crystallisation process design was endeavoured to design a multi-mode crystallisation platform through entirely digital design methods. This approach although unsuccessful could be adapted and utilised for the combinations of different processes such as the addition of an antisolvent crystalliser as a final stage MSMPR to improve the yield. On a more general note, the Compound-X model has shown that building mechanistic models do not necessarily require additional experimentation and therefore could be an insightful asset for process developers during the early stages of product development. The hope would be to include the development of mechanistic models for crystallisation process as an industry standard in the early development to better aid experimental design and recovery. This could be particularly useful given the current requirement for green manufacturing and the collective goal of reducing waste by means of more effective experimental design and utilisation of digital twins.

8 References

[1] H. J. M. Kramer and G. M. van Rosmalen, “CRYSTALLIZATION,” *Encycl. Sep. Sci.*, pp. 64–84, Jan. 2000, doi: 10.1016/B0-12-226770-2/00031-4.

[2] M. T. Lusk and A. E. Mattsson, “High-performance computing for materials design to advance energy science,” *MRS Bull.*, 2011, doi: 10.1557/mrs.2011.30.

[3] A. K. El-Zhry El-Yafi and H. El-Zein, “Technical crystallization for application in pharmaceutical material engineering: Review article,” *Asian J. Pharm. Sci.*, vol. 10, no. 4, pp. 283–291, Jul. 2015, doi: 10.1016/J.AJPS.2015.03.003.

[4] Z. Zhang, D.-W. Sun, Z. Zhu, and L. Cheng, “Enhancement of Crystallization Processes by Power Ultrasound: Current State-of-the-Art and Research Advances,” *Compr. Rev. Food Sci. Food Saf.*, vol. 14, no. 4, pp. 303–316, Jul. 2015, doi: 10.1111/1541-4337.12132.

[5] C. T. Ó’Ciardhá, K. W. Hutton, N. A. Mitchell, and P. J. Frawley, “Simultaneous Parameter Estimation and Optimization of a Seeded Antisolvent Crystallization,” *Cryst. Growth Des.*, vol. 12, no. 11, pp. 5247–5261, Nov. 2012, doi: 10.1021/cg3006822.

[6] H. M. Schoen, C. S. Grove, and J. A. Palermo, “The early history of crystallization,” *J. Chem. Educ.*, vol. 33, no. 8, p. 373, Aug. 1956, doi: 10.1021/ed033p373.

[7] Z. K. Nagy and R. D. Braatz, “Advances and new directions in crystallization control.,” *Annu. Rev. Chem. Biomol. Eng.*, vol. 3, pp. 55–75, 2012, doi: 10.1146/annurev-chembioeng-062011-081043.

[8] Siemens Process Systems Engineering Limited, “gPROMS FormulatedProducts Documentation.” London, Jul. 2022.

[9] K. Plumb, “Continuous Processing in the Pharmaceutical Industry: Changing the Mind Set,” *Chem. Eng. Res. Des.*, vol. 83, no. 6, pp. 730–738, Jun. 2005, doi: 10.1205/CHERD.04359.

[10] D. Zhang, S. Xu, S. Du, J. Wang, and J. Gong, “Progress of Pharmaceutical Continuous Crystallization,” *Engineering*, vol. 3, no. 3, pp. 354–364, Jun. 2017, doi: 10.1016/J.ENG.2017.03.023.

[11] S. L. Lee *et al.*, “Modernizing Pharmaceutical Manufacturing: from Batch to Continuous Production,” *J. Pharm. Innov.*, vol. 10, no. 3, pp. 191–199, 2015, doi: 10.1007/s12247-015-9215-8.

[12] B. Benyahia, P. D. Anandan, and C. Rielly, “Control of Batch and Continuous Crystallization Processes using Reinforcement Learning”, doi: 10.1016/B978-0-323-88506-5.50211-4.

[13] C. J. Brown *et al.*, “Enabling precision manufacturing of active pharmaceutical ingredients: workflow for seeded cooling continuous crystallisations,” *Mol. Syst. Des. Eng.*, vol. 3, no. 3, pp. 518–549, 2018, doi: 10.1039/c7me00096k.

[14] A. S. Myerson, M. Krumme, M. Nasr, H. Thomas, and R. D. Braatz, “Control Systems Engineering in Continuous Pharmaceutical Manufacturing Continuous Manufacturing

Symposium", doi: 10.1002/jps.24311.

[15] H. Siddique, C. J. Brown, I. Houson, and A. J. Florence, "Establishment of a Continuous Sonocrystallization Process for Lactose in an Oscillatory Baffled Crystallizer," *Org. Process Res. Dev.*, vol. 19, no. 12, pp. 1871–1881, Dec. 2015, doi: 10.1021/acs.oprd.5b00127.

[16] M. S. Alam, B. Ashokkumar, and A. Mohammed Siddiq, "The density, dynamic viscosity and kinematic viscosity of protic polar solvents (pure and mixed systems) studies: A theoretical insight of thermophysical properties," *J. Mol. Liq.*, vol. 251, pp. 458–469, Feb. 2018, doi: 10.1016/J.MOLLIQ.2017.12.089.

[17] R. Liang and Z. Yuan, "Computational Shape Optimization of Microreactors based on CFD Simulation and Surrogate Model driven Optimization," 2020, doi: 10.1016/B978-0-12-823377-1.50155-5.

[18] A. Mersmann, *Crystallization Technology Handbook*. Taylor & Francis, 2001. [Online]. Available: https://books.google.co.uk/books?id=BVJdDw59lDcC

[19] R. Davey and J. Garside, *From molecules to crystallizers*. Oxford University Press, 2000.

[20] N. Kubota, "A new interpretation of metastable zone widths measured for unseeded solutions," *J. Cryst. Growth*, vol. 310, pp. 629–634, 2008, doi: 10.1016/j.jcrysgro.2007.11.123.

[21] A. Cashmore, M. Haw, M. Lee, and J. Sefcik, "Understanding and Measurement of Secondary Nucleation," 2022.

[22] S. G. Agrawal and A. H. J. Paterson, "Secondary Nucleation: Mechanisms and Models," *Chem. Eng. Commun.*, vol. 202, no. 5, pp. 698–706, May 2015, doi: 10.1080/00986445.2014.969369.

[23] S. O'regan, P. J. Frawley, and O. Shardt, "The determination of the critical Reynolds number for particle-wall collisions using the lattice-Boltzmann method." [Online]. Available: https://ssrn.com/abstract=4127895

[24] M. Bravi, S. Di Cave, B. Mazzarotta, and N. Verdone, "Relating the attrition behaviour of crystals in a stirred vessel to their mechanical properties," *Chem. Eng. J.*, vol. 94, no. 3, pp. 223–229, Aug. 2003, doi: 10.1016/S1385-8947(03)00053-6.

[25] J. B. Rawlings, M. Stephen, and R. Witkowskit, "Model Identification and Control of Solution Crystallization Processes : A Review Z4y]," no. 512, pp. 1275–1296, 1993.

[26] J. W. Mullin, *Crystallization*. in Chemical, Petrochemical & Process. Elsevier Science, 2001. [Online]. Available: https://books.google.co.uk/books?id=Et0EtojQmvsC

[27] N. A. Mitchell, C. T. Ó'Ciardhá, and P. J. Frawley, "Estimation of the growth kinetics for the cooling crystallisation of paracetamol and ethanol solutions," *J. Cryst. Growth*, vol. 328, no. 1, pp. 39–49, Aug. 2011, doi: 10.1016/J.JCRYSGRO.2011.06.016.

[28] L.-M. Terdenge, J. A. Kossuch, G. Schembecker, and K. Wohlgemuth, "Potential of gassing crystallization to control the agglomeration degree of crystalline products," 2017, doi: 10.1016/j.powtec.2017.07.044.

[29] K. Pitt *et al.*, "Particle design via spherical agglomeration: A critical review of

controlling parameters, rate processes and modelling," *Powder Technol.*, vol. 326, pp. 327–343, 2018, doi: https://doi.org/10.1016/j.powtec.2017.11.052.

[30] J.-F. Pérez-Calvo, S. S. Kadam, and H. J. M. Kramer, "Determination of kinetics in batch cooling crystallization processes-A sequential parameter estimation approach," *AIChE J.*, vol. 62, no. 11, pp. 3992–4012, Nov. 2016, doi: 10.1002/aic.15295.

[31] A. Abbas and J. A. Romagnoli, "Multiscale modeling, simulation and validation of batch cooling crystallization," *Sep. Purif. Technol.*, vol. 53, no. 2, pp. 153–163, 2007, doi: 10.1016/j.seppur.2006.06.027.

[32] H. A. Jakobsen, "The Population Balance Equation," in *Chemical Reactor Modeling*, Berlin, Heidelberg: Springer Berlin Heidelberg, 2009, pp. 807–865. doi: 10.1007/978-3-540-68622-4_9.

[33] D. Verkoeijen, G. A. Pouw, G. El, M. H. Meesters, and B. Scarlett, "Population balances for particulate processes-a volume approach," *Chem. Eng. Sci.*, vol. 57, pp. 2287–2303, 2002, Accessed: Aug. 30, 2023. [Online]. Available: www.elsevier.com/locate/ces

[34] D. Ramkrishna and M. R. Singh, "Population balance modeling: current status and future prospects.," *Annu. Rev. Chem. Biomol. Eng.*, vol. 5, pp. 123–146, 2014, doi: 10.1146/annurev-chembioeng-060713-040241.

[35] A. Majumder, V. Kariwala, S. Ansumali, and A. Rajendran, "Lattice Boltzmann method for population balance equations with simultaneous growth, nucleation, aggregation and breakage," *Chem. Eng. Sci.*, vol. 69, no. 1, pp. 316–328, 2012, doi: https://doi.org/10.1016/j.ces.2011.10.051.

[36] H. M. Omar and S. Rohani, "Crystal Population Balance Formulation and Solution Methods: A Review," *Cryst. Growth Des.*, vol. 17, no. 7, pp. 4028–4041, Jul. 2017, doi: 10.1021/acs.cgd.7b00645.

[37] A. D. Randolph and M. A. Larson, "Transient and steady state size distributions in continuous mixed suspension crystallizers," *AIChE J.*, vol. 8, no. 5, pp. 639–645, 1962, doi: 10.1002/aic.690080515.

[38] S. K. Jha, S. Karthika, and T. K. Radhakrishnan, "Modelling and control of crystallization process," *Resour. Technol.*, vol. 3, no. 1, pp. 94–100, Mar. 2017, doi: 10.1016/J.REFFIT.2017.01.002.

[39] M. M. Attarakih, C. Drumm, and H.-J. Bart, "Solution of the population balance equation using the sectional quadrature method of moments (SQMOM)," *Chem. Eng. Sci.*, vol. 64, pp. 742–752, 2009, doi: 10.1016/j.ces.2008.05.006.

[40] F. Puel, G. Fã Evotte, and J. P. Klein, "Simulation and analysis of industrial crystallization processes through multidimensional population balance equations. Part 1: a resolution algorithm based on the method of classes," *Chem. Eng. Sci.*, vol. 58, pp. 3715–3727, 2003, doi: 10.1016/S0009-2509(03)00254-9.

[41] V. John, T. Mitkova, M. Roland, K. Sundmacher, L. Tobiska, and A. Voigt, "Simulations of population balance systems with one internal coordinate using finite element methods," *Chem. Eng. Sci.*, vol. 64, no. 4, pp. 733–741, 2009, doi:

https://doi.org/10.1016/j.ces.2008.05.004.

[42] K. K. Pradhan, S. Chakraverty, K. K. Pradhan, and S. Chakraverty, “Finite Element Method,” *Comput. Struct. Mech.*, pp. 25–28, Jan. 2019, doi: 10.1016/B978-0-12-815492-2.00010-1.

[43] B. E. Rapp and B. E. Rapp, “Finite Element Method,” *Microfluid. Model. Mech. Math.*, pp. 655–678, Jan. 2017, doi: 10.1016/B978-1-4557-3141-1.50032-0.

[44] R. Gunawan, I. Fusman, and R. D. Braatz, “High Resolution Algorithms for Multidimensional Population Balance Equations,” *AIChE J*, vol. 50, pp. 2738–2749, 2004, doi: 10.1002/aic.10228.

[45] D. Meimaroglou and C. Kiparissides, “Monte Carlo simulation for the solution of the bi-variate dynamic population balance equation in batch particulate systems,” *Chem. Eng. Sci.*, vol. 62, no. 18–20, pp. 5295–5299, Sep. 2007, doi: 10.1016/j.ces.2006.11.032.

[46] A. H. Bari and A. B. Pandit, “Sequential Crystallization Parameter Estimation Method for Determination of Nucleation, Growth, Breakage, and Agglomeration Kinetics,” *Ind. Eng. Chem. Res.*, vol. 57, no. 5, pp. 1370–1379, 2018, doi: 10.1021/acs.iecr.7b03995.

[47] S. Kumar and D. Ramkrishna, “On the solution of population balance equations by discretization—III. Nucleation, growth and aggregation of particles,” *Chem. Eng. Sci.*, vol. 52, no. 24, pp. 4659–4679, Dec. 1997, doi: 10.1016/S0009-2509(97)00307-2.

[48] A. W. Mahoney, F. J. Doyle, and D. Ramkrishna, “Inverse problems in population balances: Growth and nucleation from dynamic data,” *AIChE J.*, vol. 48, no. 5, pp. 981–990, May 2002, doi: 10.1002/aic.690480508.

[49] F. Févotte and G. Févotte, “A method of characteristics for solving population balance equations (PBE) describing the adsorption of impurities during crystallization processes,” *Chem. Eng. Sci.*, vol. 65, no. 10, pp. 3191–3198, May 2010, doi: 10.1016/J.CES.2010.02.009.

[50] Z. K. Nagy, M. Fujiwara, X. Y. Woo, and R. D. Braatz, “Determination of the Kinetic Parameters for the Crystallization of Paracetamol from Water Using Metastable Zone Width Experiments,” *Ind. Eng. Chem. Res.*, vol. 47, no. 4, pp. 1245–1252, Feb. 2008, doi: 10.1021/ie060637c.

[51] M. Li, D. Wilkinson, and K. Patchigolla, “Comparison of Particle Size Distributions Measured Using Different Techniques,” *Part. Sci. Technol.*, vol. 23, no. 3, pp. 265–284, 2005, doi: 10.1080/02726350590955912.

[52] R. Wakeman, “The influence of particle properties on filtration,” *Sep. Purif. Technol.*, vol. 58, no. 2, pp. 234–241, 2007, doi: https://doi.org/10.1016/j.seppur.2007.03.018.

[53] E. Simone, A. I. I. Tyler, D. Kuah, X. Bao, M. E. Ries, and D. Baker, “Optimal Design of Crystallization Processes for the Recovery of a Slow-Nucleating Sugar with a Complex Chemical Equilibrium in Aqueous Solution: The Case of Lactose,” *Org. Process Res. Dev.*, vol. 23, no. 2, pp. 220–233, 2019, doi: 10.1021/acs.oprd.8b00323.

[54] S. R. Patel and Z. V. P. Murthy, “Ultrasound assisted crystallization for the recovery of lactose in an anti-solvent acetone,” *Cryst. Res. Technol.*, vol. 44, no. 8, pp. 889–896,

2009, doi: 10.1002/crat.200900227.

[55] P. Eadala, J. P. Waud, S. B. Matthews, J. T. Green, and A. K. Campbell, “Quantifying the ‘hidden’ lactose in drugs used for the treatment of gastrointestinal conditions,” *Aliment. Pharmacol. Ther.*, vol. 29, no. 6, pp. 677–687, Mar. 2009, doi: 10.1111/j.1365-2036.2008.03889.x.

[56] A. van Kreveld and A. S. Michaels, “Measurement of Crystal Growth of α-Lactose,” *J. Dairy Sci.*, vol. 48, no. 3, pp. 259–265, Mar. 1965, doi: 10.3168/JDS.S0022-0302(65)88213-3.

[57] G. Haase and T. A. Nickerson, “Kinetic Reactions of Alpha and Beta Lactose. II. Crystallization,” *J. Dairy Sci.*, vol. 49, no. 7, pp. 757–761, Jul. 1966, doi: 10.3168/JDS.S0022-0302(66)87941-9.

[58] P. Parimaladevi and K. Srinivasan, “Influence of supersaturation level on the morphology of α-lactose monohydrate crystals,” *Int. Dairy J.*, vol. 39, no. 2, pp. 301–311, Dec. 2014, doi: 10.1016/J.IDAIRYJ.2014.08.007.

[59] J. Colin Haser, R. H. Herring, and S. Datta, “Development of QSPR Model Relating Solvent Structure to Crystal Morphology,” *Comput. Aided Chem. Eng.*, vol. 34, pp. 321–326, Jan. 2014, doi: 10.1016/B978-0-444-63433-7.50038-9.

[60] E. A. Schmitt, D. Law, and G. G. Z. Zhang, “Nucleation and Crystallization Kinetics of Hydrated Amorphous Lactose Above the Glass Transition Temperature,” *J. Pharm. Sci.*, vol. 88, no. 3, pp. 291–296, Mar. 1999, doi: 10.1021/JS980387S.

[61] A. Bhargava and P. Jelen, “Lactose Solubility and Crystal Growth as Affected by Mineral Impurities,” *J. Food Sci.*, vol. 61, no. 1, pp. 180–184, Jan. 1996, doi: 10.1111/j.1365-2621.1996.tb14754.x.

[62] S. R. Patel and Z. V. P. Murthy, “Ultrasound assisted crystallization for the recovery of lactose in an anti-solvent acetone,” *Cryst. Res. Technol.*, vol. 44, no. 8, pp. 889–896, Aug. 2009, doi: 10.1002/crat.200900227.

[63] K. R. Morison and F. M. Mackay, “Viscosity of Lactose and Whey Protein Solutions,” *Int. J. Food Prop.*, vol. 4, no. 3, pp. 441–454, Nov. 2001, doi: 10.1081/JFP-100108647.

[64] P. Walstra, J. T. M. Wouters, and T. J. Geurts, *Dairy science and technology, second edition*, 2nd ed. CRC Press, 2005. Accessed: Nov. 09, 2022. [Online]. Available: https://www.perlego.com/book/1698670/dairy-science-and-technology-pdf

[65] J. M. Johnson and F. D. Conforti, “Lactose,” in *Encyclopedia of Food Sciences and Nutrition (Second Edition)*, B. Caballero, Ed., Second Edi.Oxford: Academic Press, 2003, pp. 3472–3476. doi: https://doi.org/10.1016/B0-12-227055-X/00674-X.

[66] P. Zarmpi, T. Flanagan, E. Meehan, J. Mann, and N. Fotaki, “Biopharmaceutical aspects and implications of excipient variability in drug product performance,” *Eur. J. Pharm. Biopharm.*, vol. 111, pp. 1–15, 2017, doi: https://doi.org/10.1016/j.ejpb.2016.11.004.

[67] J. Mcleod, “Nucleation and growth of alpha lactose monohydrate : a thesis presented in partial fulfilment of the requirements for the degree of Doctor of Philosophy in Process Engineering at Massey University,” vol. Doctor of, 2007, Accessed: Apr. 22, 2020. [Online]. Available: http://hdl.handle.net/10179/1444

[68] R. A. Visser, *Crystal Growth Kinetics of Alpha-lactose Hydrate*. Druk: Cooperative Condensfabriek"Friesland" w.a., 1983. [Online]. Available: https://books.google.co.uk/books?id=PZOPNQAACAAJ

[69] E. Simone, A. N. Saleemi, and Z. K. Nagy, "Raman, UV, NIR, and Mid-IR Spectroscopy with Focused Beam Reflectance Measurement in Monitoring Polymorphic Transformations," *Chem. Eng. Technol.*, vol. 37, no. 8, pp. 1305–1313, Aug. 2014, doi: 10.1002/CEAT.201400203.

[70] J. Cornel, C. Lindenberg, and M. Mazzotti, "Quantitative application of in situ ATR-FTIR and raman spectroscopy in crystallization processes," *Ind. Eng. Chem. Res.*, vol. 47, no. 14, pp. 4870–4882, Jul. 2008, doi: 10.1021/IE800236V.

[71] T. Togkalidou, H.-H. Tung, Y. Sun, A. Andrews, and R. D. Braatz, "Solution Concentration Prediction for Pharmaceutical Crystallization Processes Using Robust Chemometrics and ATR FTIR Spectroscopy," *Org. Process Res. Dev.*, vol. 6, no. 3, pp. 317–322, May 2002, doi: 10.1021/op015516x.

[72] S. A. Schiele, R. Meinhardt, C. Eder, and H. Briesen, "ATR-FTIR spectroscopy for in-line anomer concentration measurements in solution: A case study of lactose," *Food Control*, vol. 110, p. 107024, Apr. 2020, doi: 10.1016/J.FOODCONT.2019.107024.

[73] G. James, D. Burley, D. Clements, P. Dyke, and N. Steele, *Advanced Modern Engineering Mathematics*. Pearson, 2018. [Online]. Available: https://books.google.co.uk/books?id=OiPZswEACAAJ

[74] T. Vetter, C. L. Burcham, and M. F. Doherty, "Regions of attainable particle sizes in continuous and batch crystallization processes," *Chem. Eng. Sci.*, vol. 106, pp. 167–180, 2014, doi: https://doi.org/10.1016/j.ces.2013.11.008.

[75] Eigenvector Research Inc., "Solo and PLS Toolbox User Guide," *V 1.1*. 2010.

[76] S. Y. Wong and R. W. Hartel, "Crystallization in Lactose Refining—A Review," *J. Food Sci.*, vol. 79, no. 3, pp. R257–R272, 2014, doi: 10.1111/1750-3841.12349.

[77] B. E. Butler, "Modelling Industrial Lactose Crystallisation," Doctoral thesis, University of Queensland, 1998.

[78] M. Öner, S. M. Stocks, and G. Sin, "Comprehensive sensitivity analysis and process risk assessment of large scale pharmaceutical crystallization processes," *Comput. Chem. Eng.*, vol. 135, p. 106746, 2020, doi: https://doi.org/10.1016/j.compchemeng.2020.106746.

[79] B. H. Webb, A. H. Johnson, and J. A. Alford, *Fundamentals of Dairy Chemistry*. Avi Publishing Company, 1974. [Online]. Available: https://books.google.co.uk/books?id=Mm9RAAAAMAAJ

[80] D. Henningfield, Thomas and A. Dinesen, Richard, "Process and Plant for Evaporative Concentration and Crystallization of a Viscous Lactose-Containing Aqueous Liquid," Oct. 23, 2003

[81] L. T. T. Vu, R. J. Durham, J. A. Hourigan, and R. W. Sleigh, "Dynamic modelling and simulation of lactose cooling crystallisation: from batch and semi-batch to continuous operations," *Comput. Aided Chem. Eng.*, vol. 20, no. C, pp. 493–498, Jan. 2005, doi:

10.1016/S1570-7946(05)80204-4.

[82] S. Agrawal, “Evaporative crystallization of alpha-lactose monohydrate : a thesis presented in partial fulfilment of the requirements for the degree of Doctor of Philosophy in Chemical Engineering at Massey University, Manawatu, New Zealand.,” 2012.

[83] L. Sowul and M. A. F. Epstein, “Crystallization Kinetics of Sucrose in a CMSMPR Evaporative Crystallizer,” *Ind. Eng. Chem. Process Des. Dev.*, vol. 20, no. 2, pp. 197–203, Apr. 1981, doi: 10.1021/I200013A004.

[84] J. L. Crisp, S. E. Dann, and C. G. Blatchford, “Antisolvent crystallization of pharmaceutical excipients from aqueous solutions and the use of preferred orientation in phase identification by powder X-ray diffraction,” *Eur. J. Pharm. Sci.*, vol. 42, no. 5, pp. 568–577, Apr. 2011, doi: 10.1016/J.EJPS.2011.02.010.

[85] P. Parimaladevi and K. Srinivasan, “Anti-Solvent Crystallization of Lactose Single Crystals from Alcohol-Aqueous Solution at different concentrations,” *Int. J. ChemTech Res. CODEN*, vol. 6, no. 3, pp. 1595–1597.

[86] M. Shahid, G. Sanxaridou, S. Ottoboni, L. Lue, and C. Price, “Exploring the Role of Anti-solvent Effects during Washing on Active Pharmaceutical Ingredient Purity,” *Cite This Org. Process Res. Dev*, vol. 25, pp. 969–981, 2021, doi: 10.1021/acs.oprd.1c00005.

[87] R. Wijayasinghe, D. Bogahawaththa, J. Chandrapala, and T. Vasiljevic, “Crystallization behavior and crystal properties of lactose as affected by lactic, citric, or phosphoric acid,” *J. Dairy Sci.*, vol. 103, no. 12, pp. 11050–11061, 2020, doi: https://doi.org/10.3168/jds.2020-18375.

[88] S. Y. Wong, R. K. Bund, R. K. Connelly, and R. W. Hartel, “Designing a lactose crystallization process based on dynamic metastable limit,” *J. Food Eng.*, vol. 111, no. 4, pp. 642–654, Aug. 2012, doi: 10.1016/J.JFOODENG.2012.03.003.